1987

Forward-bias current annealing of radiation damaged gallium arsenide and silicon solar cells.

Staats, Richard L.

NAVAL POSTGRADUATE SCHOOL
Monterey, California

THESIS

FOWARD-BIASED CURRENT ANNEALING OF RADIATION DAMAGED GALLIUM ARSENIDE AND SILICON SOLAR CELLS

by

Richard L. Staats

September 1987

Thesis Advisor Sherif Michael

CURITY CLASSIFICATION OF THIS PAGE

REPORT DOCUMENTATION PAGE

REPORT SECURITY CLASSIFICATION: UNCLASSIFIED	1b RESTRICTIVE MARKINGS
SECURITY CLASSIFICATION AUTHORITY	3 DISTRIBUTION/AVAILABILITY OF REPORT: Approved for Public Release; Distribution Unlimited
DECLASSIFICATION/DOWNGRADING SCHEDULE	
PERFORMING ORGANIZATION REPORT NUMBER(S)	5 MONITORING ORGANIZATION REPORT NUMBER(S)
NAME OF PERFORMING ORGANIZATION: aval Postgraduate School / 6b OFFICE SYMBOL (If applicable): 62	7a NAME OF MONITORING ORGANIZATION: Naval Postgraduate School
ADDRESS (City, State, and ZIP Code): onterey, California 93943-5000	7b ADDRESS (City, State, and ZIP Code): Monterey, California 93943-5000
NAME OF FUNDING/SPONSORING ORGANIZATION / 8b OFFICE SYMBOL (If applicable)	9 PROCUREMENT INSTRUMENT IDENTIFICATION NUMBER
ADDRESS (City, State, and ZIP Code)	10 SOURCE OF FUNDING NUMBERS: PROGRAM ELEMENT NO / PROJECT NO / TASK NO / WORK UNIT ACCESSION NO

TITLE (Include Security Classification)

FOWARD-BIAS CURRENT ANNEALING OF RADIATION DAMAGED GALLIUM ARSENIDE AND SILICON SOLAR CELLS

PERSONAL AUTHOR(S)

Richard L. Staats

TYPE OF REPORT	13b TIME COVERED	14 DATE OF REPORT (Year Month Day)	15 PAGE COUNT
Master's Thesis	FROM ____ TO ____	1987 September 24	101

SUPPLEMENTARY NOTATION

COSATI CODES			18 SUBJECT TERMS (Continue on reverse if necessary and identify by block number)
FIELD	GROUP	SUB-GROUP	Gallium Arsenide and Silicon; Solar Cells; Annealing

ABSTRACT (Continue on reverse if necessary and identify by block number)

Radiation damaged gallium arsenide and silicon solar cells were nnealed using a combination of thermal and Foward-bias Current nnealing techniques. These cells were annealed under varying current ensities from 0.125 A/cm^2 to 1.250 A/cm^2 and at temperatures from 90 C 140 C. Gallium arsenide solar cells annealed at current densities rom 0.250 A/cm^2 to 0.750 A/cm^2. Attempts to anneal silicon solar cells ailed to produce positive results at all current densities. The rimary application of this research is to determine the feasibility of n-orbit annealing of a satellite's solar array. At present, only ilicon solar cells are deployed in space to provide electric power for tellites. When GaAs solar cells become space qualified, on-orbit oward-bias Current Annealing of these solar arrays may significantly crease the end of life of orbiting satellites.

DISTRIBUTION/AVAILABILITY OF ABSTRACT	21 ABSTRACT SECURITY CLASSIFICATION
UNCLASSIFIED/UNLIMITED ☐ SAME AS RPT ☐ DTIC USERS	UNCLASSIFIED
NAME OF RESPONSIBLE INDIVIDUAL: rofessor Sherif Michael	22b TELEPHONE (Include Area Code): (408) 646-2252 / 22c OFFICE SYMBOL: 62Mi

FORM 1473, 84 MAR — 83 APR edition may be used until exhausted; All other editions are obsolete — SECURITY CLASSIFICATION OF THIS PAGE

Approved for public release; distribution is unlimited.

Foward-Biased Current Annealing of Radiation Damaged Gallium Arsenide and Silicon Solar Cells

by

Richard L. Staats
Lieutenant, United States Navy
B.A., Metropolitan State College 1979

Submitted in partial fulfillment of the
requirements for the degree of

MASTER OF SCIENCE IN ELECTRICAL ENGINEERING

from the

NAVAL POSTGRADUATE SCHOOL
September 1987

ABSTRACT

Radiation damaged gallium arsenide and silicon solar cells were annealed using a combination of thermal and Foward-bias Current Annealing techniques. These cells were annealed under varying current densities from 0.125 A/cm^2 to 1.250 A/cm^2 and at temperatures from 90°C to 140°C. Gallium arsenide solar cells annealed at current densities from 0.250 A/cm^2 to 0.750 A/cm^2. Attempts to anneal silicon solar cells failed to produce positive results at all current densities. The primary application of this research is to determine the feasibility of on-orbit annealing of a satellite's solar array. At present, only silicon solar cells are deployed in space to provide electric power for satellites. When GaAs solar cells become space qualified, on-orbit Foward-bias Current Annealing of these solar arrays may significantly increase the end of life of orbiting satellites.

TABLE OF CONTENTS

I. INTRODUCTION 10

II. SOLAR CELLS 13
- A. ATOMIC STRUCTURE 13
- B. PHOTOVOLTAIC (PV) EFFECT 13
- C. POTENTIAL BARRIER 13
- D. MINORITY CARRIERS AND DIFFUSION LENGTH 15
- E. ELECTRICAL CHARACTERISTICS 16
- F. SOLAR CELL EFFICIENCY 18
- G. EFFECTS OF TEMPERATURE 19
- H. GALLIUM ARSENIDE VERSES SILICON SOLAR CELLS 20

III. RADIATION 22
- A. RADIATION ENVIRONMENT IN SPACE 22
  - 1. Solar Flare Protons 22
  - 2. Geomagnetically Trapped Protons and Electrons 22
- B. DAMAGE EQUIVALENCE 24
- C. EFFECT OF RADIATION ON CELL MICROSTRUCTURE 24
  - 1. Inelastic Collisions with Atomic Electrons 25
  - 2. Elastic Collisions with Atomic Nuclei 25
  - 3. Inelastic Collisions with Atomic Nuclei 25
- D. IONIZATION 25
- E. PERMANENT DAMAGE THROUGH ATOMIC DISPLACEMENTS 26
- F. EFFECT OF RADIATION ON MINORITY CARRIER LIFETIME 29
- G. ELECTRICAL CHARACTERISTICS AFTER IRRADIATION 30

H. RADIATION HARDENING METHODS 30
1. Base Resistivity 30
2. Cell Thickness 30
3. Shielding 32
4. Improved Silicon Solar Cell Designs 32

IV. ANNEALING METHODS 34
A. AMBIENT DAMAGE ANNEALING 34
B. THERMAL ANNEALING 34
C. FOWARD BIAS CURRENT ANNEALING 35

V. SOLAR CELL TEST EQUIPMENT AND PROCEDURE 37
A. SOLAR SIMULATOR SYSTEM 37
B. SOLAR CELL CALIBRATION/TEST PROCEDURE 37
C. FOWARD-BIAS CURRENT ANNEALING TEST PROCEDURE 39
D. IRRADIATION OF SOLAR CELLS 39

VI. ANNEALING EXPERIMENT 40
A. EXPERIMENT TEST STANDARDS 40
B. GALLIUM ARSENIDE SOLAR CELL ANNEALING 40
C. SILICON SOLAR CELL ANNEALING 41

VII. CONCLUSIONS AND RECOMMENDATIONS 94
A. CONCLUSIONS 94
1. GaAs Annealing Experiment 94
2. Silicon Annealing Experiment 95
3. Gallium Arsenide Verses Silicon Annealing 95
B. RECOMMENDATIONS 96
1. Gallium Arsenide Solar Cells 96
2. Silicon Solar Cells 96

LIST OF REFERENCES 97

INITIAL DISTRIBUTION LIST 99

LIST OF TABLES

1. TYPICAL SILICON SOLAR CELL CHARACTERISTICS [REF. 1 P. 340] 11
2. STS AND ELV LAUNCH COSTS [REF. 2 P. 34] 12
3. ANNUAL SOLAR PROTON FLUENCE [REF. 5 P. 5-20] 23
4. ASEC P/N 2 BY 2 CENTIMETER GAAS SOLAR CELLS 41
5. EXPERIMENTAL RESULTS OF FOWARD-BIAS CURRENT ANNEALING ON GAAS SOLAR CELLS IRRADIATED BY 20-MEV ELECTRONS 43
6. EXPERIMENTAL RESULTS OF THERMAL ANNEALING ON GALLIUM ARSENIDE SOLAR CELL ASEC-23 IRRADIATED BY 1-MEV ELECTRONS 63
7. EXPERIMENTAL RESULTS OF FOWARD-BIAS CURRENT ANNEALING ON GAAS SOLAR CELL ASEC-16 IRRADIATED BY 1-MEV ELECTRONS 63
8. EXPERIMENTAL RESULTS OF THERMAL ANNEALING ON SILICON SOLAR CELLS IRRADIATED BY 1-MEV ELECTRONS 66
9. EXPERIMENTAL RESULTS OF FOWARD-BIAS CURRENT ANNEALING ON SILICON SOLAR CELLS IRRADIATED BY 1-MEV ELECTRONS 67

LIST OF FIGURES

2.1 Solar Cell Potential Barrier [ref. 3 p. 15] 14

2.2 Solar Cell in Operation [ref. 3 p. 22] 14

2.3 Solar Cell Current-Voltage Curve [ref. 1 p. 329] 16

2.4 Conventional Solar Cell I-V Curve [ref. 4 p. 3.2-1] 17

2.5 Effect of R_s on Solar Cell I-V Curve [ref. 4 p. 3 .2-2] 18

2.6 Cell Efficiency as a Function of Temperature-dependent Energy Gap [ref. 5 p. 1-32] 19

2.7 Efficiency Verses Minimum Energy Needed to Free an Orbital Electron [ref. 3 p. 27] 20

2.8 Solar Cell Efficiency as a Function of Temperature 21

3.1 Coverglass Transmittance Variations with Absorbed Dose [ref. 5 p. 3-56] 27

3.2 Effect of Increasing Fluence on P_{max} [ref. 1 p. 336] 31

3.3 Variation of P_{max} with Cell Thickness for a Given Fluence [ref. 1 p. 338] 31

3.4 Advanced Silicon Cell Designs (a) Textured Surface Cell, (b) Vertical Junction Cell [ref. 5 p. 1-38] 33

4.1 P-N junction under foward-bias 35

5.1 Solar Simulator Block Diagram [ref. 15 p. 27] 38

6.1 Cross-Section View of the ASEC AlGaAs-GaAs Solar Cell 41

6.2 I-V Curve for GaAs Solar Cell ASEC-4 [ref. 15 p. 97] 45

6.3 I-V Curve for GaAs Solar Cell ASEC-4A, Irradiated to a Fluence of 10^{15} e/cm^2 by 20-Mev Electrons 46

6.4 I-V Curve for GaAs Solar Cell ASEC-4E, Annealed at 90°C Under Various Foward-bias Current Densities 47

6.5 I-V Curve for GaAs Solar Cell ASEC-5 [ref. 15 p. 98] 48

6.6 I-V Curve for GaAs Solar Cell ASEC-5A, Irradiated to a Fluence of 10^{14} e/cm^2 by 20-Mev Electrons 49

6.7 I-V Curve for GaAs Solar Cell ASEC-5D, Annealed at 90°C Under Various Foward-bias Current Densities 50

6.8 I-V Curve for GaAs Solar Cell ASEC-7 [ref. 15 p. 100] 51
6.9 I-V Curve for GaAs Solar Cell ASEC-7A, Irradiated to a Fluence of 10^{14} e/cm^2 by 20-Mev Electrons 52
6.10 I-V Curve for GaAs Solar Cell ASEC-7D, Annealed at 130°C, Under Various Foward-bias Current Densities 53
6.11 I-V Curve for GaAs Solar Cell ASEC-8 [ref. 15 p. 101] 54
6.12 I-V Curve for GaAs Solar Cell ASEC-8A, Irradiated to a Fluence of 10^{13} e/cm^2 by 20-Mev Electrons 55
6.13 I-V Curve for GaAs Solar Cell ASEC-8C, Annealed at 115°C, Under Various Foward-bias Current Densities 56
6.14 I-V Curve for GaAs Solar Cell ASEC-9 [ref. 15 p. 102] 57
6.15 I-V Curve for GaAs Solar Cell ASEC-9A, Irradiated to a Fluence of 10^{13} e/cm^2 by 20-Mev Electrons 58
6.16 I-V Curve for GaAs Solar Cell ASEC-9B, Annealed at 115°C, Under a 1.125 A/cm^2 Foward-bias Current 59
6.17 I-V Curve for GaAS Solar Cell ASEC-10 [ref. 15 p. 103] 60
6.18 I-V Curve for GaAs Solar Cell ASEC-10A, Irradiated to a Fluence of 10^{13} e/cm^2 by 20-Mev Electrons 61
6.19 I-V Curve for GaAS Solar Cell ASEC-10D, Annealed at 100°C, Under a 0.750 A/cm^2 Foward-bias Current for 6 Hours 62
6.20 I-V Curve for GaAs Solar Cell ASEC-16F, Annealed at 100°C, Under a 0.750 A/cm^2 Foward-bias Current for 50 Hours 64
6.21 I-V Curve for GaAs Solar Cell ASEC-16H, Annealed at 100°C, Under a 0.750 A/cm^2 Foward-bias Current for 140 Hours 65
6.22 I-V Curve for Silicon Solar Cell Sil-86A, Irradiated to a Fluence of 1.8×10^{14} e/cm^2 by 1-Mev Electrons 70
6.23 I-V Curve for Silicon Solar Cell Sil-86C, Annealed at 100°C Under a 0.500 A/cm^2 Foward-bias Current for 22 Hours 71
6.24 I-V Curve for Silicon Solar Cell Sil-87A, Irradiated to a Fluence of 1.8×10^{14} e/cm^2 by 1-Mev Electrons 72
6.25 I-V Curve for Silicon Solar Cell Sil-87C, Annealed at 100°C Under a 0.750 A/cm^2 Foward-bias Current for 18 Hours 73
6.26 I-V Curve for Silicon Solar Cell Sil-88A, Irradiated to a Fluence of 1.8×10^{14} e/cm^2 by 1-Mev Electrons 74
6.27 I-V Curve for Silicon Solar Cell Sil-88C, Annealed at 100°C Under a 1.000 A/cm^2 Foward-bias Current for 22 Hours 75
6.28 I-V Curve for Silicon Solar Cell Sil-89A, Irradiated to a Fluence of 1.8×10^{14} e/cm^2 by 1-Mev Electrons 76

6.29 I-V Curve for Silicon Solar Cell Sil-89C, Annealed at 100°C Under a 1.250 A/cm^2 Foward-bias Current for 24 Hours 77

6.30 I-V Curve for Silicon Solar Cell Sil-90A, Irradiated to a Fluence of 3.7×10^{13} e/cm^2 by 1-Mev Electrons 78

6.31 I-V Curve for Silicon Solar Cell Sil-90C, Annealed at 120°C Under a 0.250 A/cm^2 Foward-bias Current for 45 Hours 79

6.32 I-V Curve for Silicon Solar Cell Sil-91A, Irradiated to a Fluence of 3.7×10^{13} e/cm^2 by 1-Mev Electrons 80

6.33 I-V Curve for Silicon Solar Cell Sil-91C, Annealed at 120°C Under a 0.500 A/cm^2 Foward-bias Current for 23 Hours 81

6.34 I-V Curve for Silicon Solar Cell Sil-92A, Irradiated to a Fluence of 3.7×10^{13} e/cm^2 by 1-Mev Electrons 82

6.35 I-V Curve for Silicon Solar Cell Sil-92C, Annealed at 120°C Under a 1.000 A/cm^2 Foward-bias Current for 23 Hours 83

6.36 I-V Curve for Silicon Solar Cell Sil-93A, Irradiated to a Fluence of 3.7×10^{13} e/cm^2 by 1-Mev Electrons 84

6.37 I-V Curve for Silicon Solar Cell Sil-93D, Annealed at 120°C Under a 1.250 A/cm^2 Foward-bias Current for 46 Hours 85

6.38 I-V Curve for Silicon Solar Cell Sil-94A, Irradiated to a Fluence of 3.7×10^{13} e/cm^2 by 1-Mev Electrons 86

6.39 I-V Curve for Silicon Solar Cell Sil-94C, Annealed at 140°C Under a 0.250 A/cm^2 Foward-bias Current for 71 Hours 87

6.40 I-V Curve for Silicon Solar Cell Sil-95A, Irradiated to a Fluence of 3.7×10^{13} e/cm^2 by 1-Mev Electrons 88

6.41 I-V Curve for Silicon Solar Cell Sil-95D, Annealed at 140°C Under a 0.750 A/cm^2 Foward-bias Current for 47 Hours 89

6.42 I-V Curve for Silicon Solar Cell Sil-96A, Irradiated to a Fluence of 3.7×10^{13} e/cm^2 by 1-Mev Electrons 90

6.43 I-V Curve for Silicon Solar Cell Sil-96D, Annealed at 140°C Under a 1.250 A/cm^2 Foward-bias Current for 95 Hours 91

6.44 I-V Curve for Silicon Solar Cell Sil-97A, Irradiated to a Fluence of 3.7×10^{13} e/cm^2 by 1-Mev Electrons 92

6.45 I-V Curve for Silicon Solar Cell Sil-97B, Annealed at 140°C Under a 1.250 A/cm^2 Foward-bias Current for 75 Hours 93

I. INTRODUCTION

Silicon solar cells are the primary source of power on nearly all Earth orbiting satellites. Typical solar array subsystems are designed to provide adequate power to the payload through End-of-Life (EOL), which can be as long as ten years. The space environment of orbiting satellites is such that the spacecraft is continually subjected to radiation from geomagnetically trapped protons and electrons and from solar flare protons. Radiation damages silicon and gallium arsenide solar cells resulting in decreased solar cell efficiency with an overall reduction in power available from the solar array. To meet EOL power requirements, the solar array must be designed to provide more power than necessary to account for radiation degradation and other degrading effects. Thus, Beginning-of-Life (BOL) power requirements must be significantly higher than at EOL. Table 1 shows typical solar cell characteristics for several Intelsat satellites [Ref. 1: p. 340].

Current trends in satellite design are to build larger satellites with longer usable lifetimes, greater complexity and increasingly greater power requirements. For solar arrays to meet these needs more efficient solar cells or larger solar arrays are needed. The maximum efficiency of silicon solar cells available today is 15%. Gallium arsenide (GaAs) solar cells with 17% efficiency have been produced, however, as of this writing no satellite equipted with a GaAs solar array has been placed in orbit. Increasing the solar array size for a given solar cell efficiency will provide more power. Yet, launch costs of up to $33,300 per pound for Space shuttle (STS) launches and $12,900 per pound for Expendable Launch Vehicle (ELV) launches may make this practice prohibitive. Table 2 provides a rough comparison of STS and ELV launch costs in FY 83 monies [Ref. 2: p. 34]. Research into increasing solar cell efficiency and measures to reduce the launch costs of satellites is an ongoing process and in the future may alleviate these constraints.

Radiation hardening existing silicon solar cells and developing radiation tolerant cells made from materials such as GaAs are some of the areas currently being investigated. This field of study focuses on the prevention of radiation damage to solar cells. Another area of research which has shown some promise is solar cell annealing using a foward-bias current. In theory, on-orbit annealing of radiation damaged solar

TABLE 1

TYPICAL SILICON SOLAR CELL CHARACTERISTICS

[REF. 1 P. 340]

			Intelsat VI	
Characteristics	*Intelsat IV*	*Intelsat V*	*K4-3/4*	*K7*
Power BOL (28°C) (mW)	55.6	133.5	177.5	307.8
POWER EOL (28°C) (mW)	45.4	116.6	156.3	230.8
BOL				
I_{mp} (A)	0.125	0.2966	0.391	0.644
V_{mp} (V)	0.445	0.450	0.454	0.478
I_{sc} (A)	0.141	0.315	0.4187	0.6887
V_{oc} (V)	0.560	0.548	0.545	0.590
Size (cm)	2 × 2	2.1 × 4.04	1.8 × 6.2	2.5 × 6.2
Thickness (cm)	0.033	0.025	0.02	0.02
Material	Si	Si	Si	Si
Base resistivity Ω · cm/type	10/N/P	10/N/P	10/N/P	10/N/P
Front junction depth (μm)	>0.3	0.2	0.2	0.2
Back surface field	No	No	No	Yes
Back surface reflector	No	No	Yes	Yes
Contact metallization	TiPdAg	TiPdAg	TiPdAg	TiPdAg
Front contact width (cm)			0.06	0.06
Antireflective coating	SiO_2	Ti_2O_3	TiO_x	$T_iO_xAl_2O_3$
Cover type	Fused silica	Ceria-doped microsheet	cmx microsheet with antireflective coating	cmx microsheet with antireflective coating
Cover thickness (cm)	0.030	0.015	0.021	0.021
Cover adhesive	DC 634-89	DC 93-500	DC 93-500	DC 93-500
Cover front surface	Polished	Polished	Polished	Textured

cells will reverse some of the effects of irradiation and return a fraction of the power lost. This process could be integrated into a satellite's electrical subsystem. Utilizing the excess power generated at BOL to supply the necessary foward-bias current, isolated sections of the array could be continuously annealed thereby reducing the overall damaging effect of incident radiation. Application of this technique will extend the useful life of the solar cell, and therefore the satellite's lifetime, or reduce the size of the array needed to meet EOL power requirements. This thesis examines the effects of Foward-biased Current Annealing on radiation damaged silicon and gallium arsenide solar cells.

TABLE 2

STS AND ELV LAUNCH COSTS [REF. 2 P. 34]

LAUNCH MISSION OR VEHICLE	GEOSYNCHRONOUS PAYLOAD, LB	LATE 1983 LAUNCH COST, RY $M	COST/LB, RY $/LB
OPTIMIZED SHUTTLE LAUNCHES			
LEASAT	2.740	14.8	5.400
FULL SHUTTLE	10.600	54.0	5.100
NONOPTIMIZED SHUTTLE LAUNCHES			
SBS/PAM-D	1.470	12.8	8.700
INTELSAT V/PAM-A	2.350	30 4	12.900
TDRS/IUS	5.000	62.8	12.600
EXPENDABLE LAUNCHES			
DELTA 3914	1.106	29.2	26.400
DELTA 3910/PAM-D	1.285	32.4	25.200
DELTA 3920/PAM-D	1.470	37.4	25.400
ATLAS/CENTAUR	2.445	50.0	20.500
TITAN III C	3.600	≈ 120 0	33.300

• UPDATE JUST PRIOR TO PUBLICATION (OCT 1980)

In Chapter II basic solar cell semiconductor theory is reviewed and significant electrical parameters are defined. The effects of temperature on solar cells is examined, while the differences, advantages and disadvantages of silicon verses gallium arsenide cells are discussed.

Chapter III defines the radiation environment of satellites in Earth orbit, the effects of radiation damage on the macroscopic structure of cells and the results of such damage to the electrical characteristics of the cell.

Various methods of annealing are discussed in Chapter IV. Emphasis is placed on Foward-biased Current Annealing with a brief review of the effects of biasing on cell structure. The test equipment and procedures used in the Foward-biased Current Annealing experiment are described in Chapter V.

In Chapter VI, irradiated gallium arsenide and silicon solar cells are annealed using a foward-biased current. Current density, annealing temperature and time are varied to determine optimum annealing parameters.

Conclusions based on the results of solar cell annealing, as well as recommendations for further testing, are discussed in Chapter VII.

II. SOLAR CELLS

A. ATOMIC STRUCTURE

The basic structure of all materials is the atom. Atoms are composed of protons, neutrons and electrons. The neutron and positively charged proton form the nucleus, while the negatively charged electron orbits the nucleus. Electrons can only exist at discrete energy levels. Overall, the atom is electrically neutral.

The silicon atom has fourteen electrons and protons. The electrons are arranged such that the four outermost electrons are in the highest energy band. This outermost band is called the valence band and. the electrons are called the valence electrons. Valence electrons can be given to, accepted from, or shared with other atoms. Large numbers of atoms, through their valence electrons, can bond together to form a solid structure of material.

The next allowed band after the valence band is called the conduction band. The energy gap from valence to conduction band is a function of the type of material. For semiconductors, the energy gap is from 0.5 ev to 2.6 ev.

B. PHOTOVOLTAIC (PV) EFFECT

When light strikes a semiconductor such as silicon, the light may be absorbed, reflected, or pass through the crystal. If absorbed light with energies greater than the energy gap strikes an electron, the electron will break its atomic bond and enter the conduction band, where the electron is free to roam. The gap left by the missing electron is called a hole. Holes, like conduction band electrons, are free to roam the crystal structure. Generation of electron-hole pairs is the central process in the conversion of light to electricity. However, when no other mechanism is involved, the light-generated electrons and holes will meander about the crystal randomly for a time and then lose their energy thermally as they return to their valence positions. To produce an electric current from electron-hole pairs, a "potential" barrier is needed [Ref. 3: p. 14].

C. POTENTIAL BARRIER

The potential barrier separates light-generated electrons and holes. Figure 2.1 shows a typical potential barrier in a solar cell. The electron-hole pairs are separated

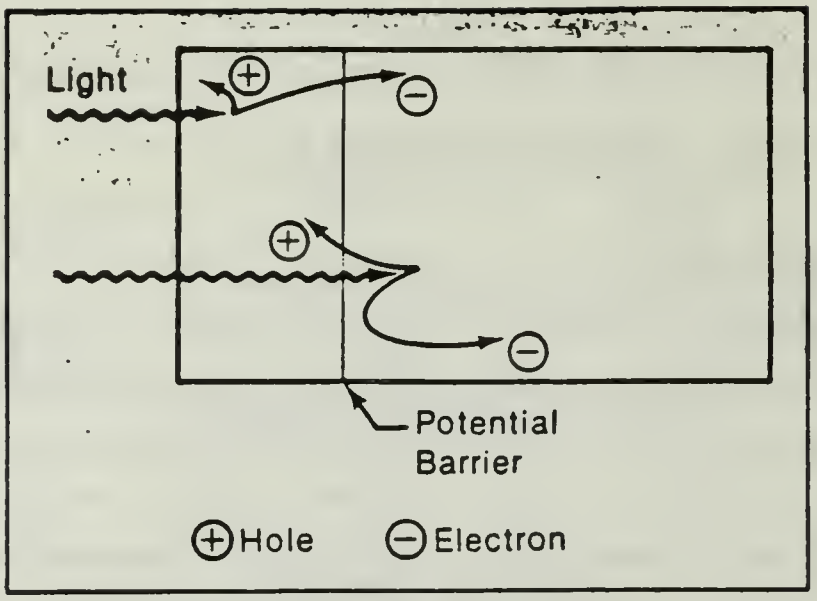

Figure 2.1 Solar Cell Potential Barrier [ref. 3 p. 15].

by the potential barrier and are less likely to recombine and lose their electrical energy. The resultant charge separation produces a voltage difference between the ends of the cell. This voltage difference can be used to drive an electric current in an external circuit as seen in Figure 2.2.

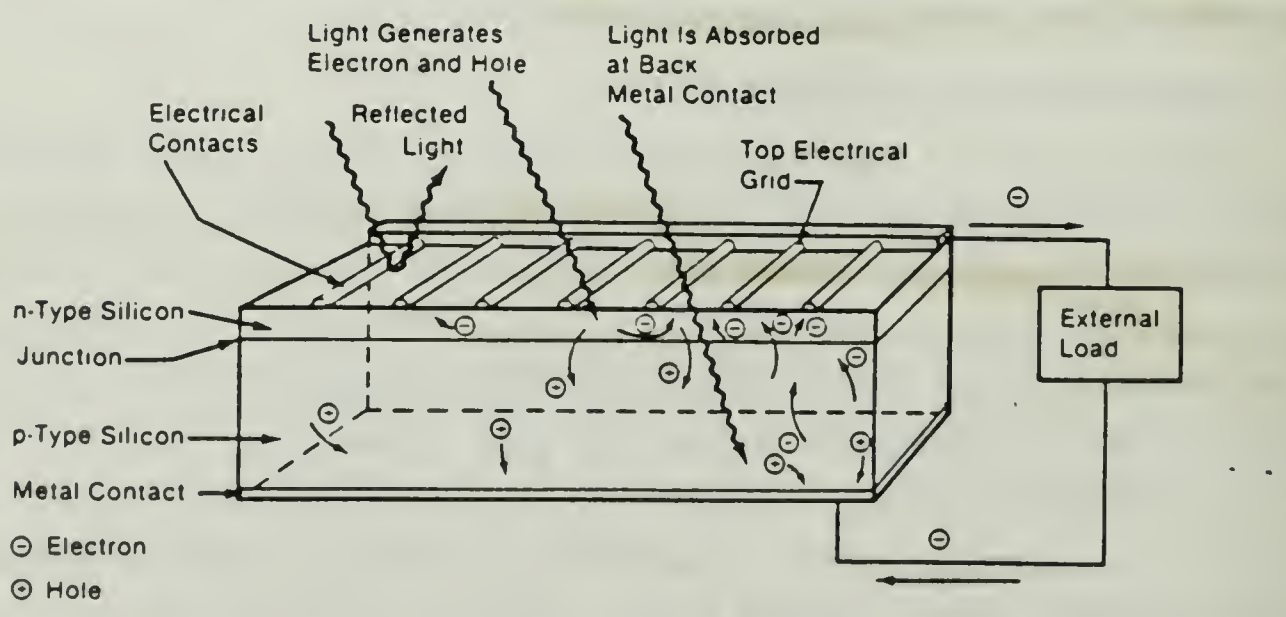

Figure 2.2 Solar Cell in Operation [ref. 3 p. 22].

Formation of the potential barrier is accomplished by altering the basic structure of the material using dopants. In a semiconductor such as silicon, the crystal lattice is altered by the addition of phosphorous or boron atoms. Unlike silicon, phosphorous has five valence electrons while, boron has three. When phosphorous is added to pure

silicon, the fifth electron does not bond with any other atom. This electron is relatively free to roam throughout the crystal, and the phosphorous atom becomes positively charged. This doped crystal is known as N-type because it has free negative charges. Conversely, when boron is added to pure silicon, one boron to silicon bond does not form. This hole acts as a free positive electron and it, also, roams the crytal lattice. The boron doped crystal is known as P-type because of the presence of free positive charges. In N-type material, the more numerous free electrons are commonly called majority carriers while the holes are called minority carriers. For P-type material, the holes are the majority carrier and the free electrons the minority carrier.

When P-type and N-type materials are joined together, charges are diffused across the junction. The free electrons in the N-type material will see a region where there are no free electrons, and hence there will be a flow of these electrons to the P-type material. The free holes in the P-type material will see a region where there are no holes, so there will be a flow of positive charged holes to the N-type material. When an excess of negative charges on the P-type material and an excess of positive charges on the N-type material form, an electrical field will be established in the region of interface of the two materials. Eventually, the electric potential becomes of such a magnitude that further diffusion of holes and electrons is prohibited. When this equilibrium is established, the construction of the P-N junction has been completed, resulting in a permanent electric field without the aid of an external electric field [Ref. 1: p. 238]. The P-N junction is typically produced by taking a wafer of P-type or N-type material and diffusing the opposite type dopant into the surface at high temperature. To form a N/P junction, N-type dopant is diffused into P-type substrate. To form a P/N junction, P-type dopant is diffused into N-type substrate.

D. MINORITY CARRIERS AND DIFFUSION LENGTH

Considering the P-region of an N/P type solar cell, the minority carriers (electrons) which do not reach the junction will recombine with the majority carriers (holes). The time required for recombination is the minority carrier lifetime, τ. After a period of time, only 1/e of these electrons will remain. These electrons will reach the junction after traveling a distance L, which is called the diffusion length. Diffusion length and minority carrier lifetime are related by the equation

$$L = \text{sqrt}(D \times \tau) \qquad (2.1)$$

where, D is the diffusion constant of the material.

The output of a solar cell is dependent on the diffusion length, which in turn, is a function of the minority carrier lifetime. Typical minority carrier diffusion lengths are about 200 microns. The effect of proton and electron irradiation is to decrease the diffusion length and ultimately reduce the electrical performance of the cell.

E. ELECTRICAL CHARACTERISTICS

Solar cells are two-terminal devices. The electrical terminal characteristics can be described by current and voltage (I-V) curves. Figure 2.3 shows the I-V curves for an

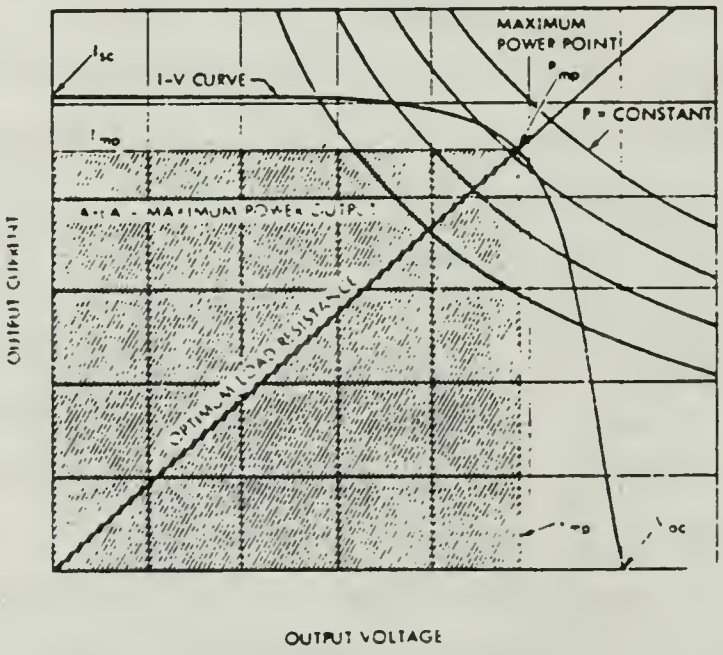

Figure 2.3 Solar Cell Current-Voltage Curve [ref. 1 p. 329].

illuminated and unilluminated solar cell. Quadrants 1 and 3 correspond to a power sink and quadrants 2 and 4 correspond to a power generator. Thus, an unilluminated solar cell is a power sink with characteristics similar to a diode. While, the illuminated solar cell is a power source. The displacement of the I-V curve in the -I direction during illumination is proportional to the illumination intensity of the source light. A conventional solar cell I-V curve is shown in Figure 2.4 where,

- I_{sc} = Short-curcuit current
- V_{oc} = Open-circuit voltage
- P_{max} = Maximum power output point
- I_{mp} = Maximum power current
- V_{mp} = Maximum power voltage
- R_{olr} = Optimum load resistance

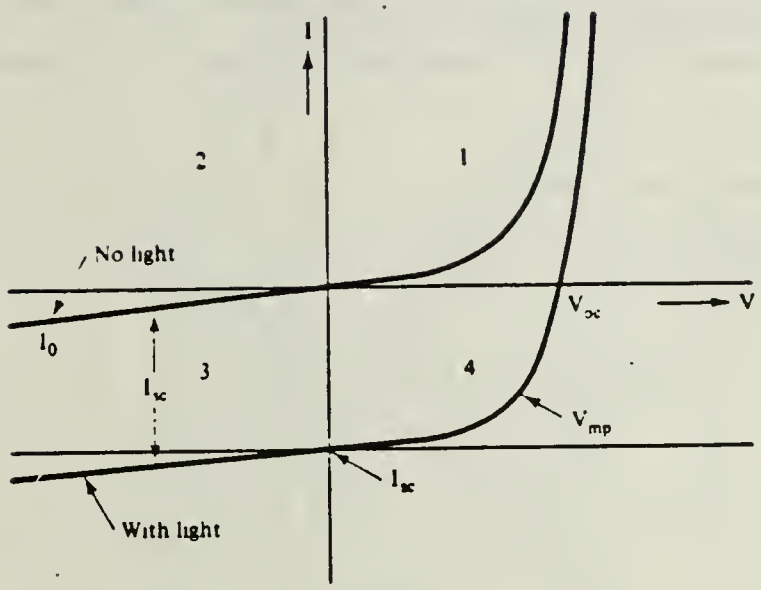

Figure 2.4 Conventional Solar Cell I-V Curve [ref. 4 p. 3.2-1].

The maximum power delivered corresponds to the area of the largest rectangle that can be drawn inside the curve. Therefore, the squarer the current-voltage characteristics, the higher the efficiency. The squareness of this curve is described by the "fill factor" where,

$$FF = \frac{V_{mp}I_{mp}}{V_{oc}I_{sc}} = \frac{P_{max}}{V_{oc}I_{sc}} \qquad (2.2)$$

The maximum power point occurs at the "knee" of the curve, which is at the intersection of I_{mp} and V_{mp}. A straight line drawn from the origin to P_{max} represents the optimum load resistance, R_{olr}, for the cell.

The series resistance, R_s, of a solar cell is an idealization of internal dissipative electrical losses which can be deduced to occur in the cell by observing its terminal behavior [Ref. 4: p. 3.2-2]. Variations in R_s are caused by humidity, temperature, heavy particle radiation, and manufactoring processes. Large variations in R_s can significantly alter a solar cell I-V curve as shown in Figure 2.5. The net effect of increased series resistance is the loss of solar cell efficiency.

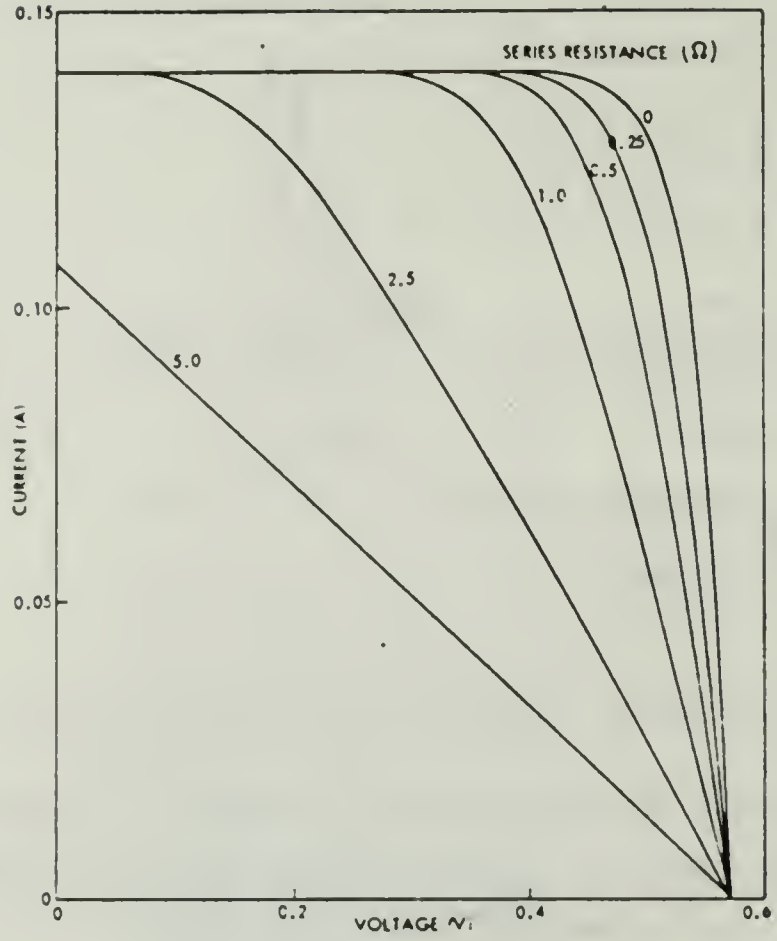

Figure 2.5 Effect of R_s on Solar Cell I-V Curve
[ref. 4 p. 3 .2-2].

F. SOLAR CELL EFFICIENCY

Solar cell efficiency, η, is defined as:

$$\eta = \frac{P_{out}}{P_{in}} = \frac{P_{out}}{(S \times \text{area})} \qquad (2.3)$$

The electrical power output of the cell, P_{out}, is optimized when P_{out} equals P_{max}. The electrical power input to the cell, P_{in}, is equal to the solar constant, S, multiplied by the active solar cell area upon which the solar energy is incident. The solar constant, S, is the total energy received from the sun on a unit area which is perpendicular to the sun's rays at the mean earth-sun distance of 1 AU. The value of S is currently taken to be 1353 W/sq.m.

G. EFFECTS OF TEMPERATURE

The conversion efficiency of solar cells is highly affected by temperature. In Figure 2.6, the net effect of increasing temperature is to decrease efficiency of all

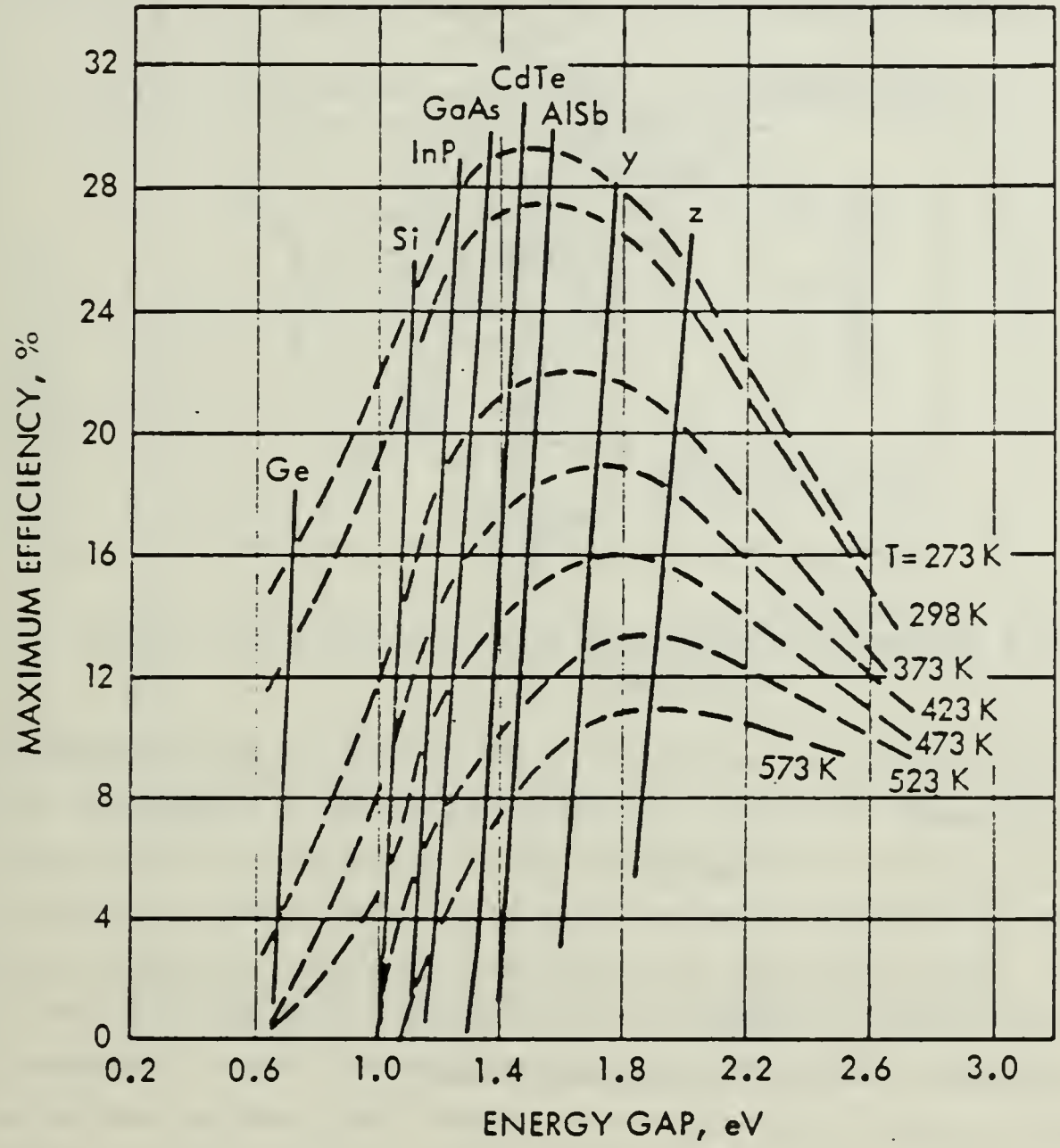

Figure 2.6 Cell Efficiency as a Function of Temperature-dependent Energy Gap [ref. 5 p. 1-32].

materials. The basic mechanism involved is the destruction of the junction between N/P or P/N materials through thermal agitation of the atomic bonds.

H. GALLIUM ARSENIDE VERSES SILICON SOLAR CELLS

The energy gap for gallium arsenide is 1.4-ev and for silicon it is 1.1-ev. Gallium arsenide solar cells are more efficient than silicon cells because the energy required to free electrons nearly coincides with the peak efficiency of the solar spectrum, as seen in Figure 2.7. Another advantage of GaAs over silicon is greater thermal stability.

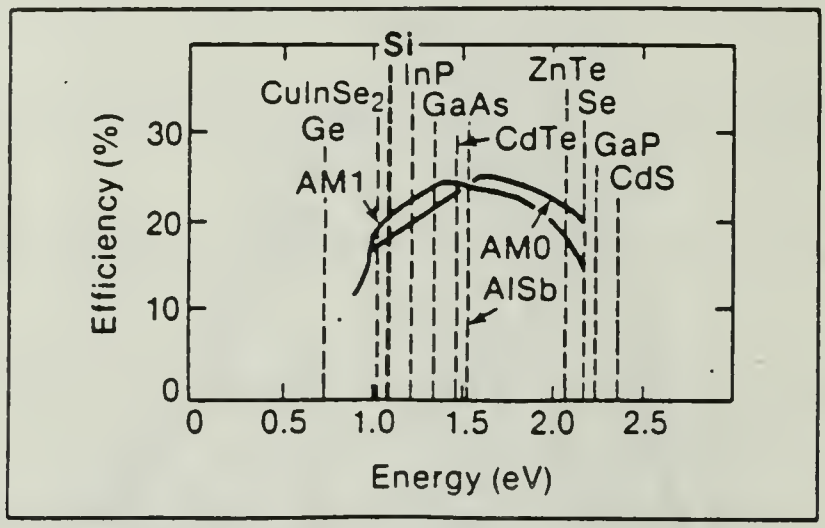

Figure 2.7 Efficiency Verses Minimum Energy Needed to Free an Orbital Electron [ref. 3 p. 27].

Figure 2.8 shows the effect of temperature on cell efficiency. A typical silicon cell degrades approximately 0.5% for every degree Celsius rise in temperature. The degradation of GaAs due to thermal environment is approximately one half that of silicon. Hence, GaAs cells are attractive for use at high temperatures such as in solar concentrators. Studies have shown that GaAs solar cells are more radiation tolerant than silicon. This makes GaAs cell solar cells ideal for use in radiation intense areas of the space environment. Finally, tests have shown GaAs cells to have a considerably better ability to anneal. From this, one can conclude that GaAs cells will be the principal solar cell in use on future satellite systems. However, there are certain disadvantages associated with their use. These are higher production costs, limited availability in production quantities, and higher mass ratio. For GaAs solar cells to be competitive with silicon solar cells, the problem of production cost and quantity must be solved. The fact that the mass of a GaAs cell is approximately twice that of a comparable silicon cell is obviated by the higher efficiency of GaAs. Studies have shown that the weight of a GaAs solar array will be less than the weight of a silicon

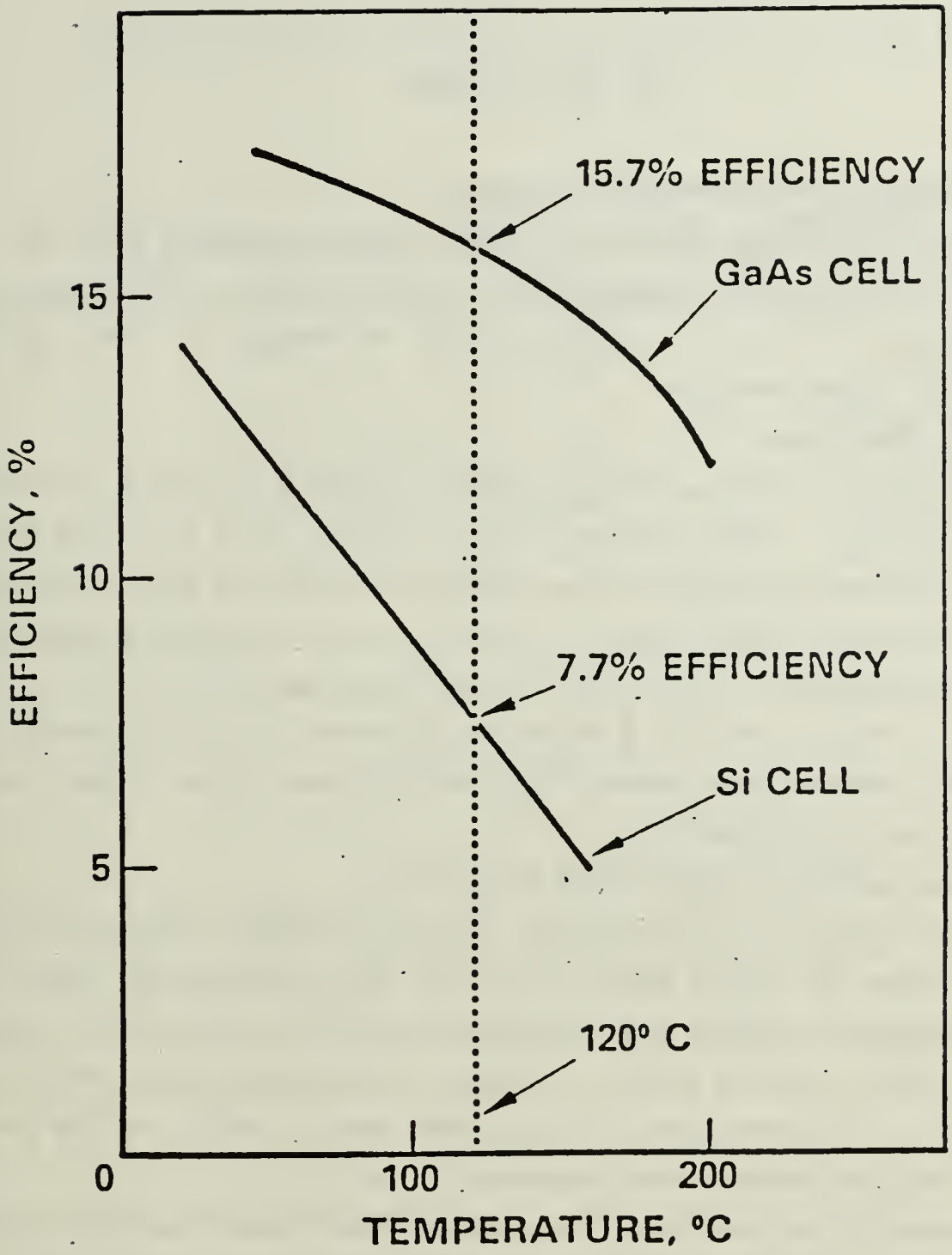

Figure 2.8 Solar Cell Efficiency as a Function of Temperature.

solar array for a given EOL power output because fewer GaAS solar cells are needed due to their higher photon conversion efficiency. In fact, studies indicate an actual weight savings can be achieved when using GaAs solar cells.

III. RADIATION

A. RADIATION ENVIRONMENT IN SPACE

Radiation in the space environment which produces damaging effects on solar cells are: solar flare protons, geomagnetically trapped protons and geomagnetically trapped electrons. By far, the principal cause of damage in solar cells are geomagnetically trapped electrons.

1. Solar Flare Protons

The ejection of large numbers of protons from the sun during a solar flare is closely associated with sunspot activity. Sunspots follow an 11 year solar cycle of increasing and decreasing activity. During a flare event, solar cells may be subjected to extremely high fluxes of solar protons. In Table 3, the observed annual integral fluence of solar flare protons from 1956 through 1979 associated with solar flare cycles 19 and 20 is shown, as well as, predicted fluences for solar cycle 21 for 1978 through 1984. Observed data indicates that protons with energies greater than 30-Mev are not uncommon during a solar flare event.

2. Geomagnetically Trapped Protons and Electrons

Protons and electrons ejected from the sun are carried by the solar wind to Earth and trapped in Earth's geomagnetic field. The mechanism by which these particles are trapped is complex and the interested reader is referred to [Ref. 5: chap 5] for further reading. The flux density of trapped protons and electrons varies due to day-night cycles, normal solar activity, solar flare activity, season, and the altitude, latitude and longitude of the orbiting spacecraft.

Trapped protons are found at an altitude from 1.5 Earth radii (alt 3,189 km) to near 6.6 Earth radii (alt 35,786 km). In general, the average energy level of all protons decrease with increasing altitude. At synchronous altitudes (alt 35,786 km), almost no protons have energies greater than 2 Mev.

Trapped electrons are primarily found in two regions, an inner region and an outer region. The inner region spans from 1.2 (alt 1,276 km) to 2.8 Earth radii (alt 11,480 km). In the outer region, the span is from 3 (alt 12,756 km) to 11 Earth radii (alt 63,780 km).

TABLE 3

ANNUAL SOLAR PROTON FLUENCE [REF. 5 P. 5-20]

Year	Number of Events	Integral Fluence (protons/cm^2)			
		Φ(>10 MeV)	Φ(>30 MeV)	Φ(>60 MeV)	Φ(>100 MeV)
1956	4	2.0×10^9	1.0×10^9		3.5×10^8
1957	9	---	4.0×10^8		2.0×10^7
1958	8	7.0×10^9	7.8×10^8		2.4×10^7
1959	6	2.2×10^{10}	4.2×10^9		4.6×10^8
1960	15	6.8×10^9	2.2×10^9		3.8×10^8
1961	6	1.6×10^9	3.5×10^8		4.2×10^7
1962	2				
1963	1				
1964		1.0×10^7	2.4×10^6		
1965	1	2.5×10^7	2.8×10^6		
1966	4	1.7×10^9	8.7×10^7	1.4×10^7	
1967	5	1.5×10^9	1.9×10^8	5.9×10^7	
1968	7	2.2×10^9	2.8×10^8	9.4×10^7	
1969	4	2.5×10^9	5.1×10^8	2.1×10^8	
1970	6	6.3×10^8	3.5×10^7	1.4×10^7	
1971	3	1.9×10^9	5.1×10^8	1.2×10^8	
1972	3	2.3×10^{10}	8.2×10^9	2.5×10^9	5.5×10^8
1973	3	1.4×10^7	6.3×10^6	3.0×10^6	
1974	5	2.8×10^8	4.2×10^7	8.2×10^6	
1975	1	3.3×10^6	2.0×10^6	1.2×10^6	
1976	1	2.1×10^7	8.6×10^6	4.2×10^6	
1977	5	2.6×10^8	8.4×10^7	3.7×10^7	
1978	11	6.3×10^9	7.9×10^8	1.4×10^8	
1979	7	8.4×10^8	1.6×10^8	4.3×10^7	
ANNUAL INTEGRAL FLUENCE PREDICTION FOR CYCLE 21 (1978 - 1984) USING SOLPRO WITH 90% CONFIDENCE LEVEL THAT CALCULATED FLUENCES WILL NOT BE EXCEEDED					
1 AL EVENT		1.7×10^{10}	7.9×10^9	2.5×10^9	5.6×10^8

Proton density reaches a peak at approximately 2 Earth radii (alt 6,378 km) while electron density peaks at 2.4 Earth radii (alt 8929 km) and 5 Earth radii (alt 25,512 km). This is the Van Allen radiation belt [Ref. 6] where the particle density may be more than 10,000 times greater than the expected average values of charged particle density of the solar wind at 1 AU.

B. DAMAGE EQUIVALENCE

As seen, electron and proton energies vary over a wide range in the space environment. To describe the effects of various types of radiation in terms of a radiation environment which can be produced under laboratory conditions, the damage equivalent 1-Mev fluence is introduced. Damage produced in solar cells by electrons of various energies can be related to the damage produced by 1-Mev electrons by damage coefficients. Similarly, the damage caused by protons of various energies can be related to the damage of 10-Mev protons.

Experimental studies indicate that a given fluence of normally incident 10-Mev protons induces the same amount of damage as 1-Mev electrons at 3000 times the fluence of the 10-Mev protons. The total 1-Mev fluence is calculated by determining the damage equivalent 1-Mev fluence for protons and electrons and then summing the results. Under laboratory conditions, a unidirectional 1-Mev electron beam that produces a similar solar cell degradation is assumed to be equivalent to the true space radiation spectrum. The validity of this concept is currently under test by Dr. Bruce Anspaugh, et al., of the Jet Propulsion Laboratory, Pasedena California. Present findings indicated the concept to be valid [Ref. 7].

C. EFFECT OF RADIATION ON CELL MICROSTRUCTURE

Highly energetic, fast moving particles of electrons are the major cause of damage in solar cells. At Low Earth Orbits (LEO) geomagnetically trapped electrons and protons are the significant contributors to solar cell degradation, while at attitudes near synchronous orbit, during periods of high solar activity, solar flare protons may add significantly to the total cell-damaging fluence. Radiation particles with energies in the range listed below are significant to solar cell damage when they impinge on solar cell covers

- Electrons 0.2 to 1-Mev
- Protons 4 to 40-Mev

Because electrons and protons have mass, charge and energy, they, or other particles generated by them, can interact with semiconductors in several ways. The principal interactions are [Ref. 5: chap 3]:

1. **Inelastic Collisions with Atomic Electrons**

Inelastic collisions of energetic protons and electrons with bound atomic electrons will cause these bound electrons to transit to an excited state (excitation) or to an unbound state (ionization). This is the dominate mechanism by which an energetic particle loses kinetic energy in an absorber.

2. **Elastic Collisions with Atomic Nuclei**

Displacement of an atom from its position in the crystal lattice can occur by coulombic interactions with the positive charge of the atomic nucleus (Rutherford scattering) or through hard sphere collisions with the nucleus. Energetically displaced atoms may in turn displace more atoms through similar collisions. The probability of hard sphere collisions is less than that for Rutherford scattering, except at higher energies.

3. **Inelastic Collisions with Atomic Nuclei**

Inelastic collisions of highly energetic protons with the atomic nucleus leaves the nucleus in an excited or activated state. The proton is absorbed by the nucleus, thus excited, the nucleus will decay emitting energetic nucleons while recoiling through the lattice structure. The moving nucleus causes additional displacements in the crystal lattice. This process is also referred to as spallation. The net effect on the microstructure of solar cells from radiation is to cause ionizations and atomic displacements to occur.

D. IONIZATION

Ionization causes permanent and temporary damage in solar cells. Permanent damage occurs in solar cell covers when ionizing radiation excites orbital electrons to the conduction band. These electrons are trapped by impurity atoms in the oxide to form charge defect complexes with subsequent darkening and degradation of the cell cover. Secondly, darkened cell covers absorb more light which increases the cell operating temperature and reduces illumination of the cell. Both mechanisms reduce solar cell efficiency and hence, power output. The fractional loss in output power can be estimated using "wide-band" transmission loss data. The "wide-band" transmittance is defined as the solar cell I_{sc} with an irradiated coverglass in place divided by the solar cell I_{sc} with the unirradiated coverglass in place. Because V_{oc} is proportional to

$\ln(I_{sc})$, the following relation can be developed to estimate the change in P_{max} due to coverglass darkening:

$$P_{max}/P_{maxo} = T(\ln(TI_{sc})/\ln(I_{sc})) \qquad (3.1)$$

where,

- P_{max}/P_{maxo} = The fractional change in P_{max}
- T = "wide-band" transmission of irradiated coverglass
- I_{sc} = Short circuit current with unirradiated coverglass

In Figure 3.1, "wide-band" transmittance is shown for various absorbed doses. The absorbed doses were produced by 1-Mev electron irradiations at room temperature, in an air environment which included no ultraviolet illumination. Electron radiation penetration was sufficient to produce uniform dose throughout the entire coverglass, coating and filter.

Temporary damage of solar cells occurs when ionization of valence electrons to the conduction band creates electron-hole pairs. This process is similar to that generated by light photons. However, roughly three times the normal energy is required to produce the same effect. Ionization by this mechanism is a beneficial interaction.

E. PERMANENT DAMAGE THROUGH ATOMIC DISPLACEMENTS

Highly energetic, fast moving particles are capable of producing atomic displacements in the crystal lattice of silicon and GaAs solar cells. These displaced atoms and their associated vacancies undergo other reactions and finally form permanent, stable defects which produce significant changes in the equilibrium carrier concentrations and minority carrier lifetime of the irradiated cell. To displace an atom, a minimum displacement energy, E_d, is required. For GaAs, the energy required is 25-ev [Ref. 8] and for silicon the displacement energy is 12.9-ev [Ref. 5: p. 3-7]. If the electron threshold energy level, E_t, is known one can derive the displacement energy using:

$$E_d = 2(m_e E_t / M m_e C^2)(E_t + 2m_e C^2) \qquad (3.2)$$

where,

- E_d = Displacement energy (Mev)
- E_t = Threshold energy (Mev)

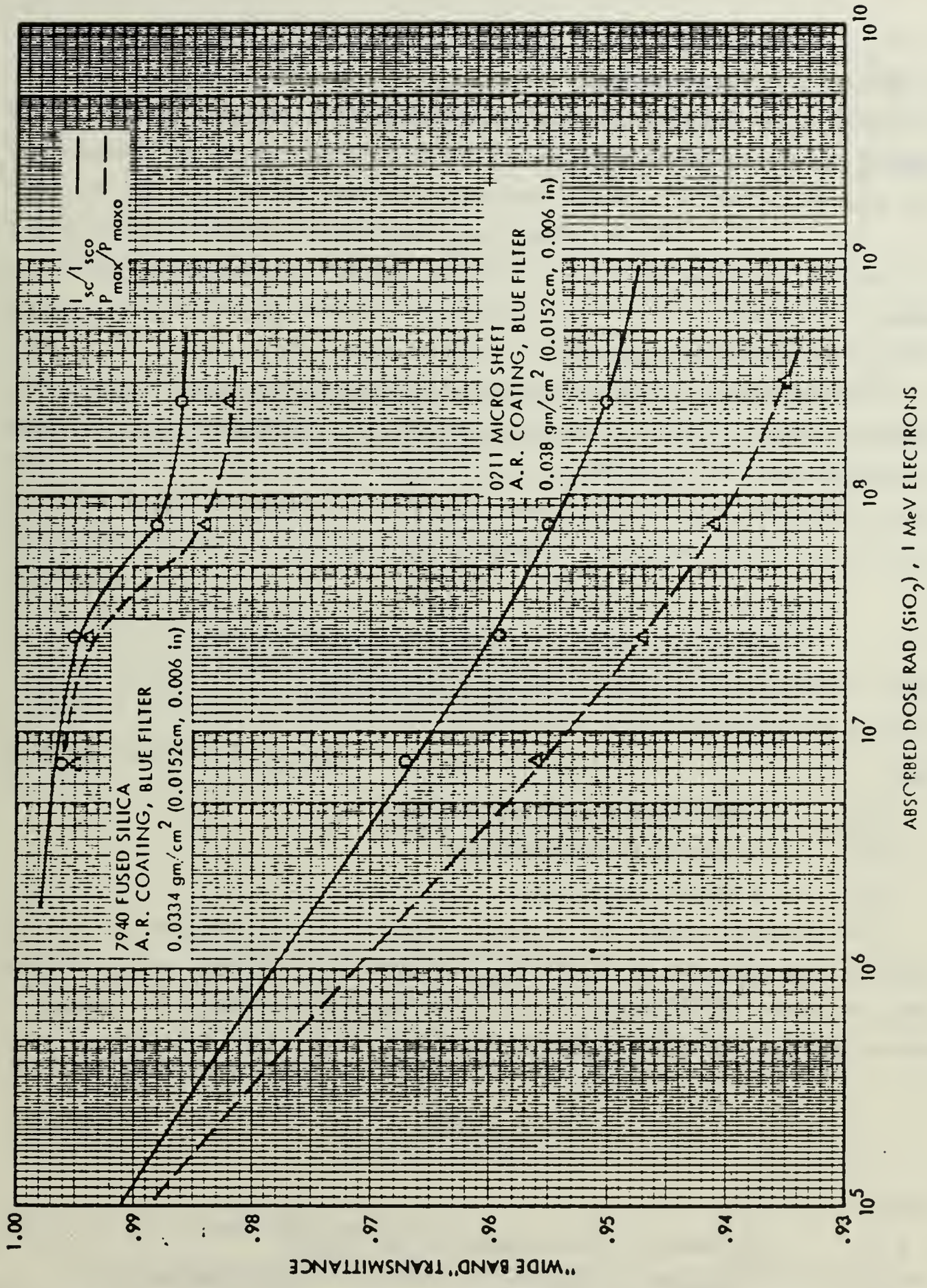

Figure 3.1 Coverglass Transmittance Variations with Absorbed Dose [ref. 5 p. 3-56].

- m_e = Electron mass
- M = Atomic weight
- m_eC^2 = Electronic mass-energy equivalence (0.511Mev)

Similarly, for proton threshold energies:

$$E_d = ((4Mm_p)/(m_p + M)^2)E_t \quad (3.3)$$

where,

- m_p = Proton mass

Particles below the threshold level cannot produce displacement damage. The maximum energy, E_{max}, that can be transferred from irradiation particle to lattice atom is determined using [Ref. 9]:

$$E_{max} = (4E_i m_p m_a)/(m_p + m_a)^2 \quad (3.4)$$

$$E_{max} = ((E_i + 2m_eC^2)/(m_aC^2))2E_i \quad (3.5)$$

where

- E_{max} = Maximum energy transferred (ev)
- E_i = Incident particle energy (ev)
- m_a = mass of lattice atom

The maximum energy for protons is calculated from Equation 3.4 and for electrons using Equation 3.5. When E_{max} is greater than or equal to E_d, sufficient energy is possesed by moving particles to cause atomic displacements. The number of atomic displacements can be estimated from:

$$N_d = n_a\sigma\gamma\Phi \quad (3.6)$$

where,

- N_d = Number of displacements per unit volume
- n_a = Number of atoms per unit volume of absorber (atoms/cm^3)
- σ = Displacement cross section (cm^2)
- γ = Average displacements per primary displacement

- Φ = Radiation fluence (particle/cm^2)

The displacement cross section, σ, for 1-Mev electrons and protons in silicon are $68 \times E^{-24} cm^2$ and $3.5 \times E^{-20} cm^2$, respectively. While the average number of displacements per primary displacement, γ, for electrons is 1.53 and 4.8 for protons. Thus, one can conclude that proton displacement collisions are much more likely than electron collision displacements.

Neutron displacement damage can occur in absorber material. However, the displacement cross section for a 1-Mev neutron is $2.4 \times E^{-24} cm^2$ which is well below those for 1-Mev protons and 1-Mev electrons. The probability of atomic displacement via neutron collision is relatively small. When neutron collisions do occur, they are hard sphere collisions rather than coulombic collsions, since neutrons are uncharged particles. The average energy transferred to the recoiling atom is about 70-Kev. At this higher energy level secondary collisions between silicon atoms will displace about 1500 additional atoms with the damage clustered near the site of the primary displacement.

F. EFFECT OF RADIATION ON MINORITY CARRIER LIFETIME

The principal effect of radiation is to decrease minority carrier diffusion length (lifetime) of the solar cell. The minority carrier lifetime, τ, after irradiation by electrons and protons can be found using:

$$1/\tau = 1/\delta + 1/\alpha + 1/\beta \qquad (3.7)$$

where,

- $1/\delta$ = Minority carrier lifetime before irradiation
- $1/\alpha$ = Minority carrier lifetime due to electron irradiation
- $1/\beta$ = Minority carrier lifetime due to proton irradiation

Conversely, if the total electron and proton fluence is known one can use:

$$1/\tau = 1/\delta + k_\tau \Phi \qquad (3.8)$$

where, k_τ is the damage coefficient (lifetime).

Since, the diffusion length, L, varies as a function of τ, the diffusion length can be found by substituting Equation 2.1 into Equation 3.8 and solving. Thus, the final expression becomes:

$$1/L^2 = 1/L_o^2 + k_L \Phi \quad (3.9)$$

where,

- L_o = Initial minority carrier diffusion length
- k_L = k_τ/D = Damage coefficient (diffusion length)

In practice, minority carrier lifetime and diffusion length measurements are difficult to make in the laboratory. Another more convienient way to characterize the degrading effect of radiation is to measure the change in electrical parameters of the irradiated cell.

G. ELECTRICAL CHARACTERISTICS AFTER IRRADIATION

Irradiation of solar cells by electrons and protons will cause permanent degradation to the following electrical parameters: R_s (series resistance), η (cell efficiency), I_{sc} (short circuit current), V_{oc} (open circuit voltage), and P_{max} (maximum power point). Degradations in I_{sc} and V_{oc} will decrease the shape and size of the I-V curve. The fill factor, FF, is relatively insensitive to uniformly penetrating radiation. If the fill factor is known and assumed constant then, using Equation 2.2, one can determine P_{max} from V_{oc} and I_{sc}. This is the basis by which the effect of radiation on solar cells is commonly evaluated. Radiation damage is cumulative with each particle adding to the total fluence of the cell. Figure 3.2 shows the effect of increasing fluence on the maximum power of various types of silicon cells.

H. RADIATION HARDENING METHODS

Many methods are employed to harden solar cells against radiation damage from energetic electrons and protons which are found in the satellite environment. A few of these methods are discussed below.

1. Base Resistivity

Increasing the base resistivity of a solar cell will increase the radiation resistance while decreasing the overall cell efficiency. For low fluence missions, low base resistivity (1 to 3 Ωcm) cells provide the highest power output, and for high fluence missions, high base resistivity (7 to 14 Ωcm) provides the largest output [Ref. 4: p. 3.1-3].

2. Cell Thickness

Radiation degrades the red (long-wavelength) response of cells.. If the cell thickness is made smaller than, or equal to, the mean diffusion length, then the red

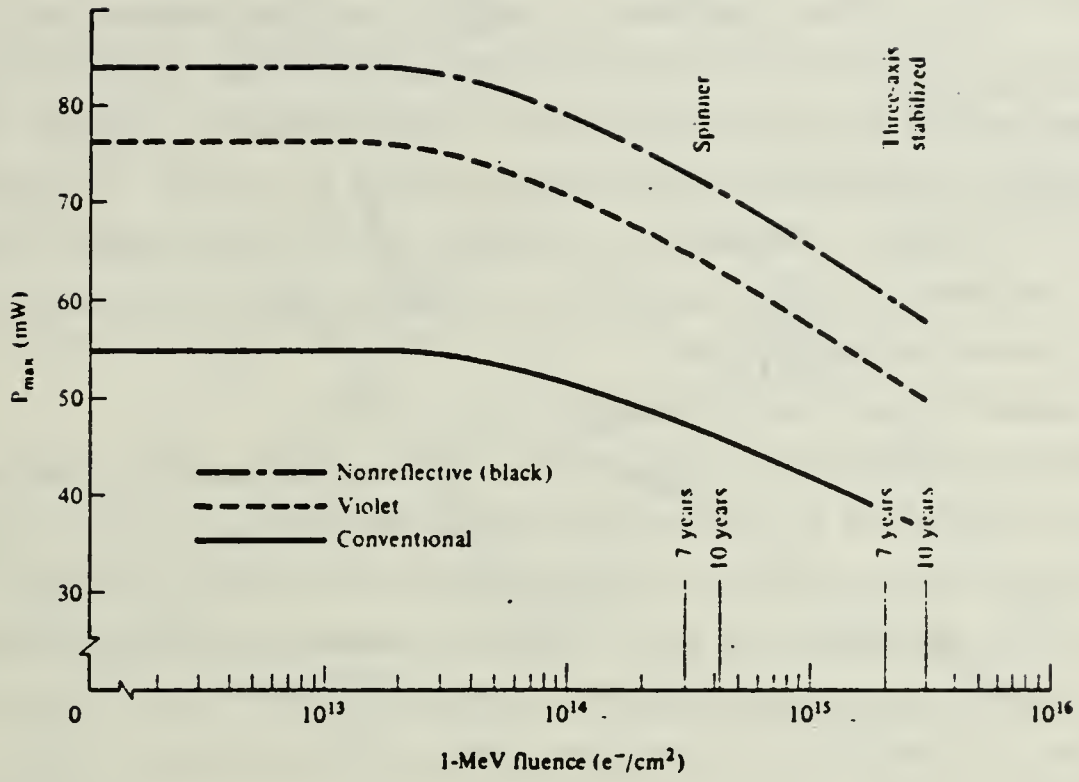

Figure 3.2 Effect of Increasing Fluence on P_{max} [ref. 1 p. 336].

response will be reduced. Consequently, reducing the thickness of a solar cell increases radiation hardness while reducing solar cell efficiency. As can be seen from Figure 3.3,

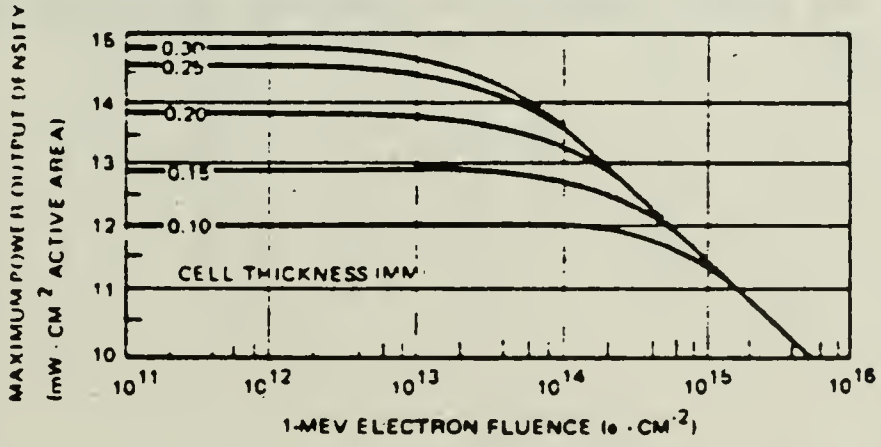

Figure 3.3 Variation of P_{max} with Cell Thickness for a Given Fluence [ref. 1 p. 338].

the effect of thickness on electric power output decreases as the radiation dosage increases.

3. **Shielding**

Low energy proton penetration is confined to shallow regions near the front surface of the cell where the P-N junction of most cells is located. Protons which come to rest near the P-N junction introduce shunt paths across the junction. This can cause significant degradations in the electrical output of the cell. To prevent low energy proton damage, coverglasses are installed on the front surfaces. Back side shielding is employed to prevent penetration by radiation which may cause a reduction in minority carrier lifetime of the cell.

4. **Improved Silicon Solar Cell Designs**

Increasing the spectral response of solar cells to blue and ultraviolet regions of the spectrum will increase the radiation hardness of the cell and improve cell efficiency. Shallow junction (Violet) cells have been developed with increased response in these regions and with efficiencies near 14.5%. Another method of increasing efficiency and radiation hardness is to modify the front surfaces of the cells in a manner which increases the red response and produces electron-hole pairs nearer the junction. Textured surface (Black) cells using pyramidal construction, as seen in Figure 3.4 (a), reduces reflectivity and causes electron-hole pairs generated by long wavelength light to be created near the junction. The vertical junction cell of Figure 3.4 (b) acts in a fashion that is very similar to the textured surface cell. Vertical junction cells with efficiencies of 15% and textured surface cells with 15.5% efficiencies have been produced. Experiments by Green, et al. [Ref. 10], using a microgrooved Passivated Emitter Solar Cell (PESC) structure has produced silicon solar cells with AM0 efficiencies of 18%.

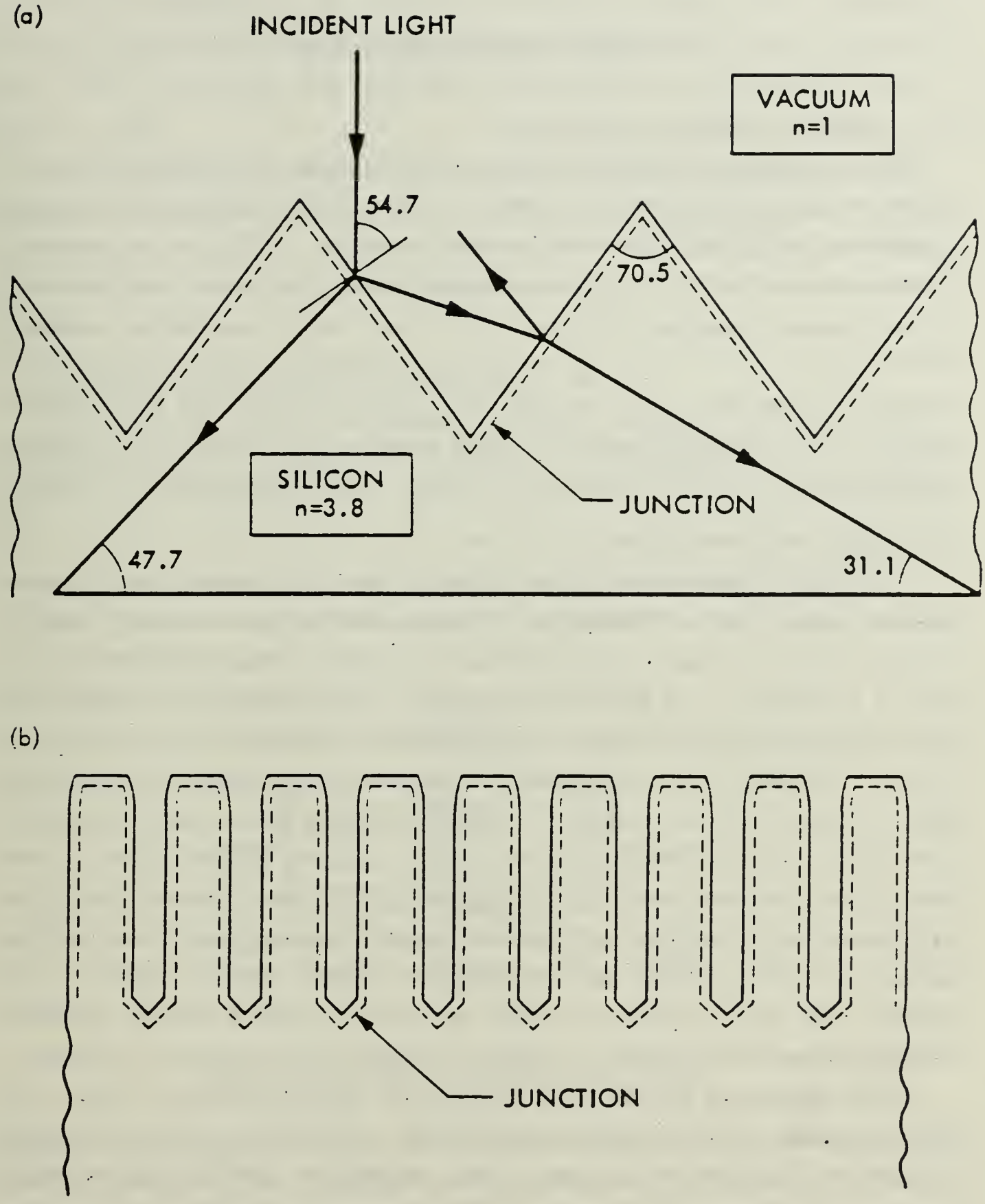

Figure 3.4 Advanced Silicon Cell Designs (a) Textured Surface Cell, (b) Vertical Junction Cell [ref. 5 p. 1-38].

IV. ANNEALING METHODS

A. AMBIENT DAMAGE ANNEALING

In the laboratory, solar cells irradiated with electrons and protons have been observed to anneal under ambient conditions. In the space environment, this damage annealing occurs simultaneously with solar cell irradiation. Damage annealing occurs at temperatures above 25°C with proton damage annealing being more significant than electron damage annealing [Ref. 4: p. 3.3-4]. For electron irradiation, annealing recovery rates of up to 10% in I_{SC} occur in several days to a month. While, proton irradiated recovery rates of up to 20% in I_{SC} have been observed in 22 months [Ref. 5: p. 3-44]. Although benificial, ambient annealing of solar cells do not provide significant results. To achieve higher recovery rates, elevated temperatures are needed.

B. THERMAL ANNEALING

Elevating the base temperature of a solar cell through the introduction of heat is the most common method of annealing. Thermal annealing raises the energy level of all atoms within the structure being annealed. The amount of energy imparted to each atom is a function of the annealing temperature. Atoms displaced by proton and electron irradiation produce vacancies and interstitials. Vacancies are the vacant lattice sites left by displaced atoms, while interstitials are atoms which occupy interstitial sites within the lattice structure. Recovery of radiation damage occurs when the displaced atoms diffuse to and fill nearby vacancies. In order to move a displaced atom to a new location, the atom must pass over an energy barrier. The energy barrier is called the activation energy, Q, and heat supplies the atom with the energy needed to exceed this barrier. Since P-N junction cells are made by diffusing dopant atoms into the substrate, care must be taken when using the thermal annealing process. Excessive annealing temperatures increases the diffusion of dopants away from the P-N junction.

Prior experiments by Day, et al. [Ref. 11], on thermal annealing of silicon and gallium arsenide solar cells irradiated by 250-Kev and 1.5-Mev protons, sets upper limits on the annealing temperature. Using unirradiated control cells, isochronal anneals were performed in 25°C steps with 20 minutes of annealing time per step. Day showed that thermal degradation of the cell occured at temperatures above 450°C for silicon and 350°C for GaAs. At these elevated temperatures, the adhesives used in the

manufacture of solar cells begins to degrade and the soldered metal contacts will fail. Research by Yamaguchi, et al. [Ref. 12], on electron irradiated GaAs solar cells showed that these cells exhibit three recovery stages at 150 - 200°C, 250 - 350°C and 400 - 500°C. For silicon cells, significant recovery does not occur below 200°C [Ref. 5: p. 3-42].

In experiments conducted by Loo, et al. [Ref. 13], observations strongly suggest that continuous annealing of GaAs solar cells exposed to electron fluxes of the space environment can be effective at temperatures as low as 150°C. Thermal annealing temperatures lower than 150°C could be possible in low flux areas near geosynchronous orbit.

C. FOWARD BIAS CURRENT ANNEALING

In Foward-bias Current Annealing, a positive voltage is applied to the P (positive) side of the P-N junction of the solar cell. The magnitude of this voltage is varied to supply the desired current density across the cell. Under illumination and without external biasing, the solar cell is foward-biased by incident photons. A solar cell can be foward-biased in either an illuminated or unilluminated condition.

Figure 4.1 shows a typical P-N junction under foward-bias. The external current

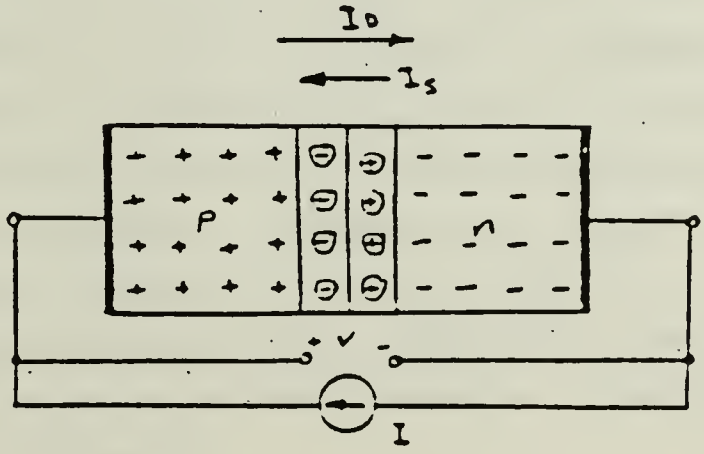

Figure 4.1 P-N junction under foward-bias.

will cause holes to be extracted from the N region and electrons from the P region of the cell. As the holes enter the P region and electrons enter the N region they become majority carriers. These majority carriers will cause a narrowing of the carrier-depletion region of the junction and a reduction of the barrier voltage. Since the diffusion current, I_D, is a function of this voltage it must increase in magnitude.

Hence, minority carrier concentration increases. The exact mechanism under which Foward-bias Current Annealing reduces radiation damage in solar cells is unknown. However, applying an external bias to an illuminated or unilluminated cell will increase the cell temperature and minority carrier concentrations. These conditions could improve minority carrier lifetime and diffusion lengths in the cell being annealed.

Previous experiments by Clark [Ref. 14], on GaAs solar cells have shown that low current densities at or near 0.5 A/cm^2 are effective in solar cell annealing. In the main experiment, Clark used a 0.5 A/cm^2 current to foward-bias the test cell. The ambient temperature of the cell was maintained at a constant temperature of 90°C and the cell was annealed for 48 hours. Under these conditions, recovery of 28-30% of lost efficiency was reported. Experiments using a combination of thermal annealing followed by Foward-bias Current Annealing have produced recoveries to near 90% of original efficiencies. Another possible annealing method would be to simultaneously anneal an irradiated solar cell at elevated temperatures near optimum for that type of cell while introducing a foward-biasing current. Such a method would take advantage of both aspects of annealing and could produce satisfactory results.

V. SOLAR CELL TEST EQUIPMENT AND PROCEDURE

A. SOLAR SIMULATOR SYSTEM

A solar simulator system is used to measure the electrical parameters of the cell under test at varying intensities of light. Standard tests are made at light intensities equal to AM0, however, measurements can be made at AM1 or at other suitable levels. The light source for this system is provided by a Kratos model SS 2500 Solar Simulator. The Kratos Solar Simulator uses a zenon arc lamp which produces light intensities that closely approximates the spectral distribution of light found at AM0.

The cell under test is placed on a brass test block which is water cooled by a temperature controlled water circulator. This enables testing of the cell at the desired temperature. A vacuum pump is attached to the cell block and it provides electrical and thermal contact between the cell and test block. The test block is electrically connected to a switching module which allows the user to select N/P or P/N junction solar cells, run or calibration functions, and test or setup functions. Digital multimeters are connected to the switching module to allow for direct reading of open circuit voltage, V_{OC}, and short circuit current, I_{SC}, of the cell.

An IBM PC/XT computer is connected to a Hewlett Packard model 3478A Digital Multimeter and IEEE-488 General Purpose Interface Bus (GPIB). Electrical connections to the test block via the switching module allows voltage and current measurements to be made using computer controlled software programs. To measure the current-voltage characteristics of the cell under test, a Hewlett Packard model 5901B Power Supply Programmer and a 6825A Bipolar Power Supply are used to sink the current generated by the cell under illumination. A simplified block diagram of this system is shown in Figure 5.1.

B. SOLAR CELL CALIBRATION/TEST PROCEDURE

Prior to testing a cell, the Solar Simulator System must be calibrated to standard temperature and intensity, usually AM0, using a standard solar cell. A standard cell with known V_{OC}, and I_{SC} values is placed on the test block. The cell is illuminated by the zenon arc lamp. After the test block and cell configuration has reached thermal equilibrium, the intensity of the incident light is adjusted until the voltage-current characteristics of the cell match the values provided. The I-V characteristics of the cell

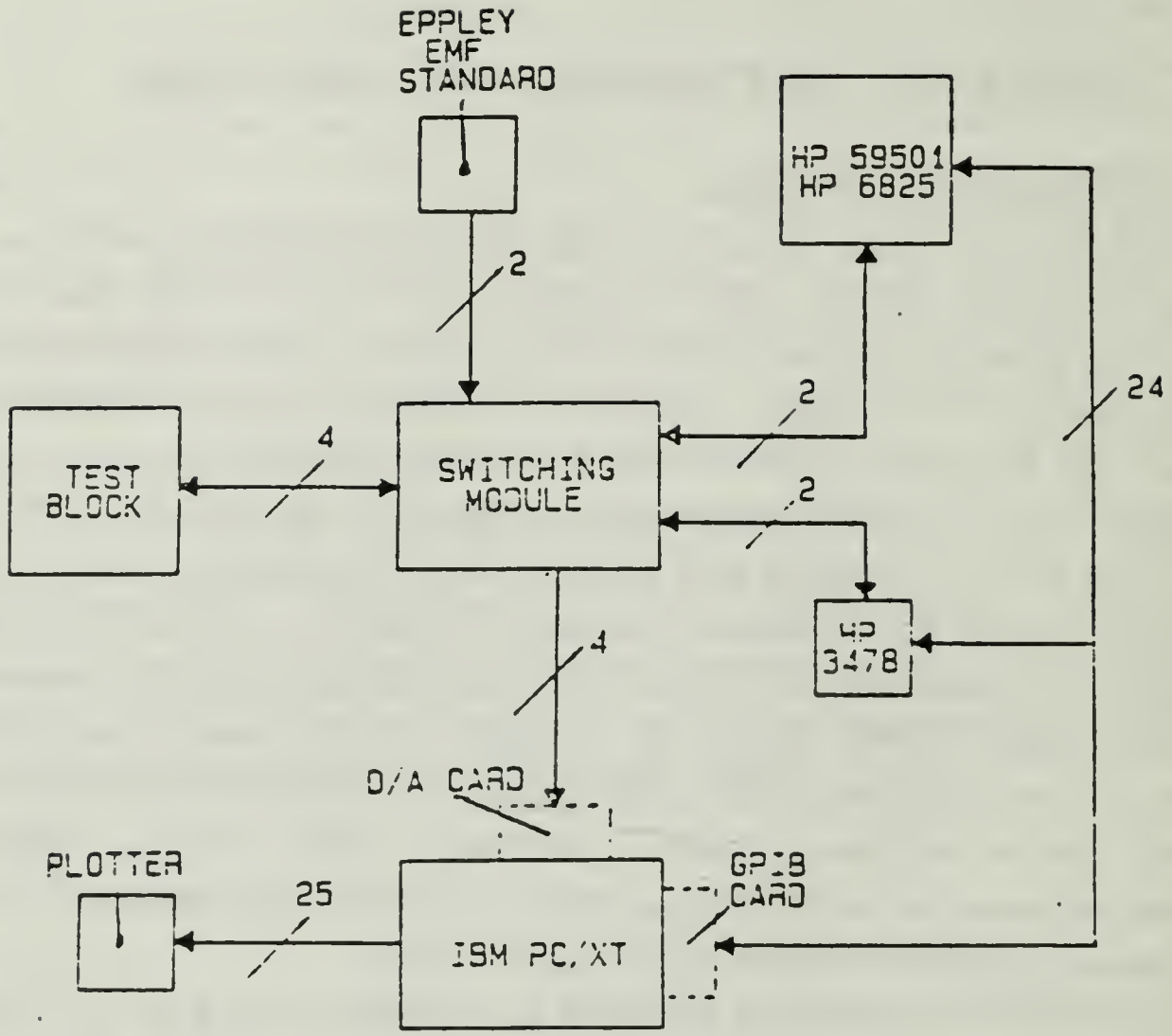

Figure 5.1 Solar Simulator Block Diagram [ref. 15 p. 27].

are determined using the computer-controlled software programs. Initiation of the program in the run/test mode steps down the voltage of the cell from V_{oc} to zero voltage, while the current steps up from zero current to I_{sc}. During the step down process, voltage and current measurements are made. The measured data can be used to plot the I-V curve of the standard solar cell on the Hewlett Packard 7475A Plotter. Duplication of electrical characteristics provided by the manufaturer of the standard cell ensure calibration of the Solar Simulator System at the correct intensity and temperature. Other cells may now be tested with confidence. The system described in this and preceeding paragraphs of the chapter was designed and installed by D. W. Gold [Ref. 15].

C. FOWARD-BIAS CURRENT ANNEALING TEST PROCEDURE

The electrical characteristics of an irradiated solar cell are determined using the calibrated solar simulator. Then the cell is placed on a test bed which is electrically connected to a current/voltage power supply where an appropriate foward-biasing current is applied to the cell. The test bed is placed in an oven with an incandenscent 75 watt lamp. The lamp is used to provide illumination of the cell at approximately AM1, while the oven provides variable thermal anneal temperatures. The cell under test is Foward-bias Current Annealed with or without AM1 illumination or thermal anneal, as appropriate, for a specified period of time. Upon completion of the anneal process, the cell is returned to the solar simulator test block where the electrical characteristics of the cell are measured and compared to pre-anneal results.

D. IRRADIATION OF SOLAR CELLS

Solar cells used in this experiment were irradiated at the Jet Propulsion Laboratory (JPL), Pasadena, CA and at the Naval Postgraduate School (NPS), Monterey, CA. The JPL system is a Dynamitron Linear accelerator. The cells at JPL were irradiated by 1-Mev electrons. The NPS system is a Linear accelerator (LINAC). These cells were irradiated by 20-Mev electrons.

VI. ANNEALING EXPERIMENT

A. EXPERIMENT TEST STANDARDS

Annealing of each cell was accomplished by placing the cell in an oven and illuminating the cell under test with a 75 watt incandescent lamp. The lamp foward-biased the cell and closely approximated AM1 conditions. Cell temperature and foward-bias current densities were varied. At appropriate time intervals, the cell was removed from the oven and allowed to cool to room temperature. Current and voltage characteristics of the cell were measured using the calibrated Solar Simulator System as described in Chapter V. All measurements were made at AM0 and at 28°C unless otherwise stated.

B. GALLIUM ARSENIDE SOLAR CELL ANNEALING

The GaAs solar cells used in this experiment were manufactured by the Applied Solar Energy Corporation (ASEC). The manufactured characteristics of these cell are shown in Table 4. A cross sectional view of the cell is shown in Figure 6.1. Solar cells ASEC-4, ASEC-5, ASEC-7, ASEC-8, ASEC-9 and ASEC-10 were obtained from thesis research conducted by D.W Gold [Ref. 15]. As part of his thesis, Gold irradiated these cells with 20-Mev electrons using the NPS Linear accelerator. Irradiation fluence levels were from 10^{13} e/cm^2 to 10^{15} e/cm^2. These cells were Foward-bias Current Annealed at various current densities and temperatures. Table 5 summarizes the results of Foward-bias Current Annealing on cells ASEC-4, ASEC-5, ASEC-7, ASEC-8, ASEC-9, and ASEC-10. Figures 6.2 through 6.19 show pre-irradiation, post-irradiation and final annealing I-V curves for each cell annealed.

Solar cells ASEC-16 and ASEC-23 were irradiated at the JPL Linear accelerator by 1-Mev electrons. Fluence levels for these cells are 1.8×10^{14} e/cm^2 and 3.7×10^{13} e/cm^2 , respectively. To determine the effect of thermal annealing on GaAs solar cells, cell ASEC-23 was thermally annealed at 100°C. The results of this anneal are shown in Table 6. Solar cell ASEC-16 was annealed at 100°C and with a foward-bias current density of 0.750 A/cm^2. Table 7 summarizes the results of annealing on this cell. Figures 6.20 and 6.21 show the maximum annealed efficiency and final annealing I-V curves for cell ASEC-16.

TABLE 4

ASEC P/N 2 BY 2 CENTIMETER GAAS SOLAR CELLS

Substrate thickness	300 uM
N layer thickness	9 uM
P junction layer thickness-Zn doped	0.5 uM
P window - $Al_xGa_{1-x}As$ ($x \sim .86-.9$) thickness	0.1 uM
P contact material	Au - Zn - Ag
N contact material	Au - Ni - Ge - Ag
Anti-reflection coating	TiO_2, Al_2O_3

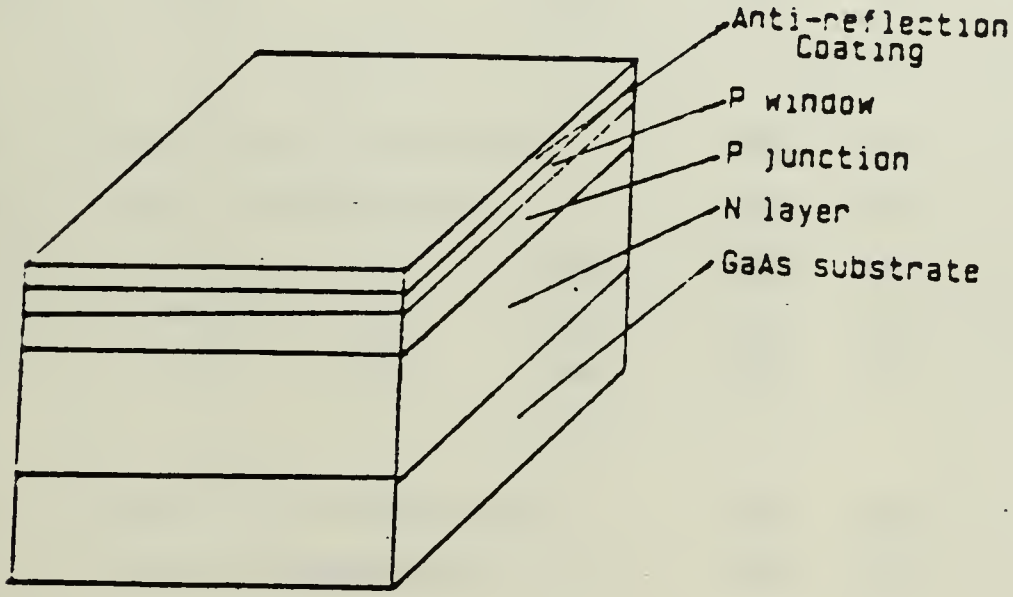

Figure 6.1 Cross-Section View of the ASEC AlGaAs-GaAs Solar Cell.

C. SILICON SOLAR CELL ANNEALING

The silicon solar cells annealed in this experiment were manufactured by the Applied Solar Energy Corporation (ASEC). These 10 Ω N/P junction solar cells are 2cm × 2cm and have characteristics similar to those of the gallium arsenide solar cells used in the previous experiment. All of the silicon solar cells were irradiated at the JPL

Linear accelerator by 1-Mev electrons. Solar cells Sil-86 through Sil-89 were irradiated to a fluence level of 1.8×10^{14} e/cm^2 while the remaining silicon cells were irradiated to a fluence of 3.7×10^{13} e/cm^2. Solar cells Sil-99 and Sil-100 were thermally annealed at 120°C and 140°C, respectively. Table 8 shows the results of this annealing. Solar cells Sil-86 through Sil-97 were Foward-bias Current Annealed at various current densities and temperatures. Experimental results are summarized in Table 9. Post-irradiation and final annealing current-voltage characteristics and curves are shown in Figures 6.22 through 6.45.

TABLE 5

EXPERIMENTAL RESULTS OF FOWARD-BIAS CURRENT ANNEALING ON GAAS SOLAR CELLS IRRADIATED BY 20-MEV ELECTRONS

Solar Cell	Anneal Temp (C)	Anneal Time (hrs)	Current Density (A/cm^2)	V_{oc} (mV)	I_{sc} (mA)	P_{max} (mW)	η (%)
ASEC-4	Prior to Irradiation			990	116	88	16.3
ASEC-4A	After Irradiation			783	75	44	8.2
ASEC-4B	90	16	0.125	783	75	44	8.2
ASEC-4C	90	2	0.250	809	82	50	9.2
ASEC-4D	90	1	0.375	806	77	46	8.5
ASEC-4E	90	1	0.625	808	80	48	8.9
ASEC-5	Prior to Irradiation			963	120	90	16.6
ASEC-5A	After Irradiation			897	108	75	13.8
ASEC-5B	90	2	0.500	905	109	76	14.2
ASEC-5C	90	1	0.625	904	106	74	13.8
ASEC-5D	90	17	1.000	754	104	49	9.0
ASEC-7	Prior to Irradiation			982	118	89	16.5
ASEC-7A	After Irradiation			903	110	75	14.0
ASEC-7B	130	2	0.750	902	109	75	13.8
ASEC-7C	130	2	1.000	850	111	63	11.7
ASEC-7D	130	17	1.000	177	107	4	0.9

TABLE 5

EXPERIMENTAL RESULTS OF FOWARD-BIAS CURRENT ANNEALING ON GAAS SOLAR CELLS IRRADIATED BY 20-MEV ELECTRONS (CONT'D.)

Solar Cell	Anneal Temp (C)	Anneal Time (hrs)	Current Density (A/cm^2)	V_{oc} (mV)	I_{sc} (mA)	P_{max} (mW)	η (%)
ASEC-8	Prior to Irradiation			975	116	89	16.5
ASEC-8A	After Irradiation			949	115	84	15.6
ASEC-8B	115	2	0.750	953	114	85	15.7
ASEC-8C	115	2	1.000	784	115	44	8.2
ASEC-9	Prior to Irradiation			948	119	89	16.4
ASEC-9A	After Irradiation			928	116	86	15.9
ASEC-9B	115	16	1.250	250	103	7	1.4
ASEC-10	Prior to Irradiation			957	116	89	16.5
ASEC-10A	After Irradiation			937	116	86	16.0
ASEC-10B	100	1	0.750	941	114	86	16.0
ASEC-10C	100	2	0.750	941	116	87	16.1
ASEC-10D	100	3	0.750	940	116	88	16.3

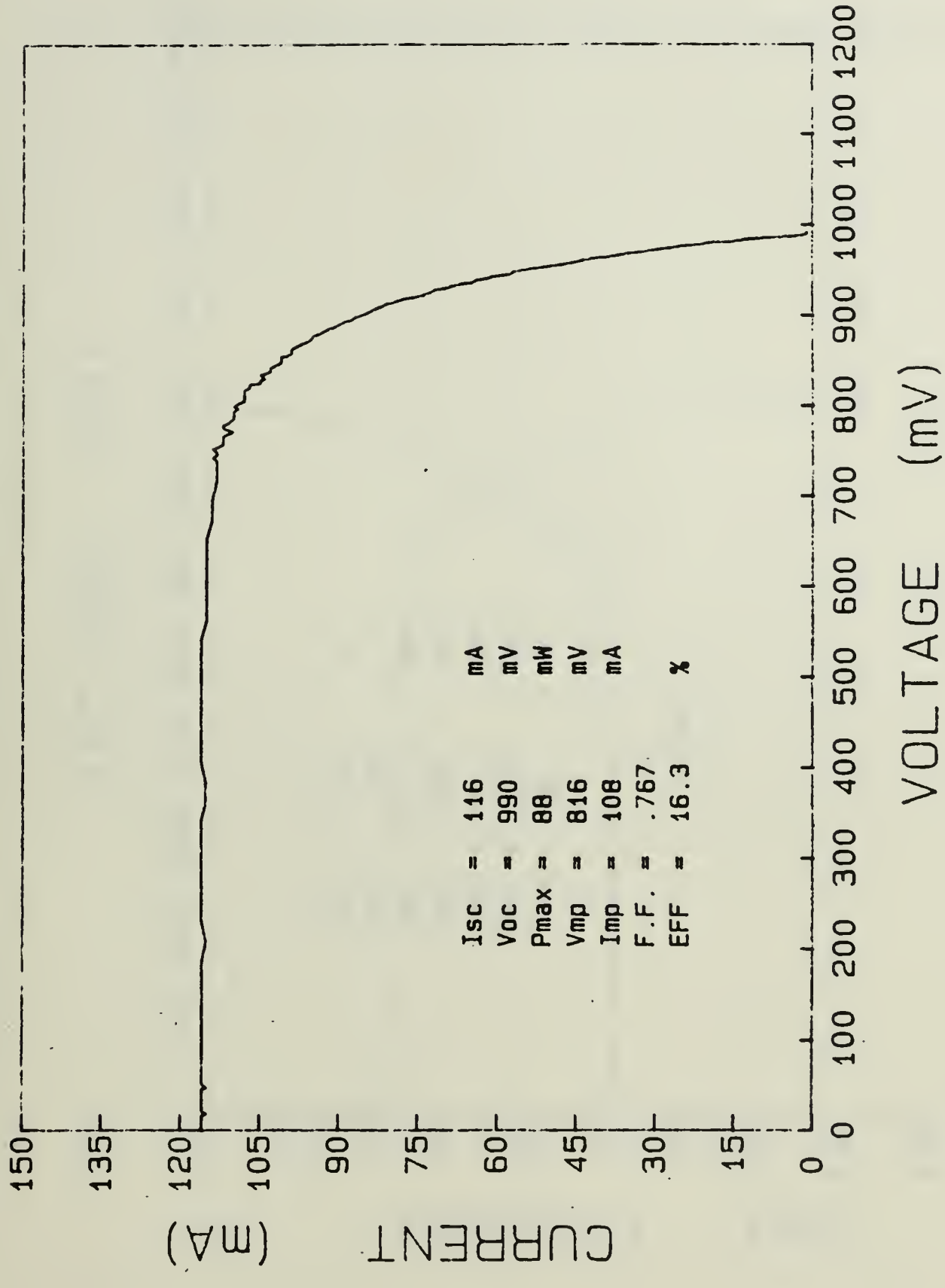

Figure 6.2 I-V Curve for GaAs Solar Cell ASEC-4 [ref. 15 p. 97].

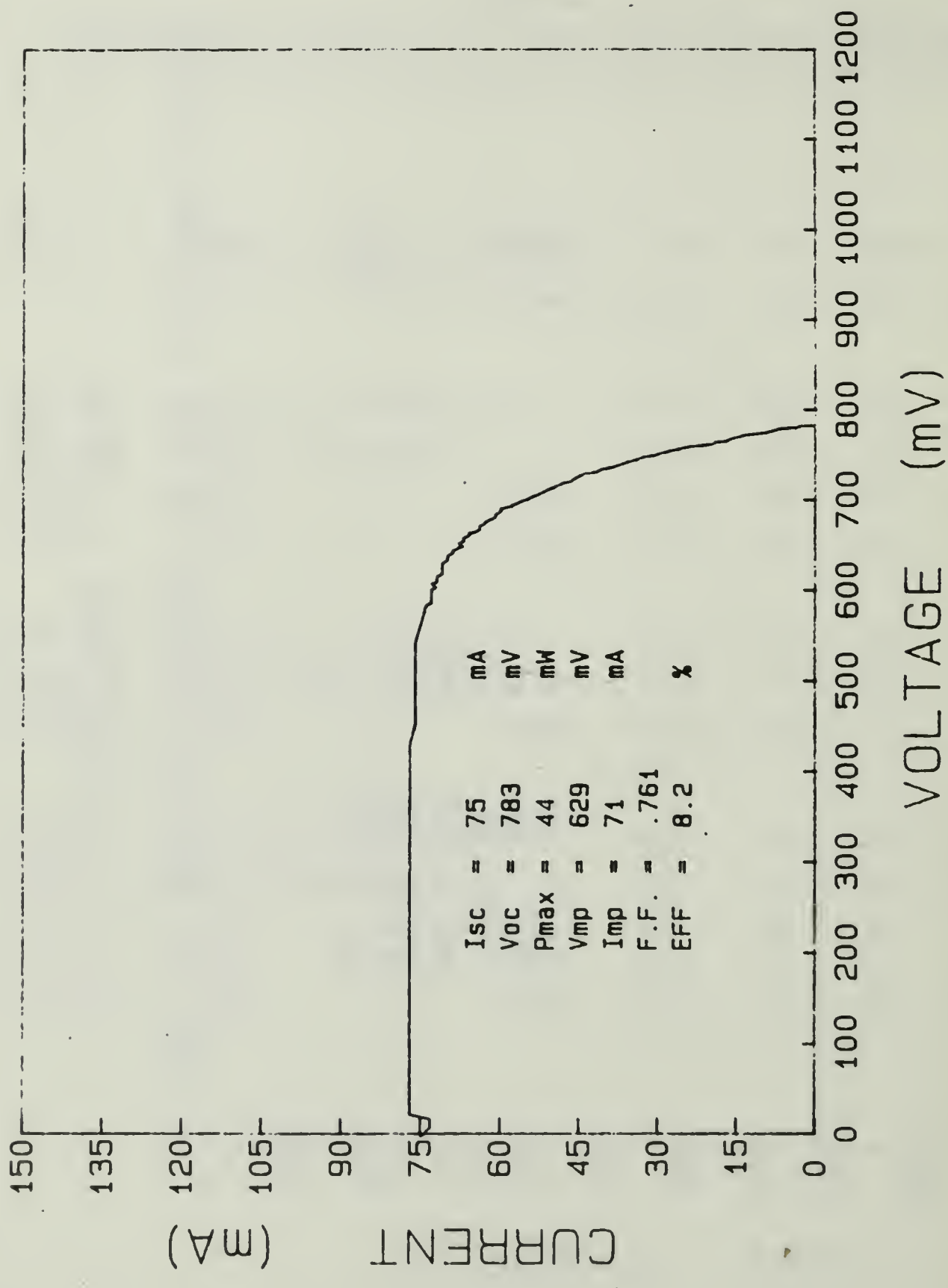

Figure 6.3 I-V Curve for GaAs Solar Cell ASEC-4A, Irradiated to a Fluence of 10^{15} e/cm^2 by 20-Mev Electrons.

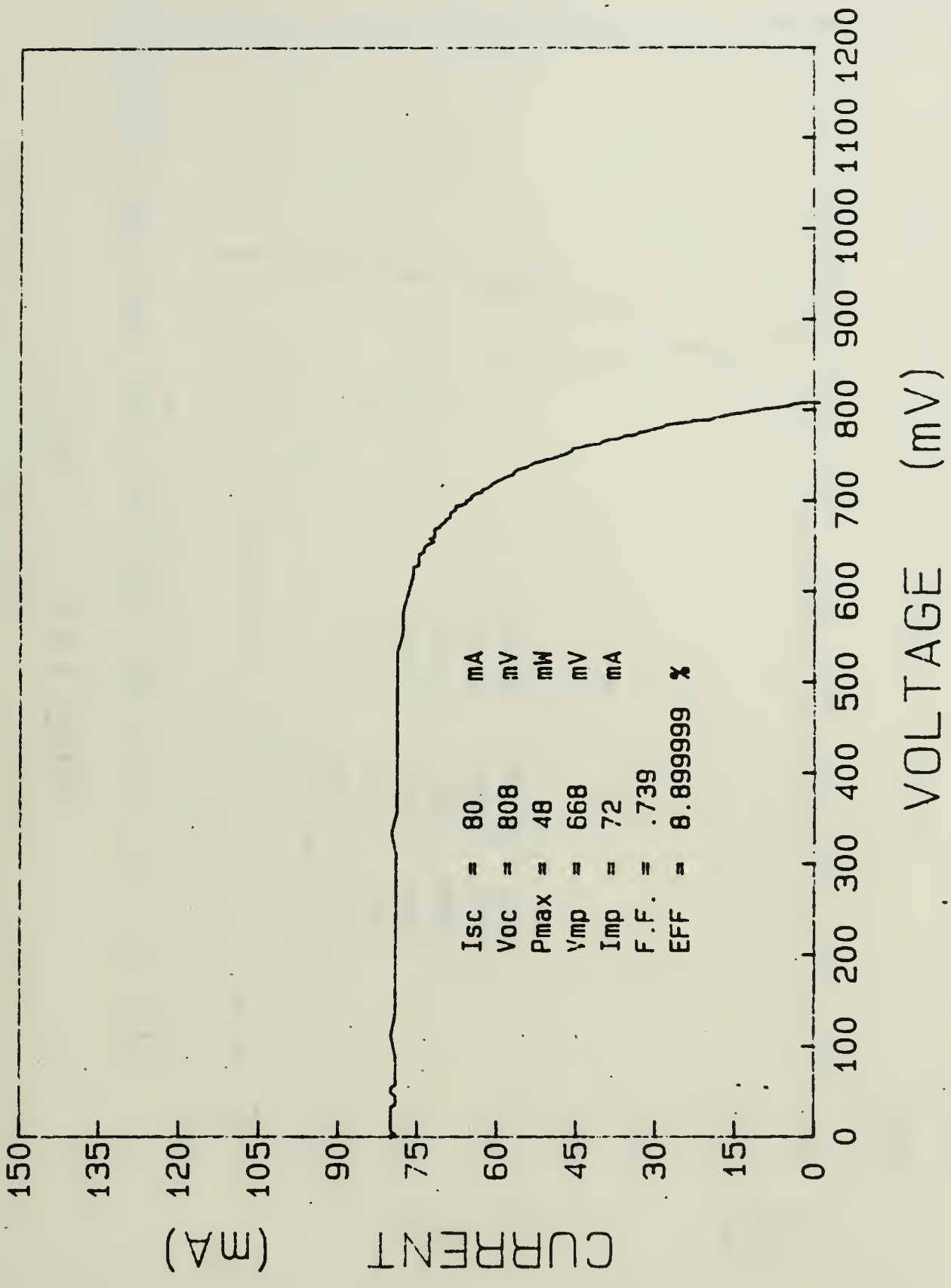

Figure 6.4 I-V Curve for GaAs Solar Cell ASEC-4E, Annealed at 90°C Under Various Foward-bias Current Densities.

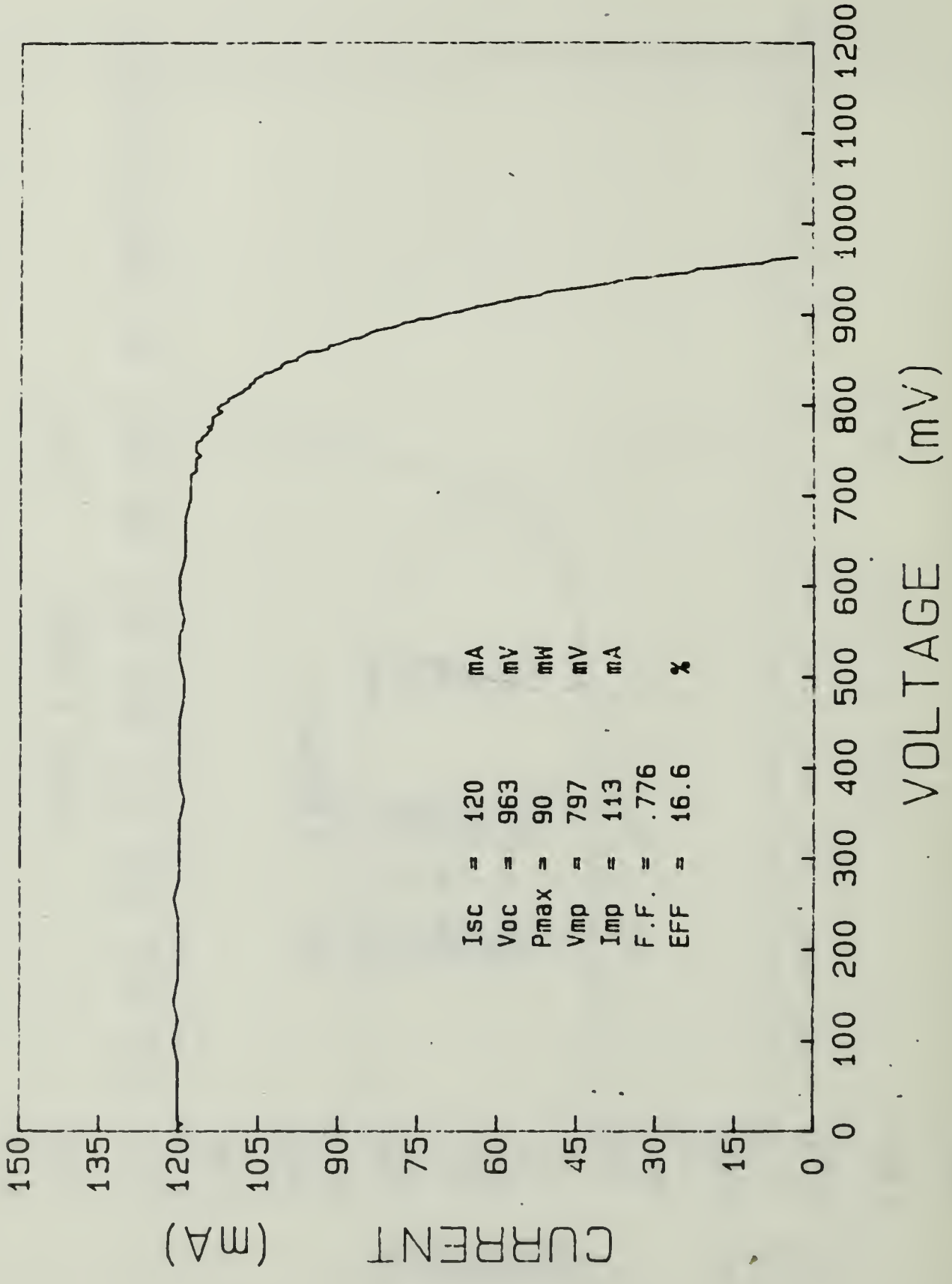

Figure 6.5 I-V Curve for GaAs Solar Cell ASEC-5 [ref. 15 p. 98].

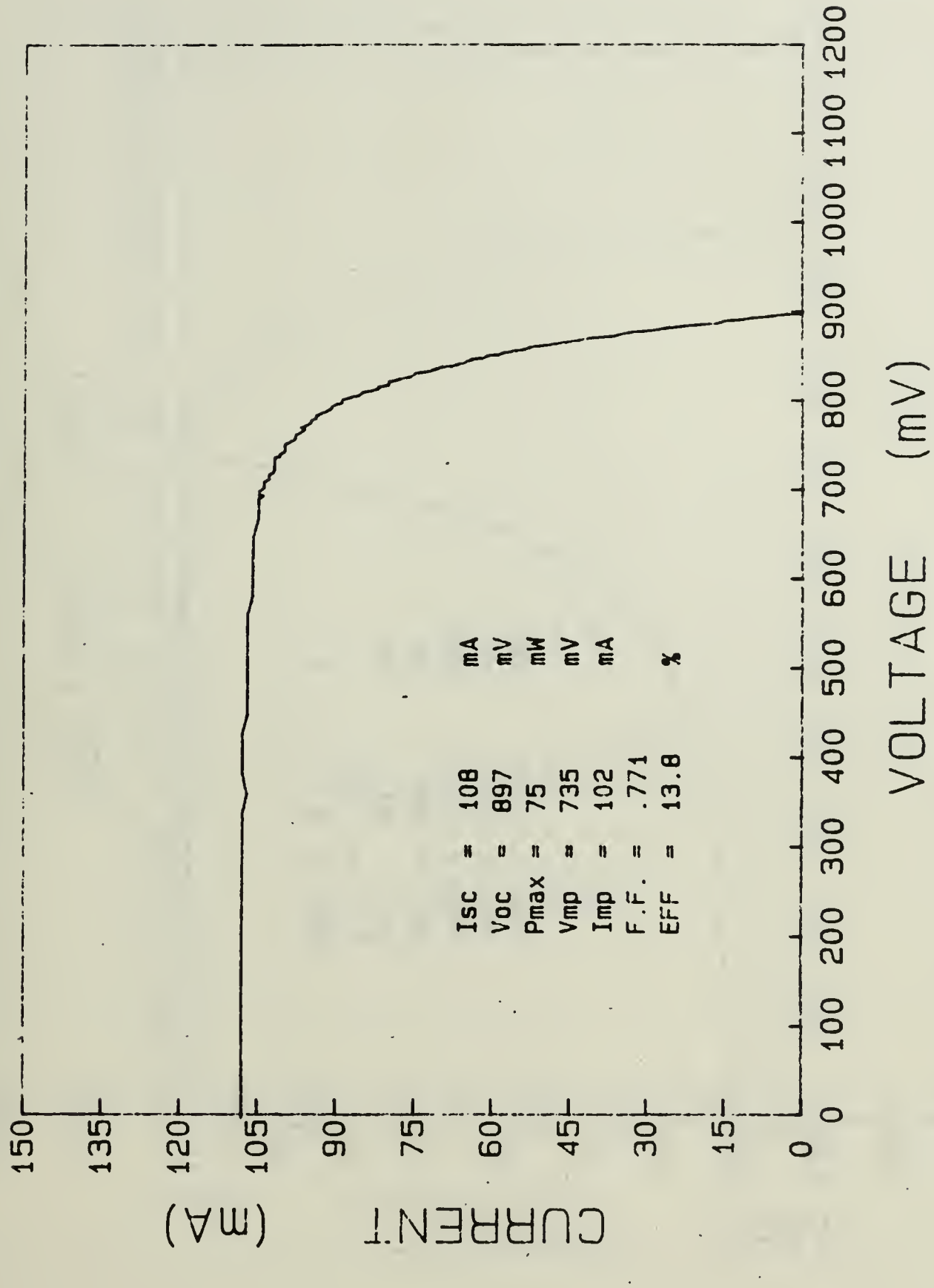

Figure 6.6 I-V Curve for GaAs Solar Cell ASEC-5A, Irradiated to a Fluence of 10^{14} e/cm^2 by 20-Mev Electrons.

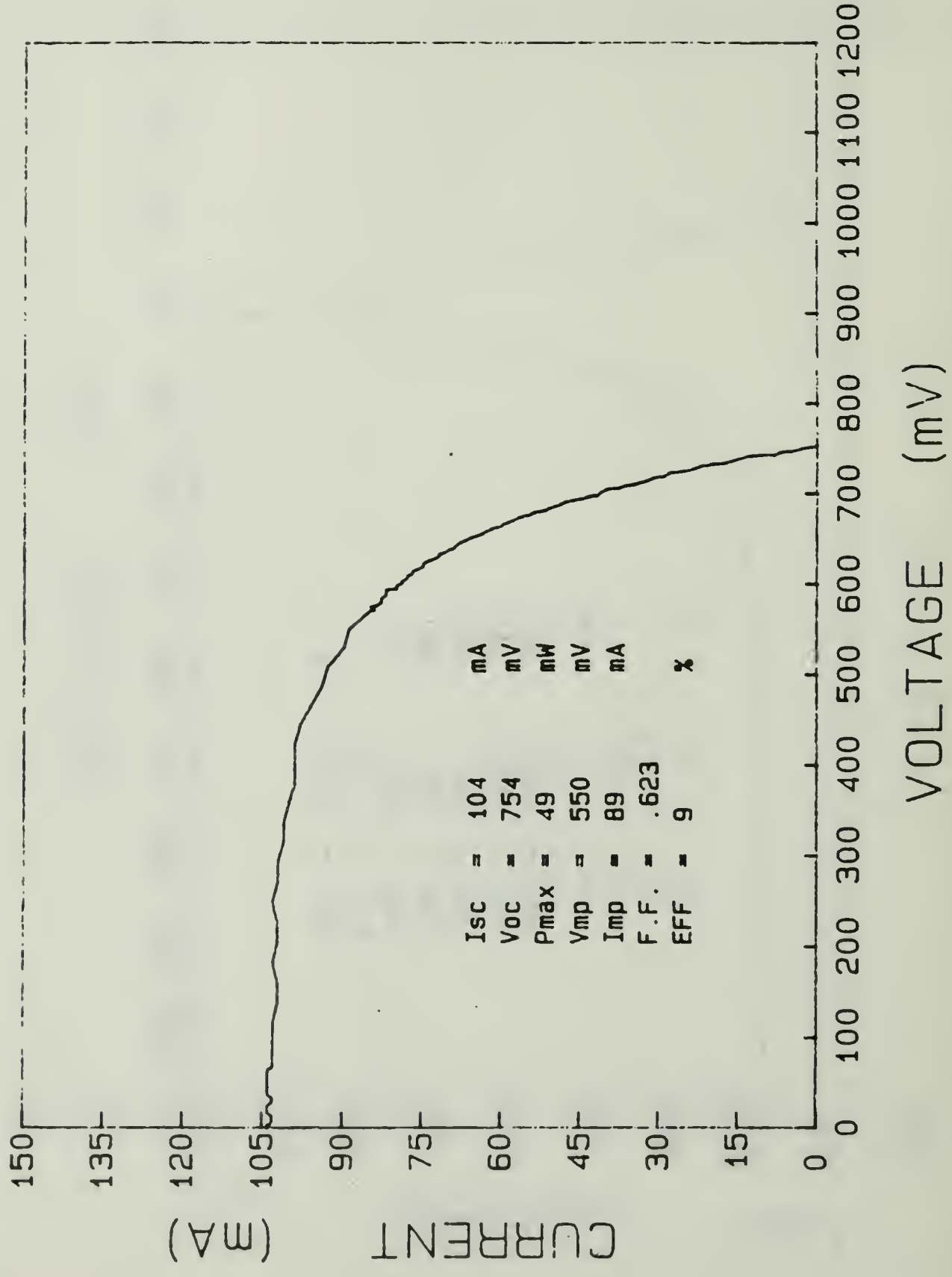

Figure 6.7 I-V Curve for GaAs Solar Cell ASEC-5D, Annealed at 90°C Under Various Foward-bias Current Densities.

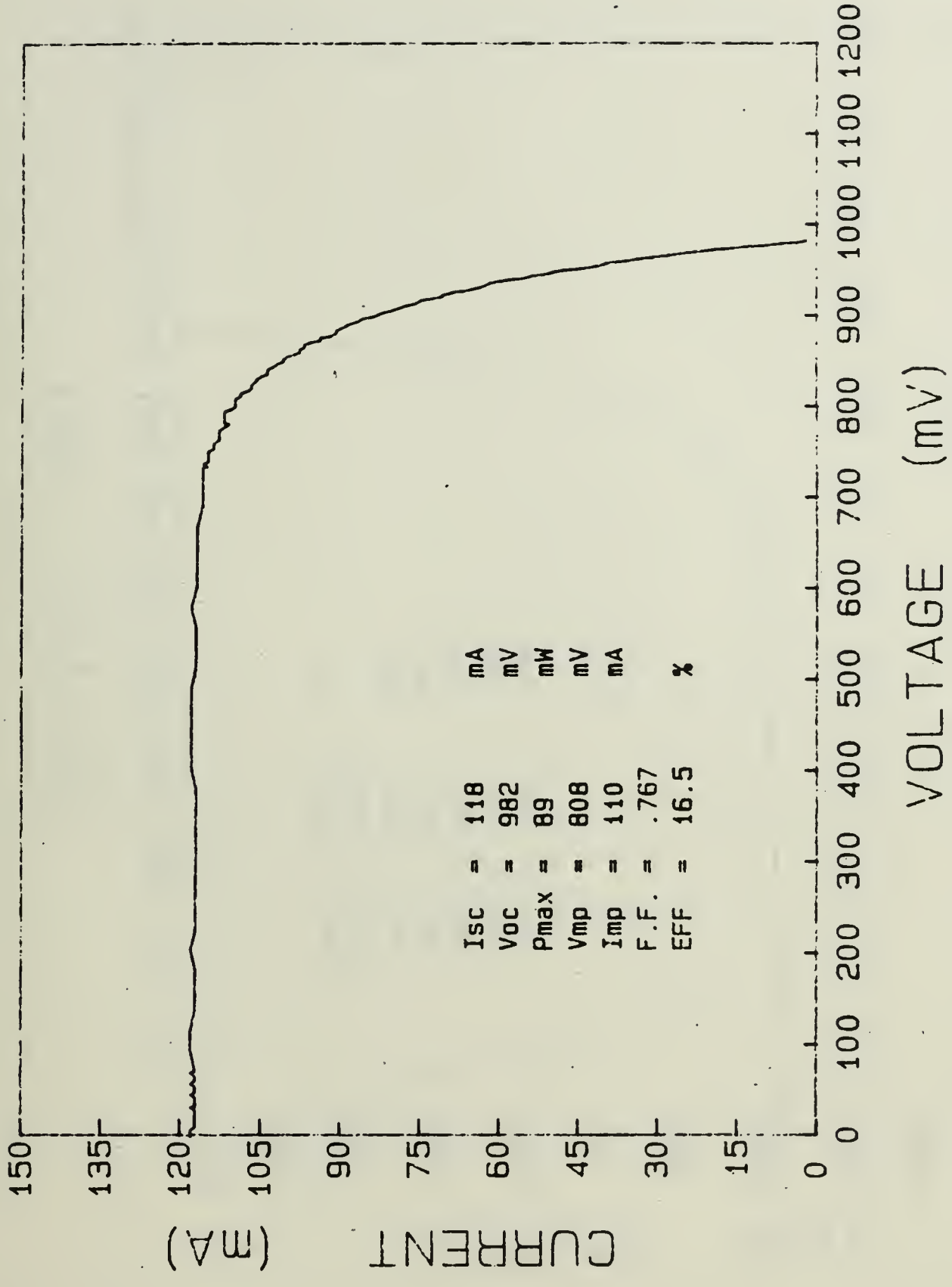

Figure 6.8 I-V Curve for GaAs Solar Cell ASEC-7 [ref. 15 p. 100].

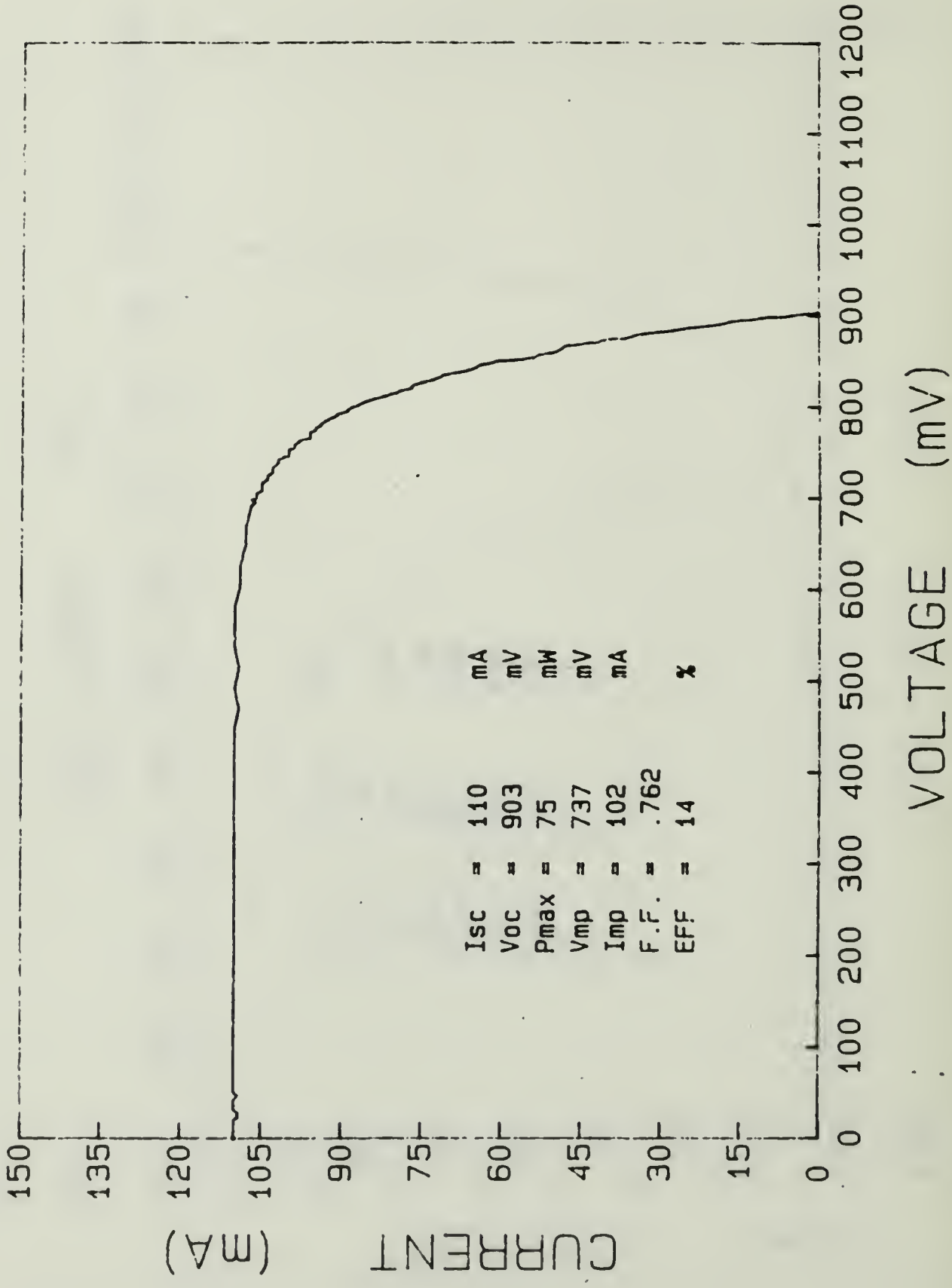

Figure 6.9 I-V Curve for GaAs Solar Cell ASEC-7A, Irradiated to a Fluence of 10^{14} e cm^{-2} by 20-Mev Electrons.

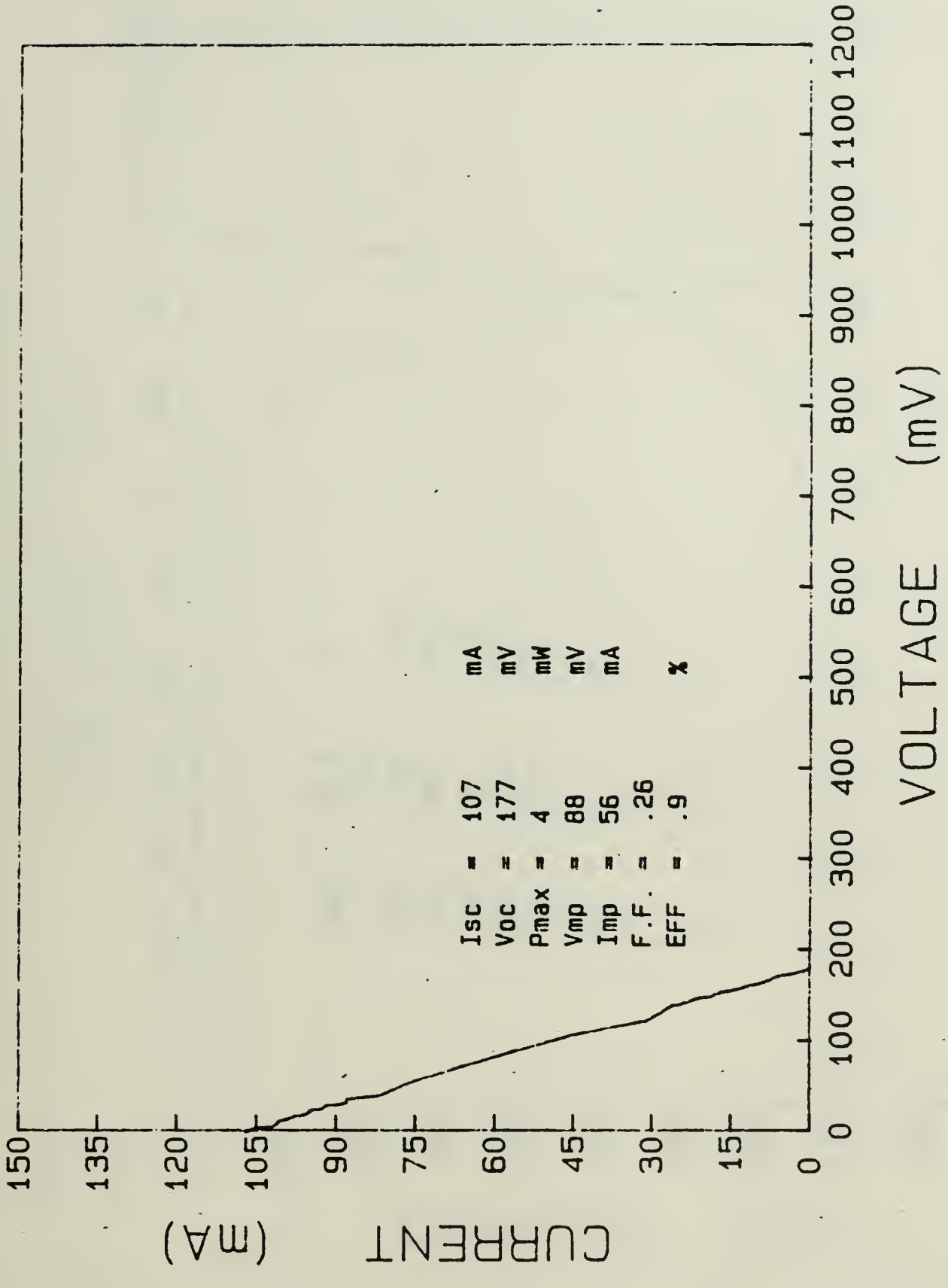

Figure 6.10 I-V Curve for GaAs Solar Cell ASEC-7D, Annealed at 130°C, Under Various Foward-bias Current Densities.

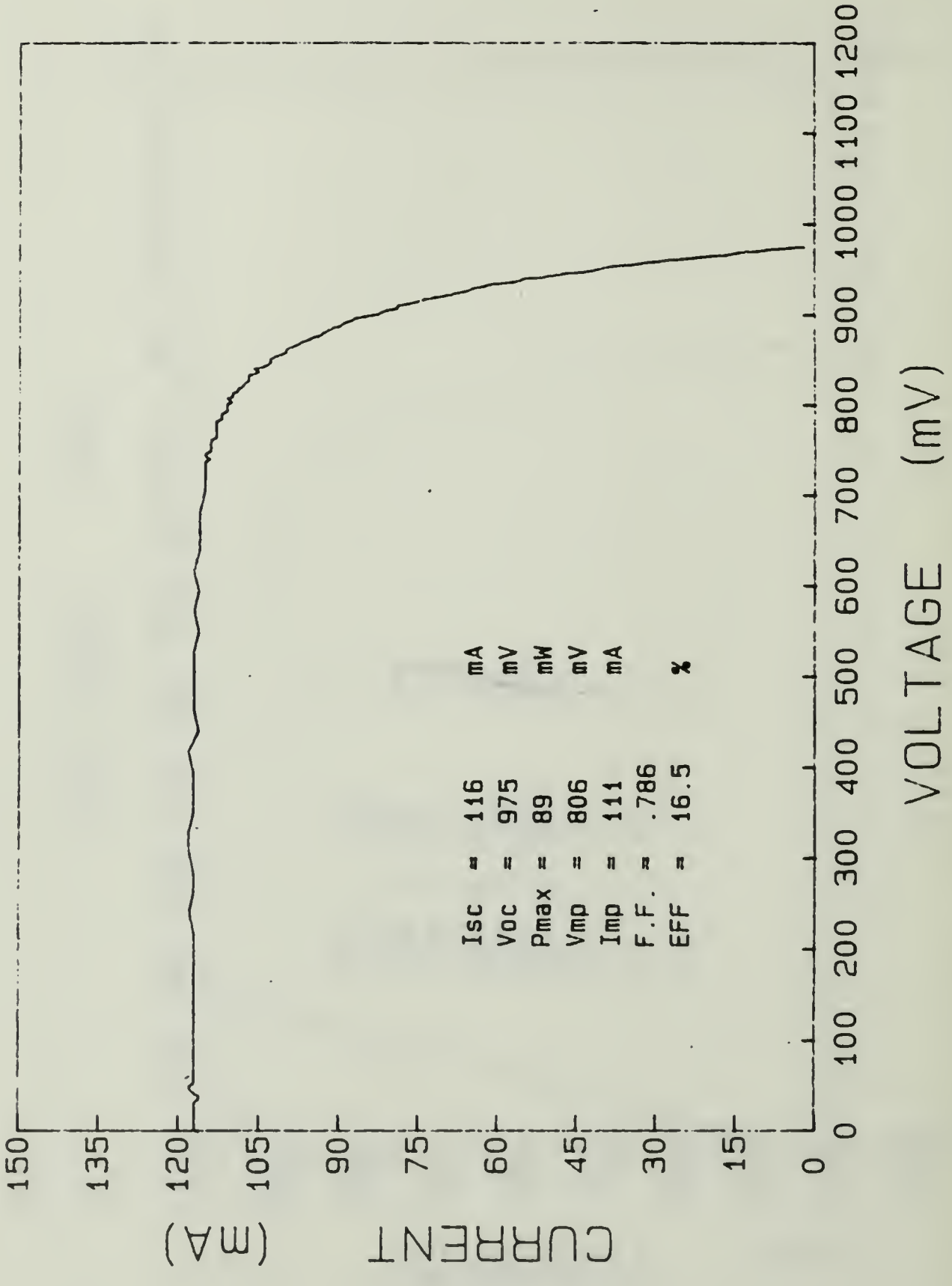

Figure 6.11 I-V Curve for GaAs Solar Cell ASEC-8 [ref. 15 p. 101].

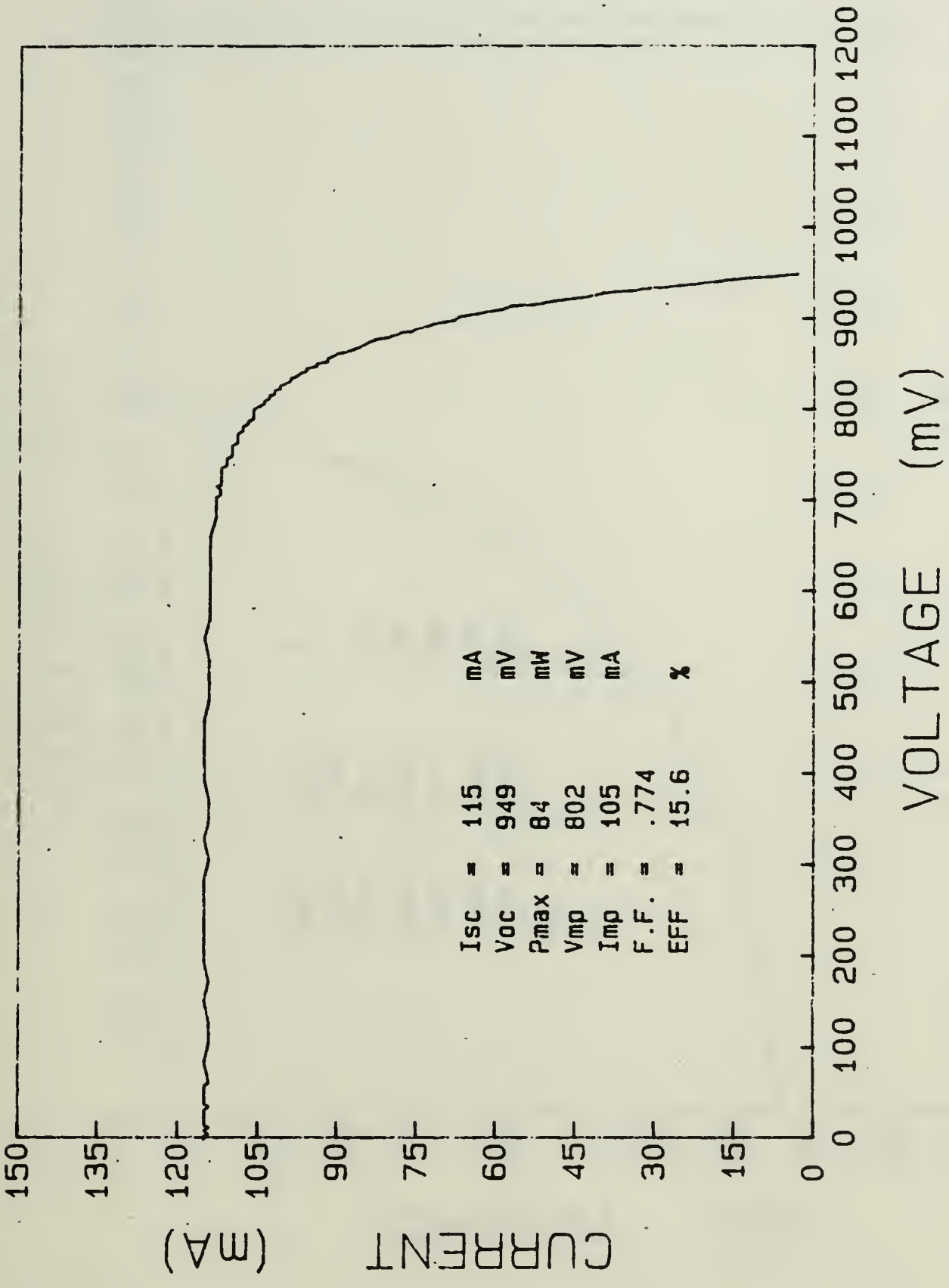

Figure 6.12 I-V Curve for GaAs Solar Cell ASEC-8A, Irradiated to a Fluence of 10^{13} e/cm^2 by 20-Mev Electrons.

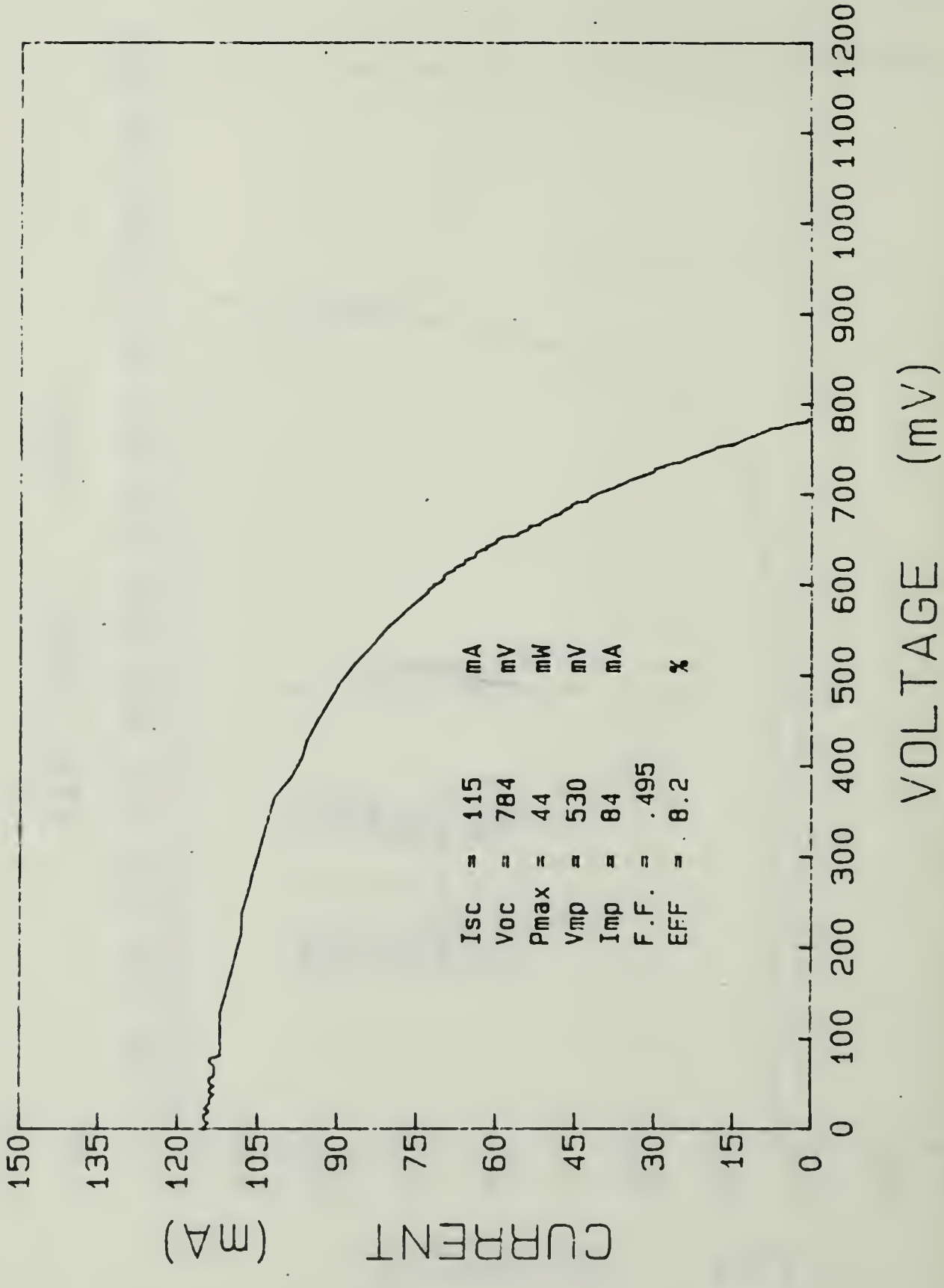

Figure 6.13 I-V Curve for GaAs Solar Cell ASEC-8C, Annealed at 115°C, Under Various Foward-bias Current Densities.

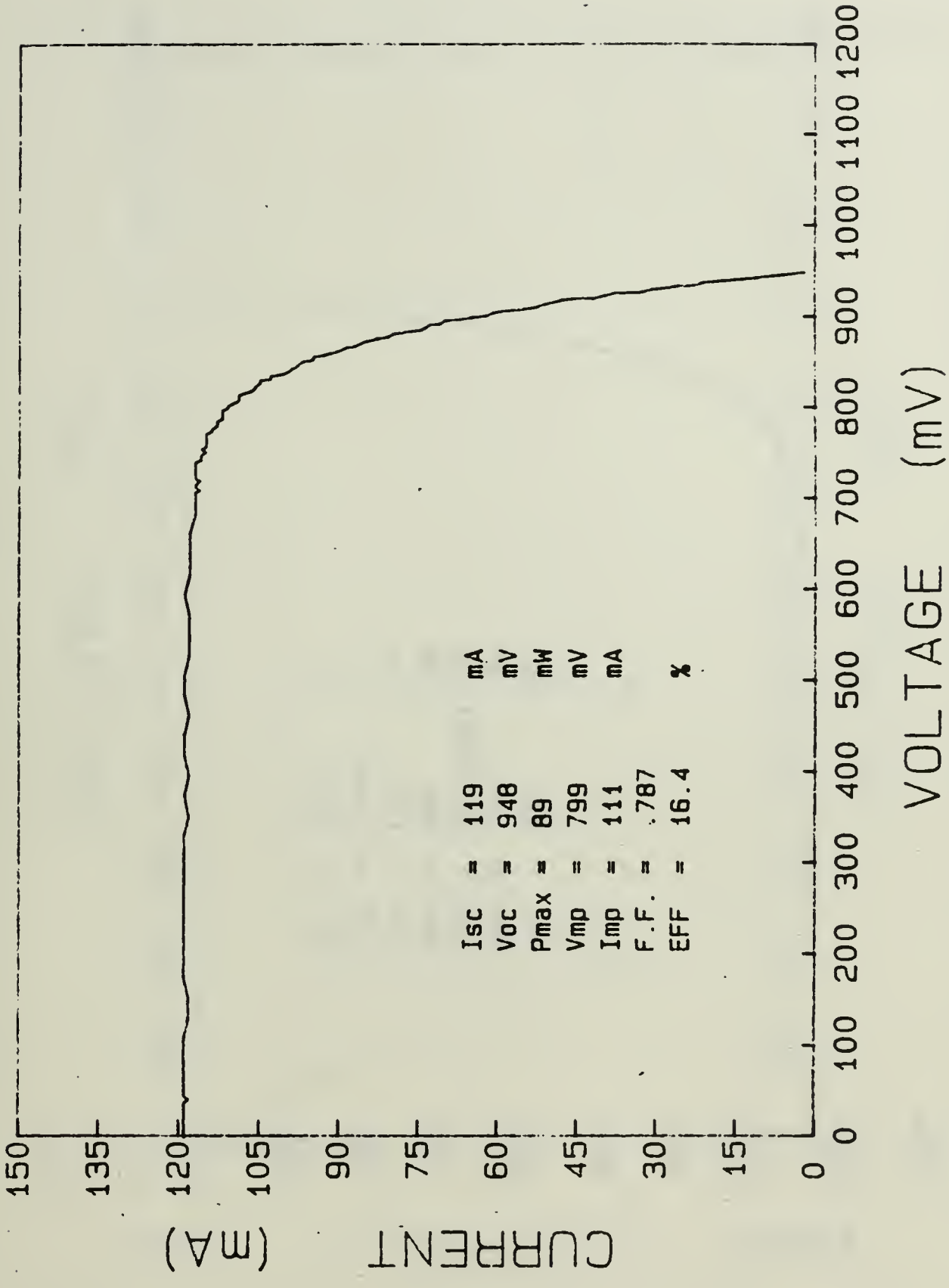

Figure 6.14 I-V Curve for GaAs Solar Cell ASEC-9 [ref. 15 p. 102].

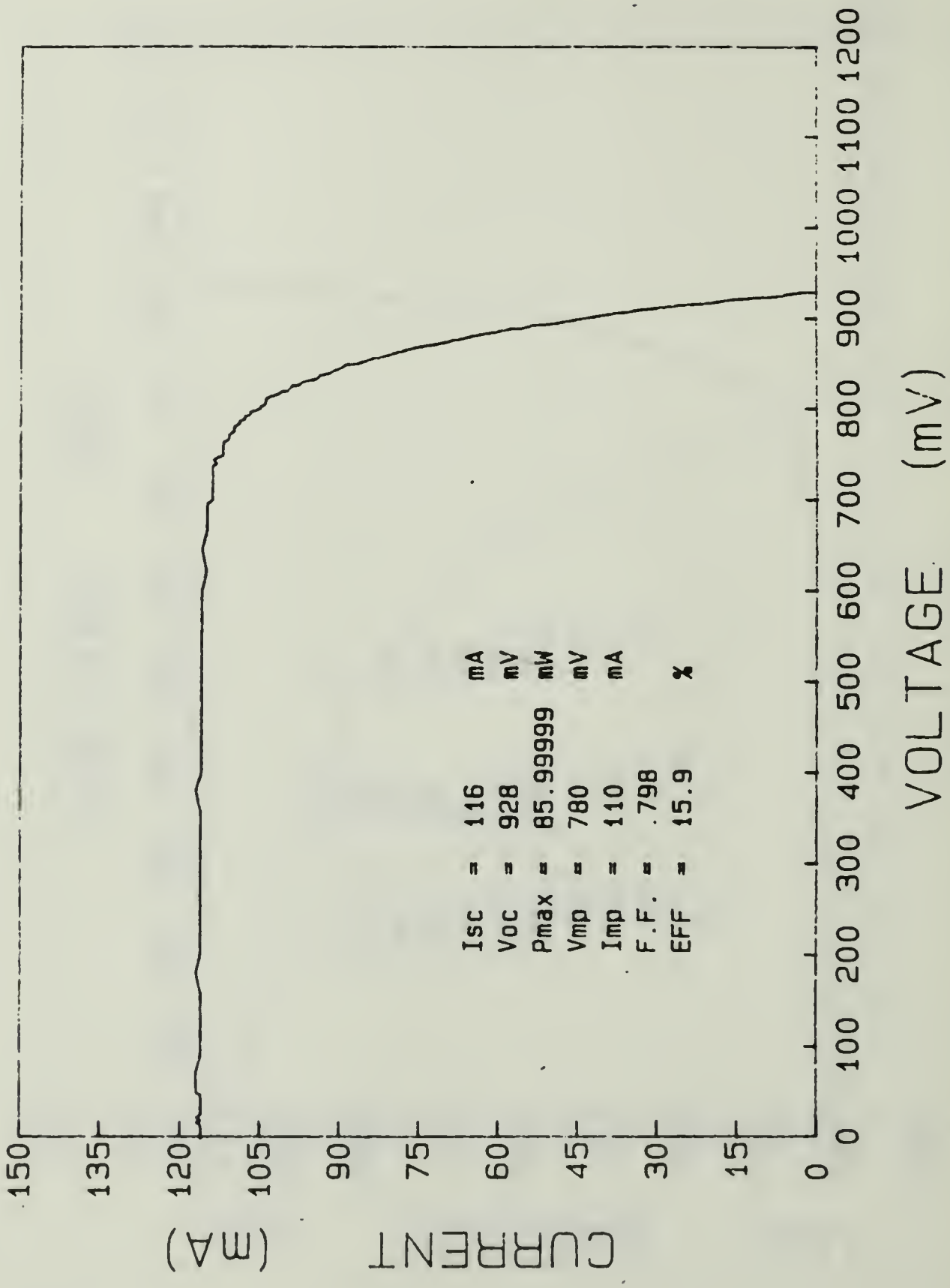

Figure 6.15 I-V Curve for GaAs Solar Cell ASEC-9A, Irradiated to a Fluence of 10^{13} e.cm^{-2} by 20-Mev Electrons.

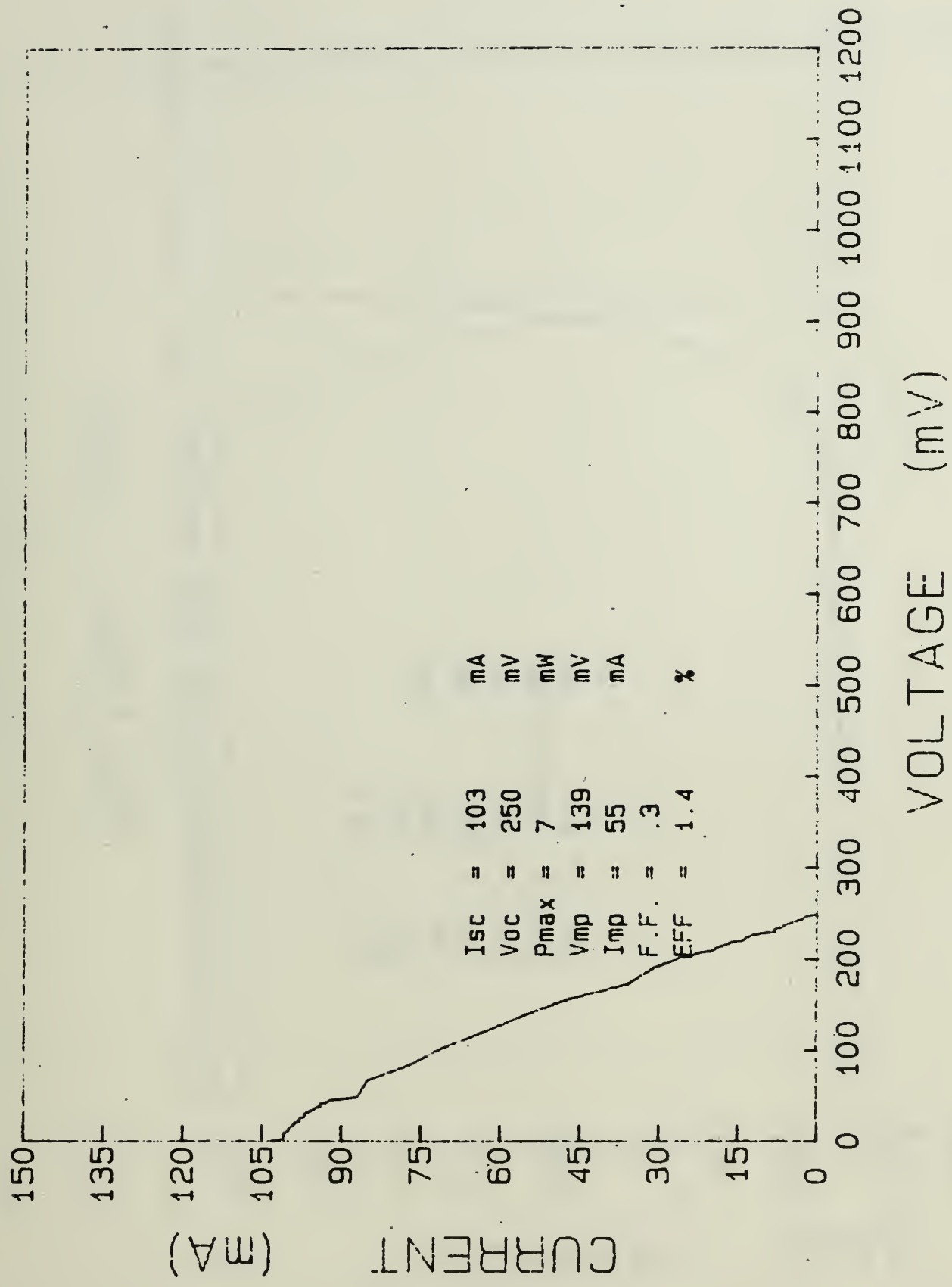

Figure 6.16 I-V Curve for GaAs Solar Cell ASEC-9B, Annealed at 115°C, Under a 1.125 A/cm^2 Foward-bias Current.

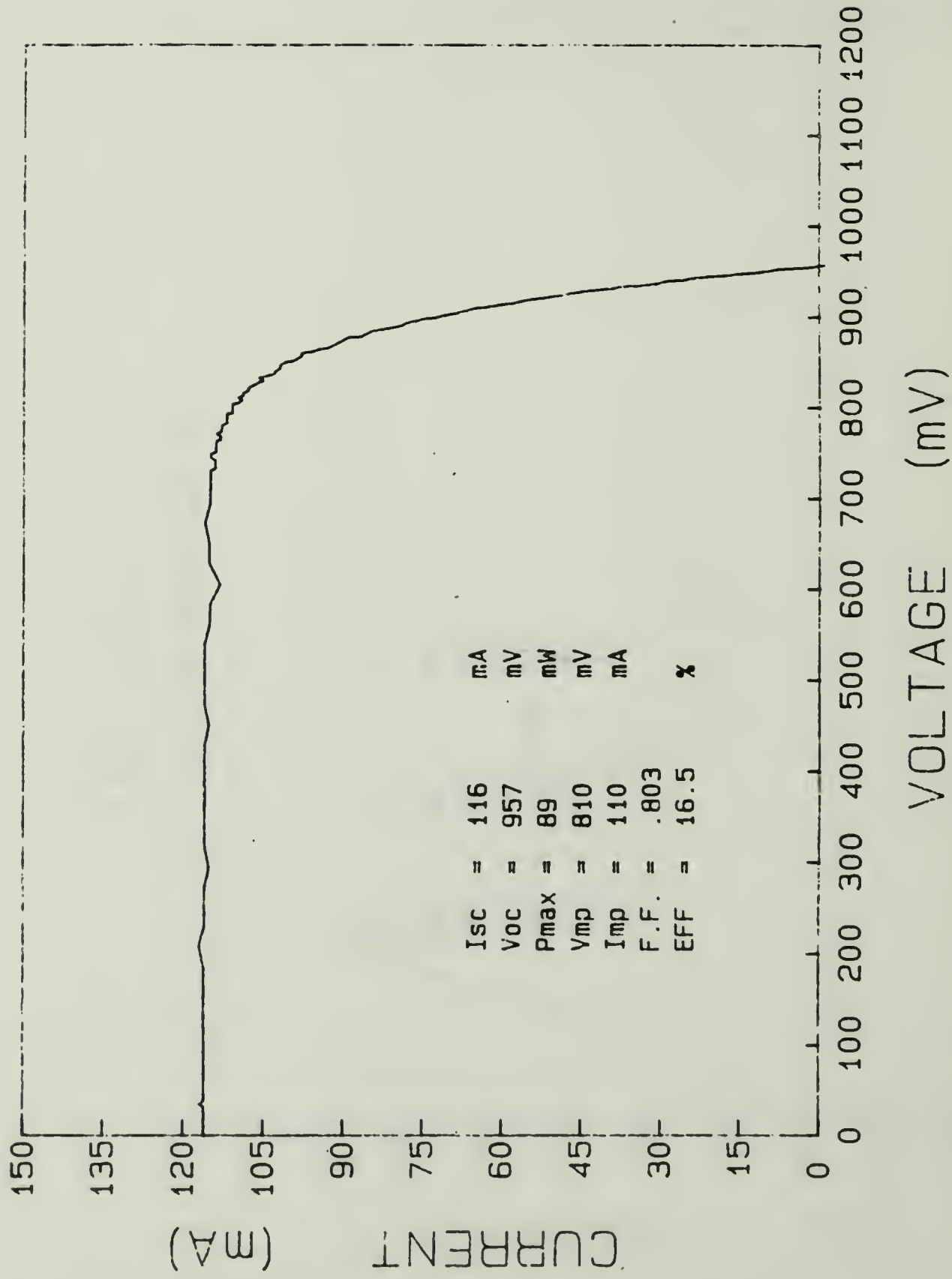

Figure 6.17 I-V Curve for GaAS Solar Cell ASEC-10 [ref. 15 p. 103].

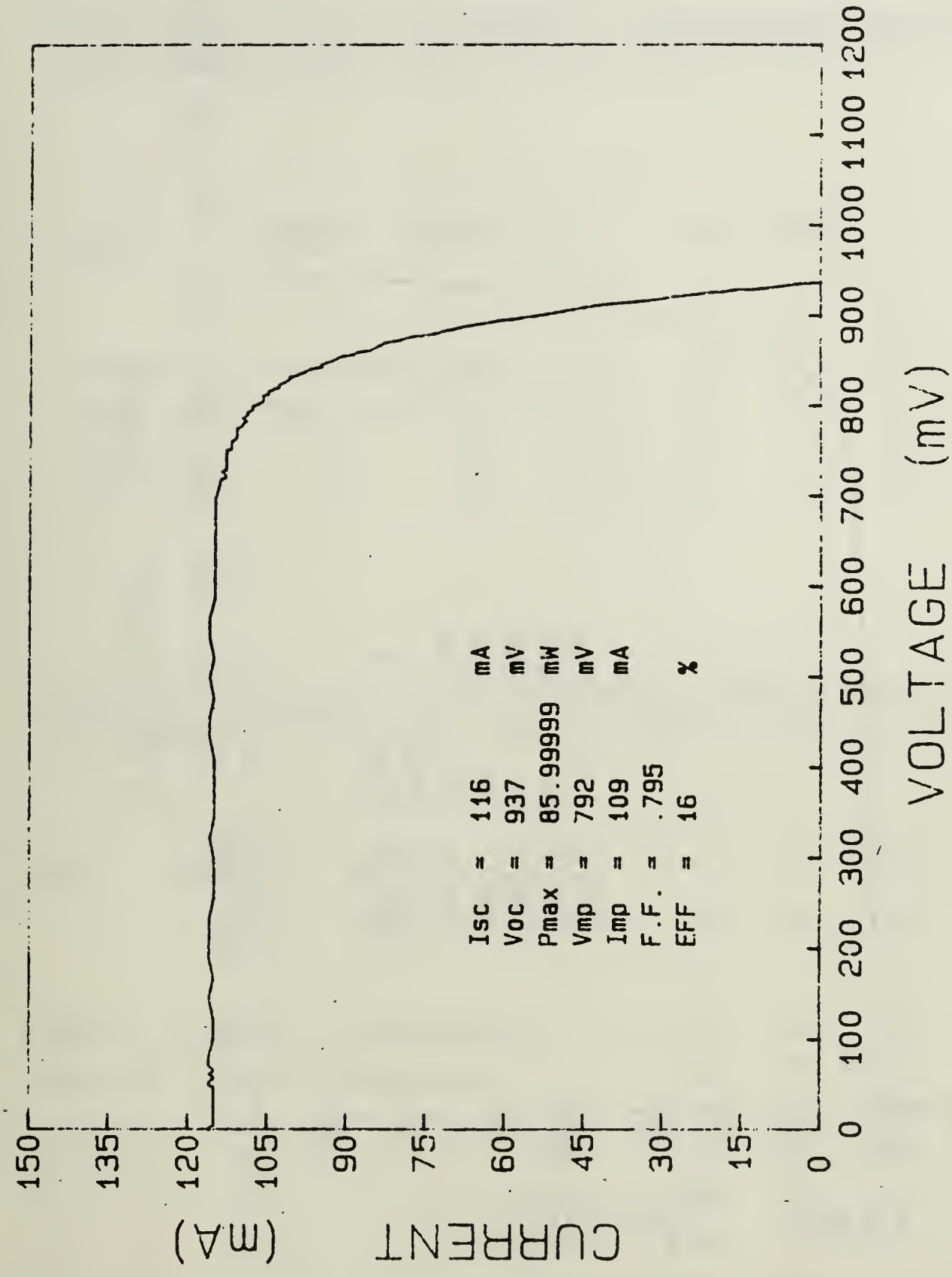

Figure 6.18 I-V Curve for GaAs Solar Cell ASEC-10A, Irradiated to a Fluence of 10^{13} e/cm^2 by 20-Mev Electrons.

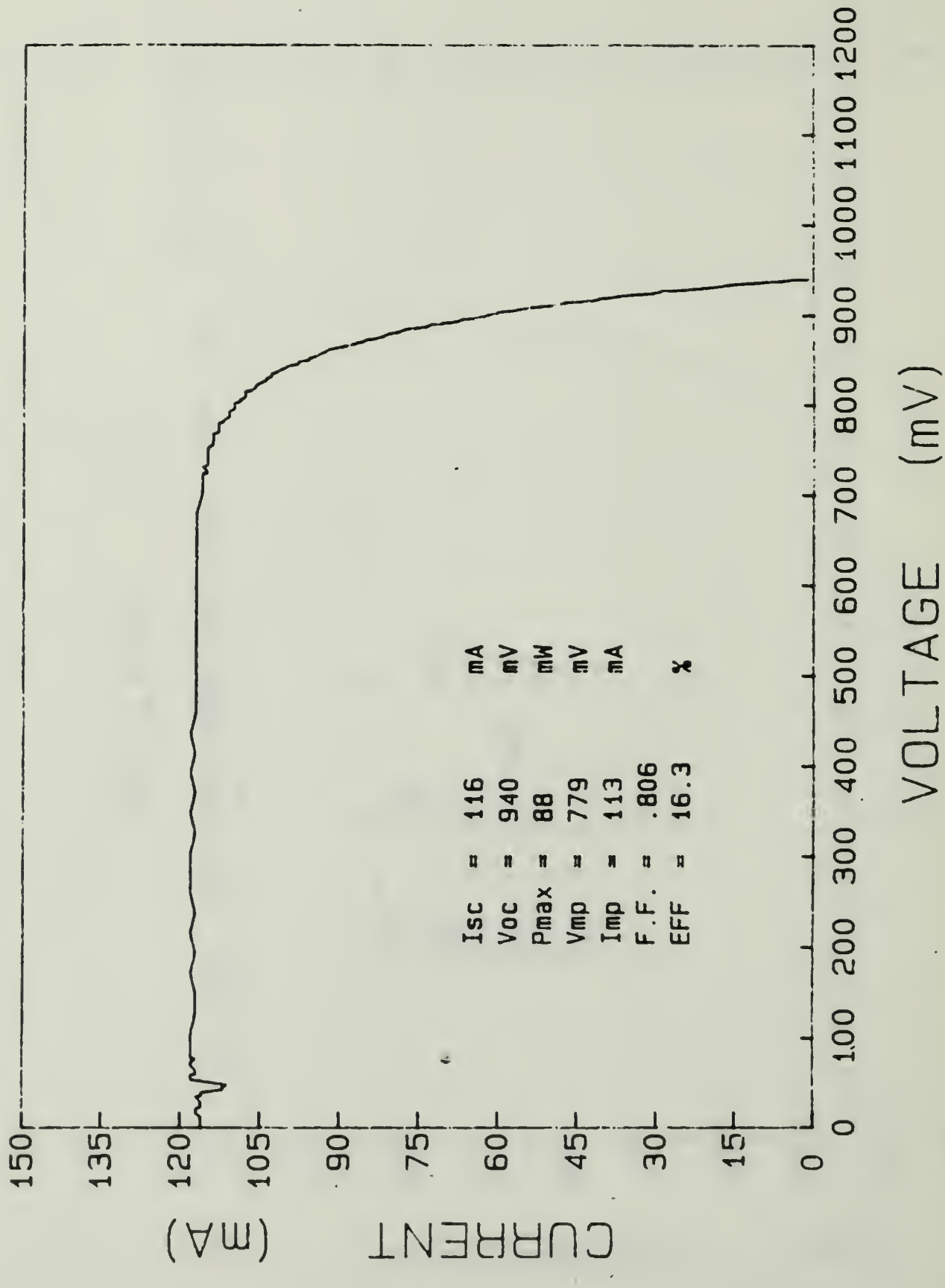

Figure 6.19 I-V Curve for GaAS Solar Cell ASEC-10D, Annealed at 100°C, Under a 0.750 A/cm^2 Foward-bias Current for 6 Hours.

TABLE 6

EXPERIMENTAL RESULTS OF THERMAL ANNEALING ON GALLIUM ARSENIDE SOLAR CELL ASEC-23 IRRADIATED BY 1-MEV ELECTRONS

Solar Cell	Anneal Temp (C)	Anneal Time (hrs)	V_{oc} (mV)	I_{sc} (mA)	P_{max} (mW)	η (%)
ASEC-23	Pre-irradiation		916	116	86	15.8
ASEC-23A	Post-irradiation		885	112	79	14.6
ASEC-23B	100	5	884	112	79	14.7
ASEC-23C	100	18	884	112	79	14.7

TABLE 7

EXPERIMENTAL RESULTS OF FOWARD-BIAS CURRENT ANNEALING ON GAAS SOLAR CELL ASEC-16 IRRADIATED BY 1-MEV ELECTRONS

Solar Cell	Anneal Temp (C)	Anneal Time (hrs)	Current Density (A/cm^2)	V_{oc} (mV)	I_{sc} (mA)	P_{max} (mW)	η (%)
ASEC-16	Prior to Irradiation			972	116	89	16.4
ASEC-16A	After Irradiation			883	73	53	9.8
ASEC-16B	100	2	0.750	889	76	54	10.0
ASEC-16C	100	2	0.750	892	78	55	10.2
ASEC-16D	100	2	0.750	894	81	57	10.6
ASEC-16E	100	17	0.750	899	83	58	10.8
ASEC-16F	100	27	0.750	899	91	62	11.6
ASEC-16G	100	18	0.750	893	93	60	11.2
ASEC-16H	100	72	0.750	848	84	48	8.8

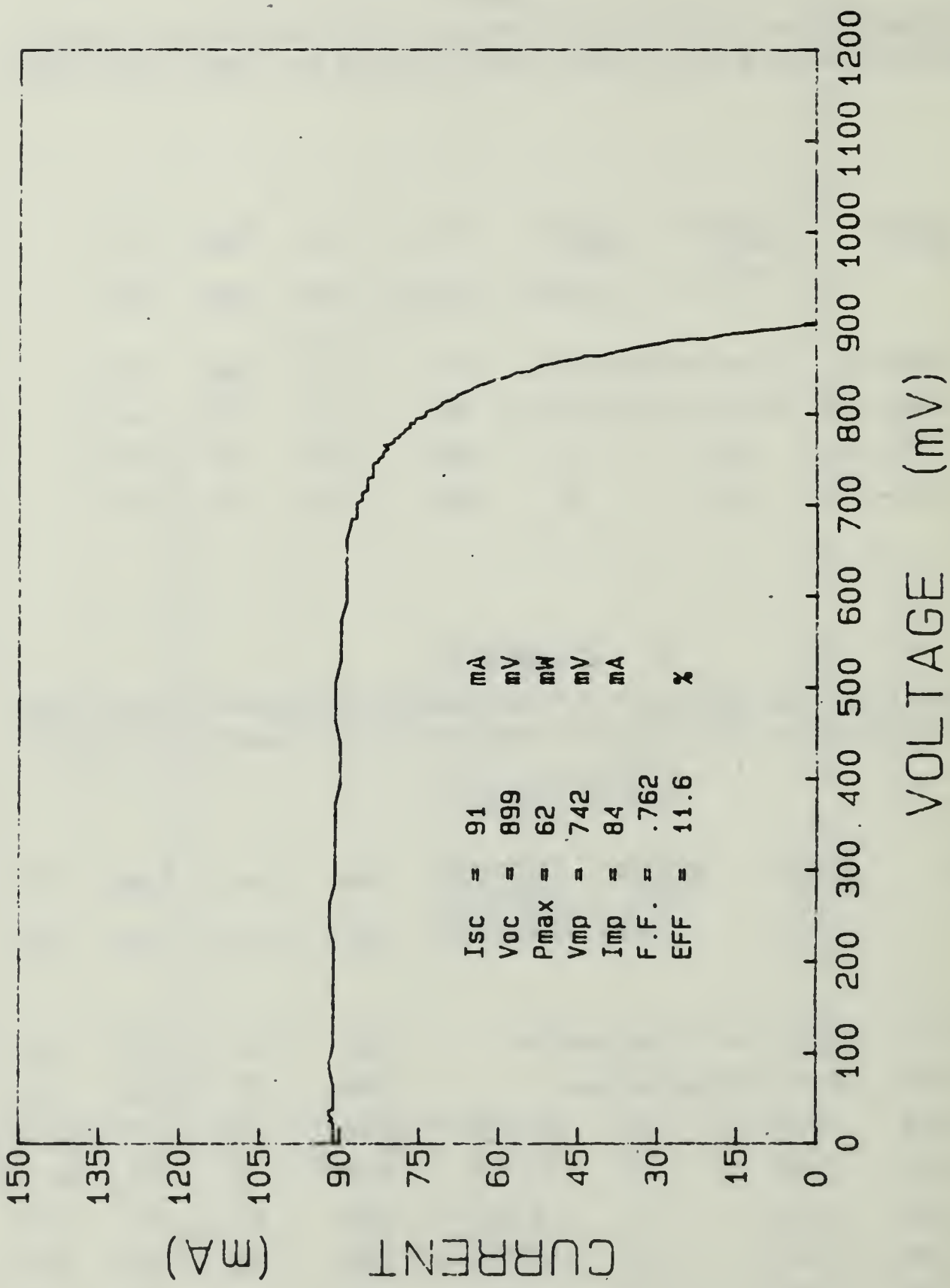

Figure 6.20 I-V Curve for GaAs Solar Cell ASEC-16F, Annealed at 100°C, Under a 0.750 A/cm^2 Foward-bias Current for 50 Hours.

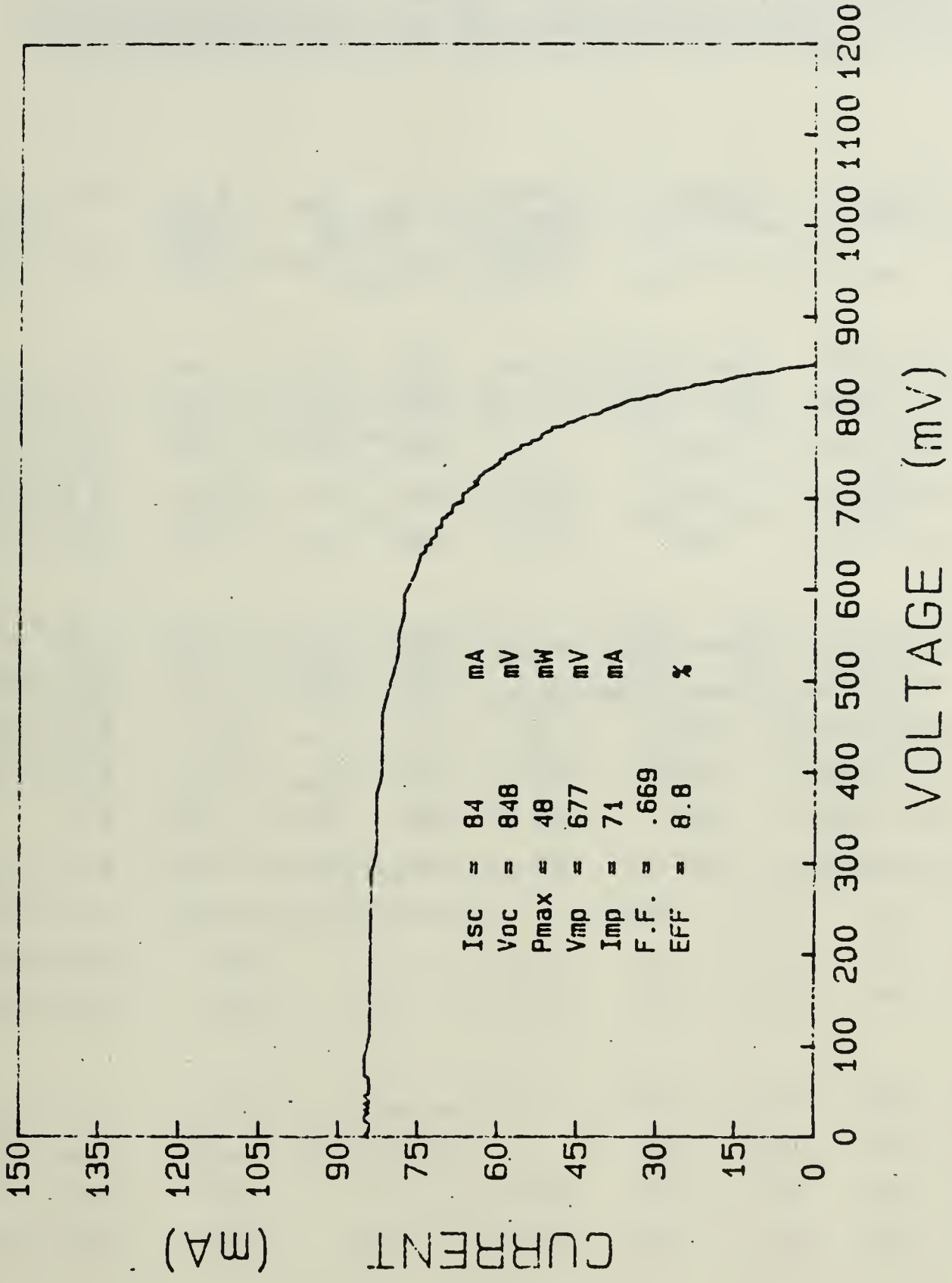

Figure 6.21 I-V Curve for GaAs Solar Cell ASEC-16H, Annealed at 100°C, Under a 0.750 A/cm^2 Foward-bias Current for 140 Hours.

TABLE 8

EXPERIMENTAL RESULTS OF THERMAL ANNEALING ON SILICON SOLAR CELLS IRRADIATED BY 1-MEV ELECTRONS

Solar Cell	Anneal Temp (C)	Anneal Time (hrs)	V_{oc} (mV)	I_{sc} (mA)	P_{max} (mW)	η (%)
Sil-99	Pre-irradiation		550	147	64	11.8
Sil-99A	Post-irradiation		505	132	51	9.4
Sil-99B	120	4	504	132	51	9.4
Sil-99C	120	18	501	134	50	9.4
Sil-99D	120	24	499	136	50	9.2
Sil-100	Pre-irradiation		551	149	65	12.0
Sil-100A	Post-irradiation		506	136	50	9.2
Sil-100B	140	5	503	136	50	9.3
Sil-100C	140	66	497	136	51	9.4
Sil-100D	140	24	495	135	50	9.3
Sil-100E	140	24	495	135	50	9.3

TABLE 9

EXPERIMENTAL RESULTS OF FOWARD-BIAS CURRENT ANNEALING ON SILICON SOLAR CELLS IRRADIATED BY 1-MEV ELECTRONS

Solar Cell	Anneal Temp (C)	Anneal Time (hrs)	Current Density (A/cm^2)	V_{oc} (mV)	I_{sc} (mA)	P_{max} (mW)	η (%)
Sil-86	Prior to Irradiation			554	151	66	12.1
Sil-86A	After Irradiation			480	130	46	8.5
Sil-86B	100	4	0.500	471	130	45	8.4
Sil-86C	100	18	0.500	464	122	42	7.8
Sil-87	Prior to Irradiation			553	150	65	12.1
Sil-87A	After Irradiation			479	126	45	8.3
Sil-87B	100	4	0.750	466	125	43	8.0
Sil-87C	100	14	0.750	467	120	42	7.8
Sil-88	Prior to Irradiation			554	151	66	12.3
Sil-88A	After Irradiation			481	133	48	8.9
Sil-88B	100	4	1.000	472	129	45	8.3
Sil-88C	100	18	1.000	470	126	44	8.1
Sil-89	Prior to Irradiation			556	150	66	12.2
Sil-89A	After Irradiation			482	128	46	8.6
Sil-89B	100	4	1.250	469	123	43	8.0
Sil-89C	100	20	1.250	469	123	43	8.0

TABLE 9

EXPERIMENTAL RESULTS OF FOWARD-BIAS CURRENT ANNEALING ON SILICON SOLAR CELLS IRRADIATED BY 1-MEV ELECTRONS (CONT'D.)

Solar Cell	Anneal Temp (C)	Anneal Time (hrs)	Current Density (A/cm^2)	V_{oc} (mV)	I_{sc} (mA)	P_{max} (mW)	η (%)
Si1-90	Prior to Irradiation			549	150	65	12.0
Si1-90A	After Irradiation			503	142	54	9.9
Si1-90B	120	3	0.250	494	136	50	9.2
Si1-90C	120	42	0.250	488	134	48	8.9
Si1-91	Prior to Irradiation			552	150	65	12.0
Si1-91A	After Irradiation			506	138	53	9.9
Si1-91B	120	5	0.500	494	131	49	9.0
Si1-91C	120	18	0.500	494	127	48	8.8
Si1-92	Prior to Irradiation			552	149	65	12.0
Si1-92A	After Irradiation			506	140	53	9.9
Si1-92B	120	5	1.000	495	135	49	9.1
Si1-92C	120	18	1.000	496	133	49	9.1
Si1-93	Prior to Irradiation			552	149	65	12.0
Si1-93A	After Irradiation			505	137	52	9.7
Si1-93B	120	4	1.250	496	132	46	8.6
Si1-93C	120	18	1.250	497	133	48	9.0
Si1-93D	120	24	1.250	498	135	50	9.3

TABLE 9

EXPERIMENTAL RESULTS OF FOWARD-BIAS CURRENT ANNEALING ON SILICON SOLAR CELLS IRRADIATED BY 1-MEV ELECTRONS (CONT'D.)

Solar Cell	Anneal Temp (C)	Anneal Time (hrs)	Current Density (A/cm^2)	V_{oc} (mV)	I_{sc} (mA)	P_{max} (mW)	η (%)
Sil-94	Prior to Irradiation			552	146	64	11.8
Sil-94A	After Irradiation			506	131	50	9.2
Sil-94B	140	5	0.250	497	129	48	8.9
Sil-94C	140	66	0.250	497	133	49	9.1
Sil-95	Prior to Irradiation			548	150	65	12.0
Sil-95A	After Irradiation			504	138	52	9.6
Sil-95B	140	5	0.750	492	133	49	9.1
Sil-95C	140	18	0.750	492	136	49	9.2
Sil-95D	140	24	0.750	492	138	50	9.3
Sil-96	Prior to Irradiation			556	150	66	12.2
Sil-96A	After Irradiation			507	136	51	9.6
Sil-96B	140	5	1.250	500	137	50	9.3
Sil-96C	140	18	1.250	503	138	51	9.5
Sil-96D	140	72	1.250	502	139	52	9.6
Sil-97	Prior to Irradiation			551	149	65	12.0
Sil-97A	After Irradiation			506	135	52	9.6
Sil-97B	140	72	1.250	507	137	53	9.8

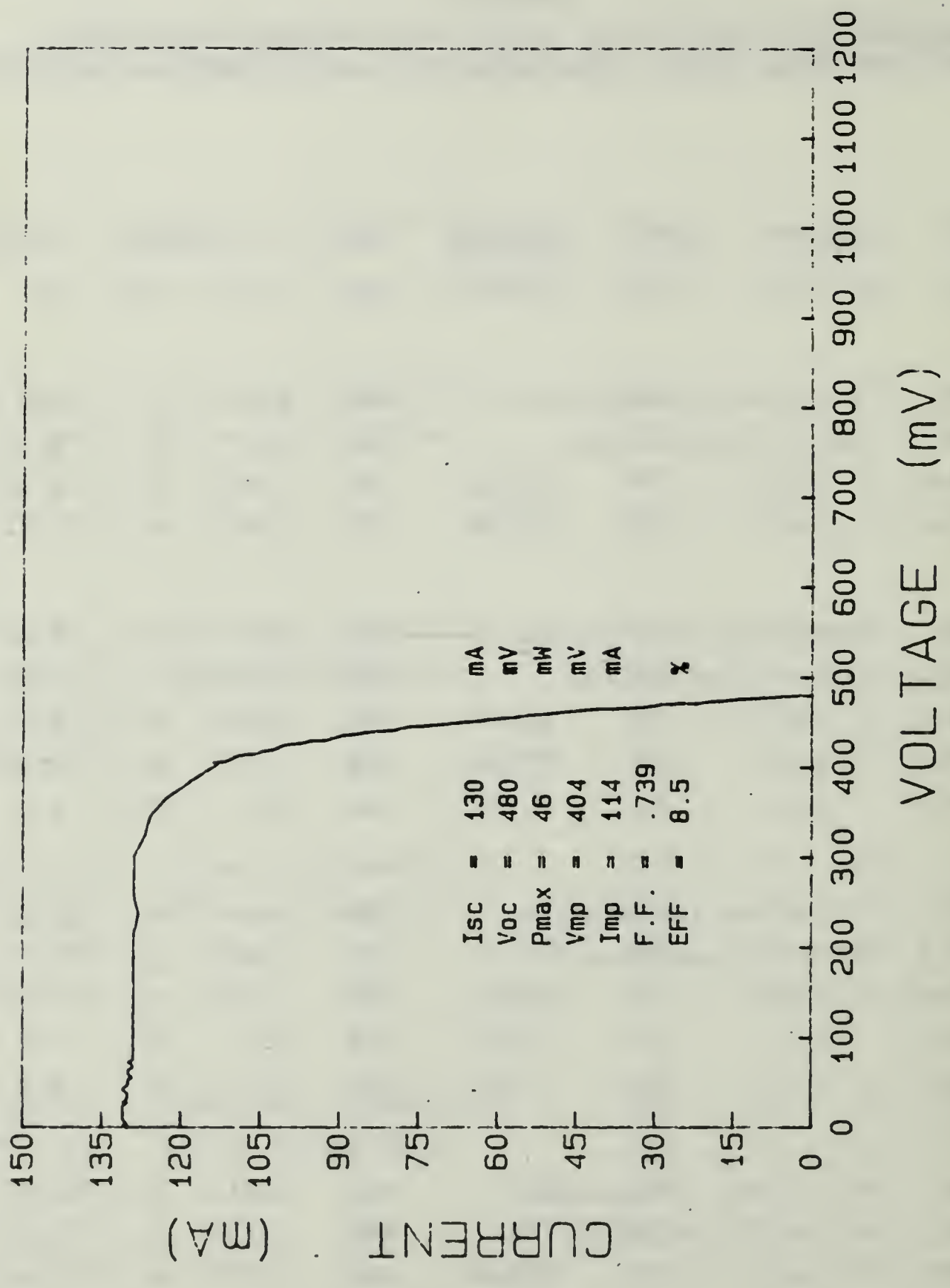

Figure 6.22 I-V Curve for Silicon Solar Cell Sil-86A, Irradiated to a Fluence of 1.8×10^{14} e/cm^2 by 1-Mev Electrons.

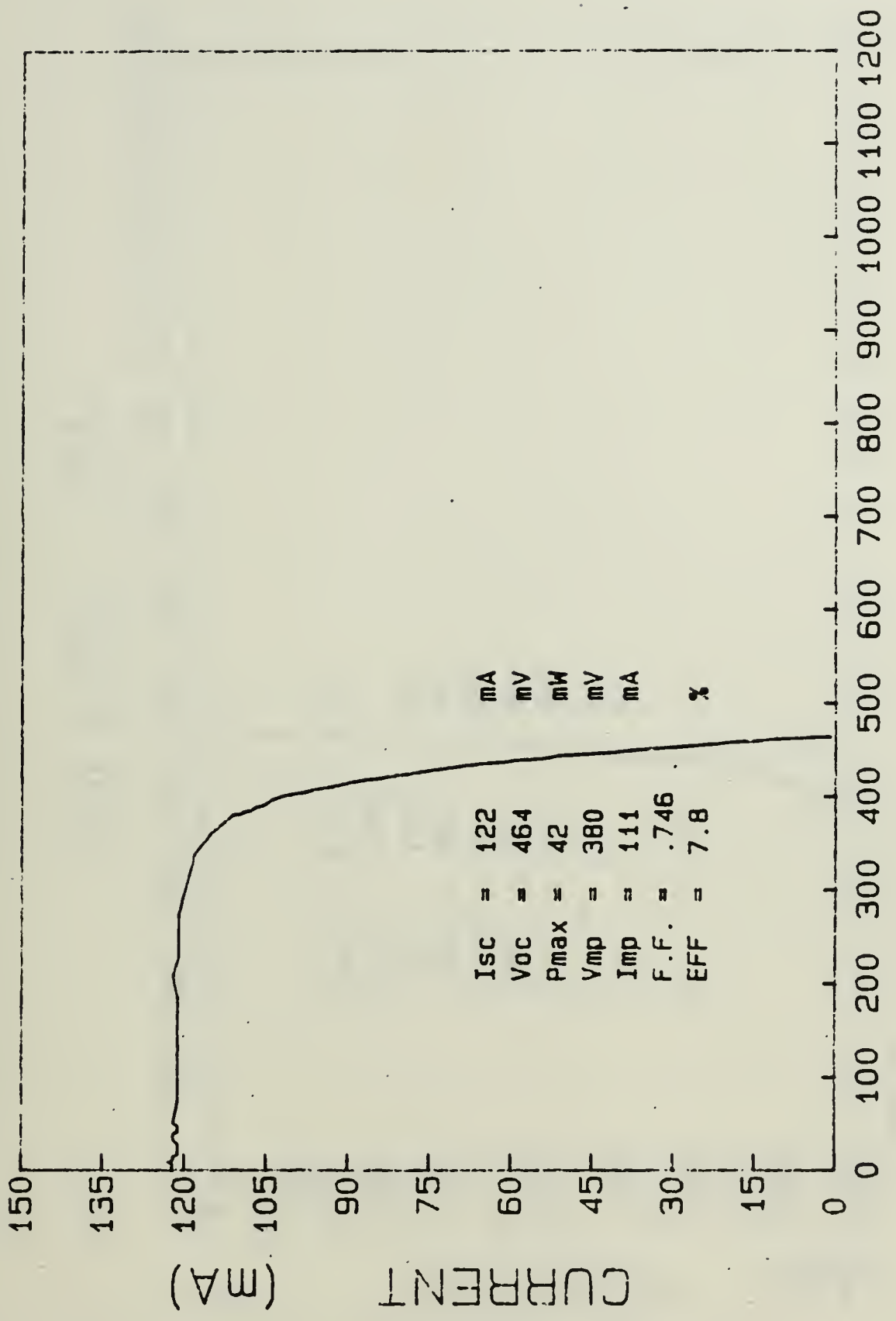

Figure 6.23 I-V Curve for Silicon Solar Cell Sil-86C, Annealed at 100°C Under a 0.500 A/cm^2 Foward-bias Current for 22 Hours.

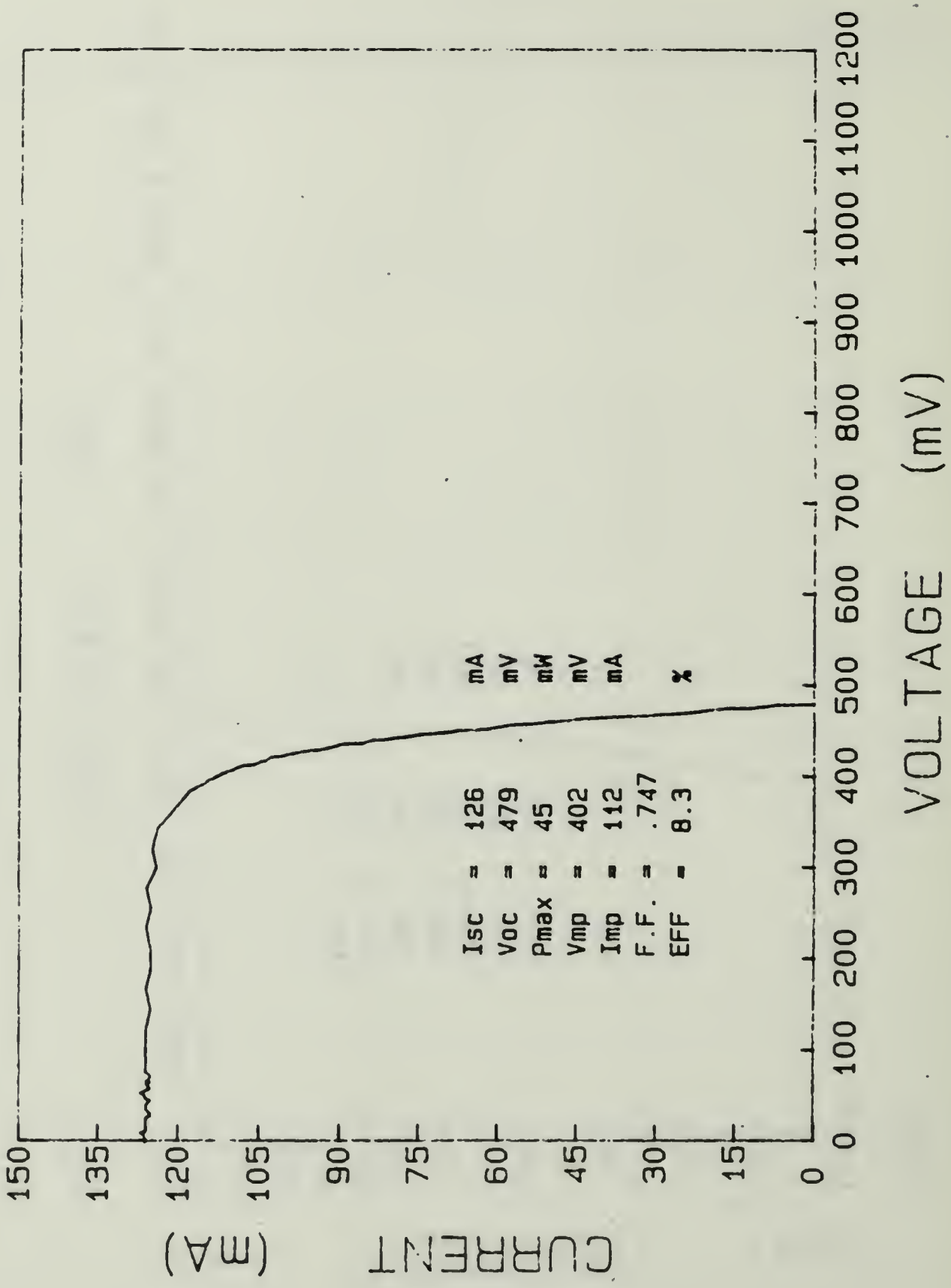

Figure 6.24 I-V Curve for Silicon Solar Cell Sil-87A, Irradiated to a Fluence of 1.8×10^{14} e/cm^2 by 1-Mev Electrons.

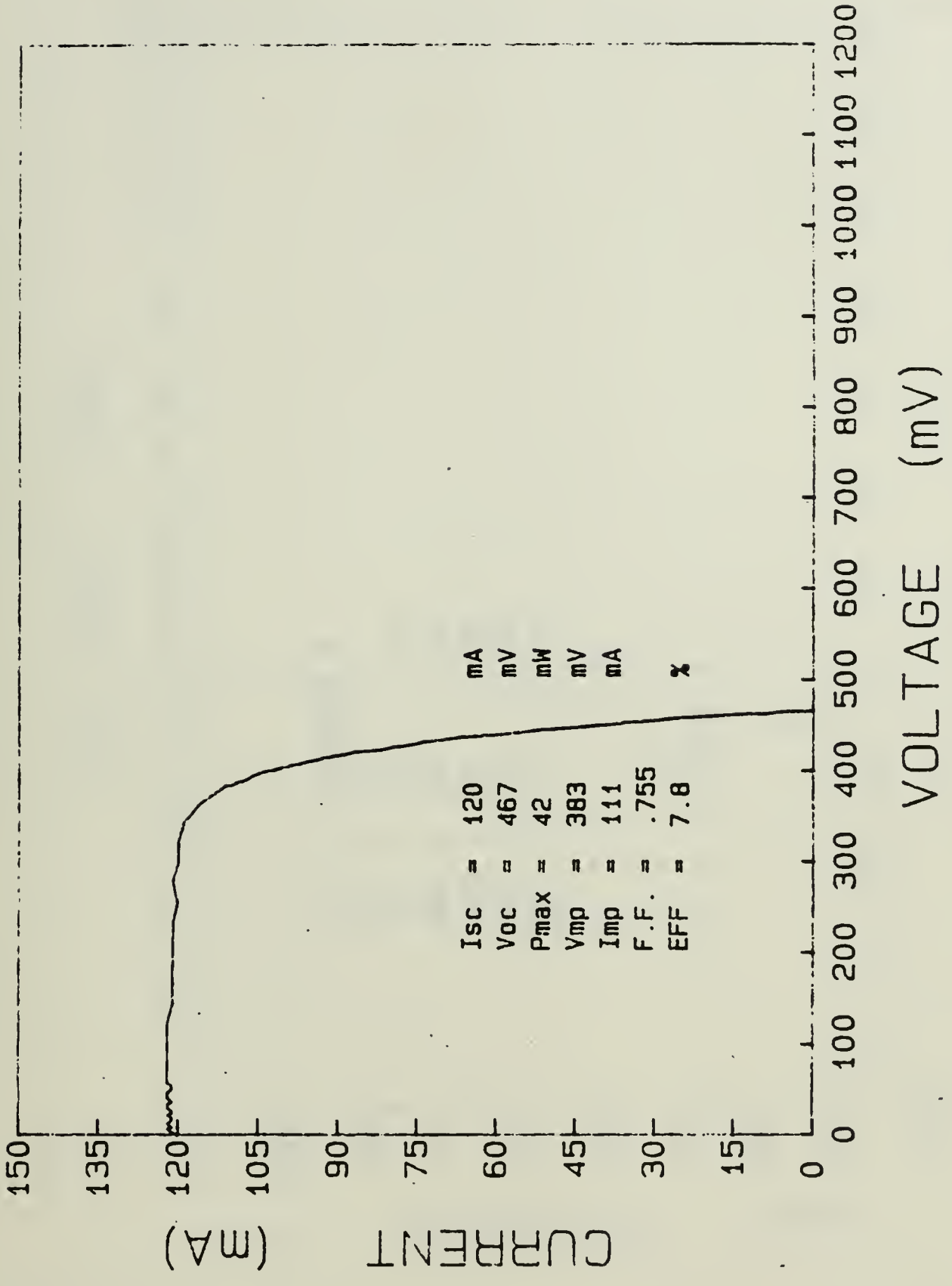

Figure 6.25 I-V Curve for Silicon Solar Cell Sil-87C, Annealed at 100°C Under a 0.750 A·cm^{-2} Foward-bias Current for 18 Hours.

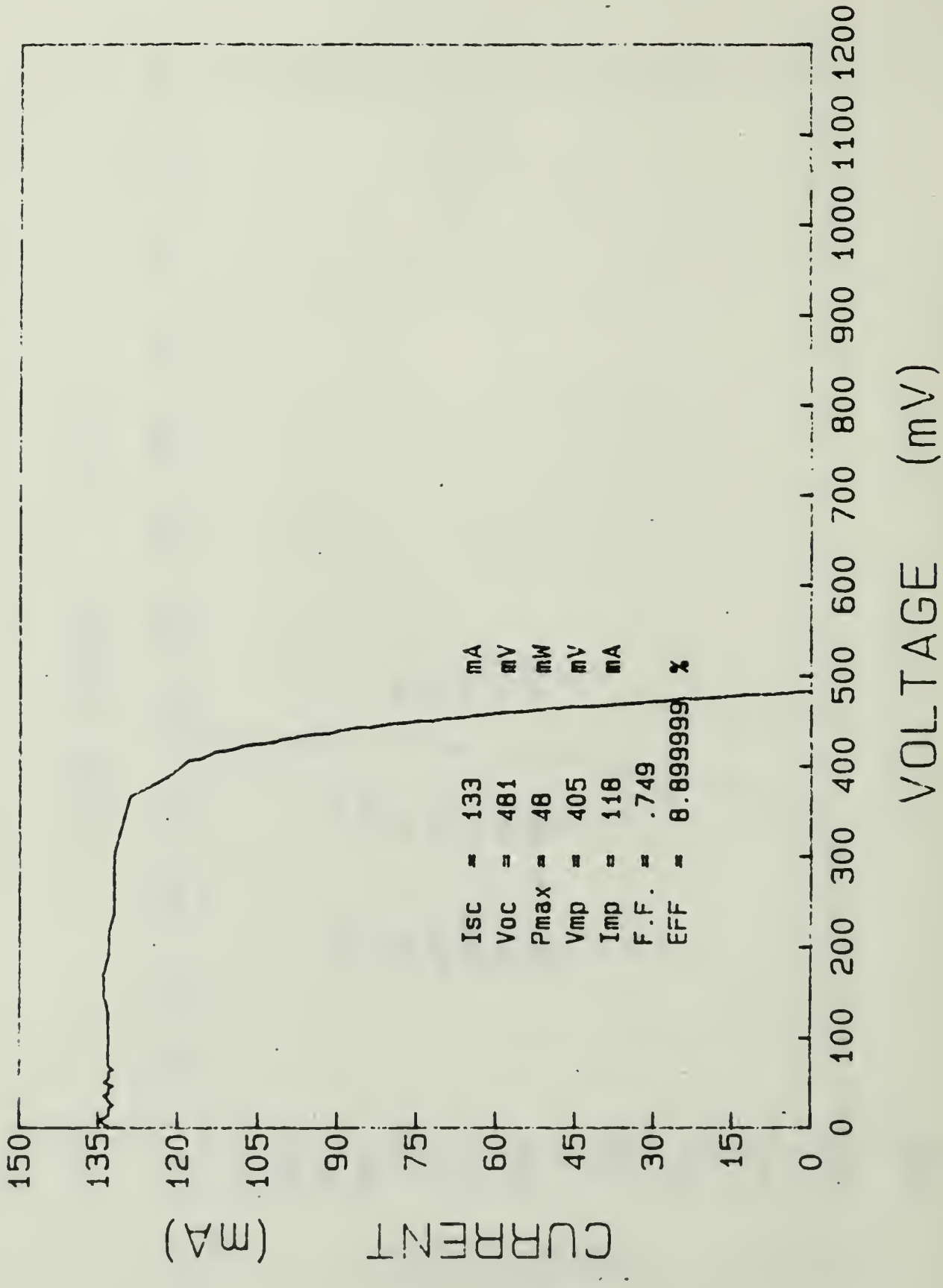

Figure 6.26 I-V Curve for Silicon Solar Cell Sil-88A, Irradiated to a Fluence of 1.8×10^{14} e cm^2 by 1-Mev Electrons.

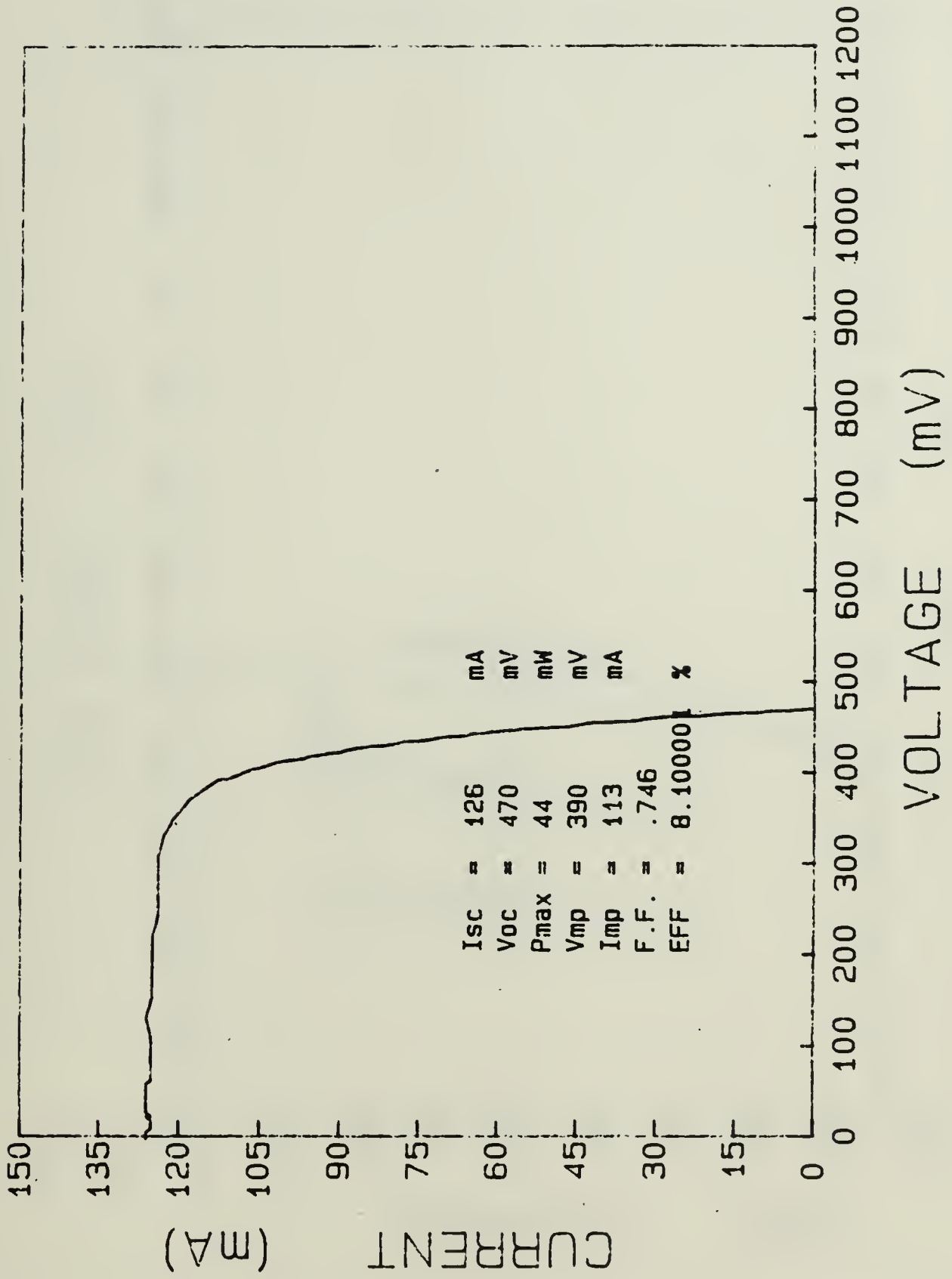

Figure 6.27 I-V Curve for Silicon Solar Cell Sil-88C, Annealed at 100°C Under a 1.000 A/cm^2 Foward-bias Current for 22 Hours.

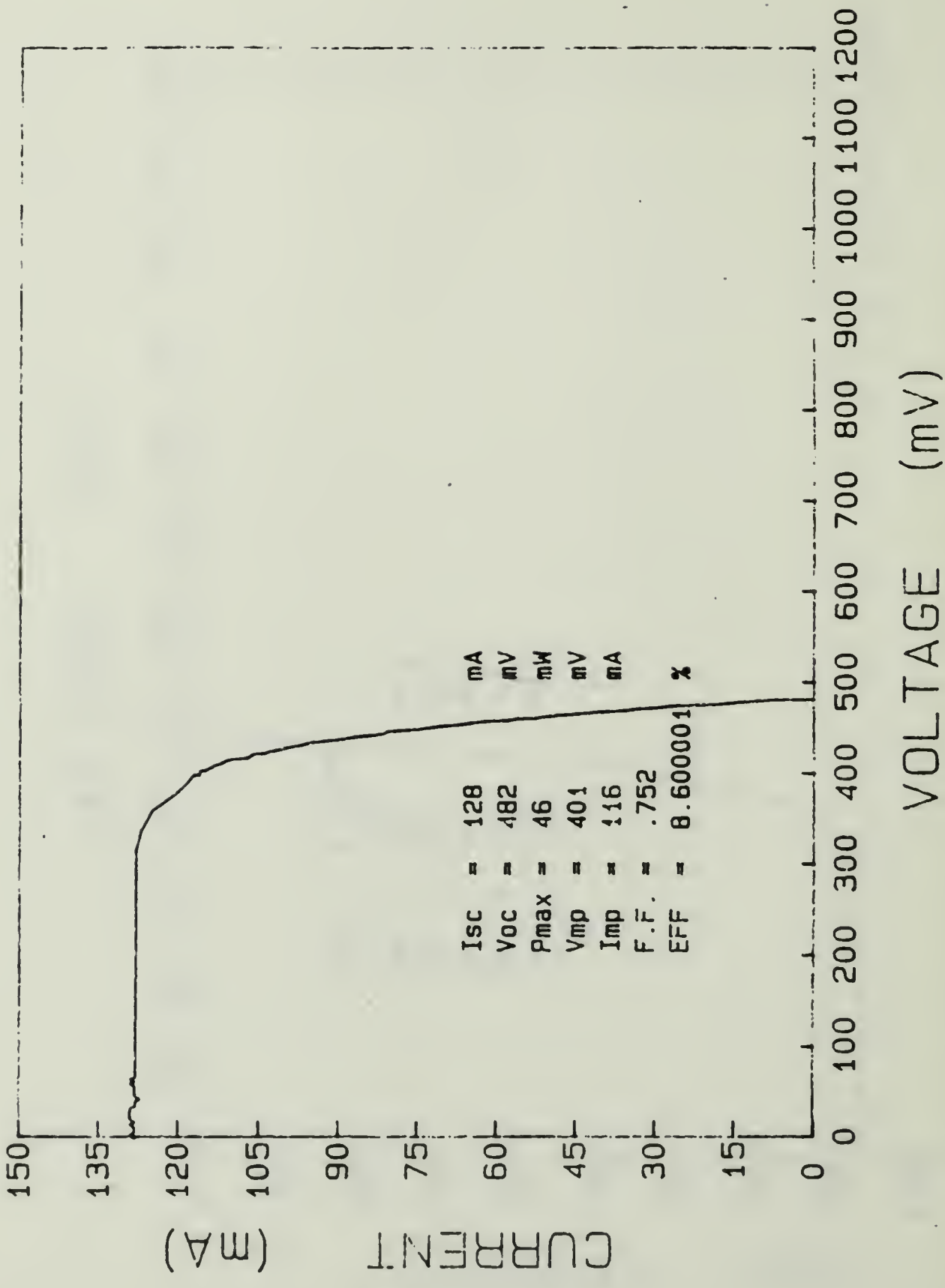

Figure 6.28 I-V Curve for Silicon Solar Cell Sil-89A, Irradiated to a Fluence of 1.8×10^{14} e/cm^2 by 1-Mev Electrons.

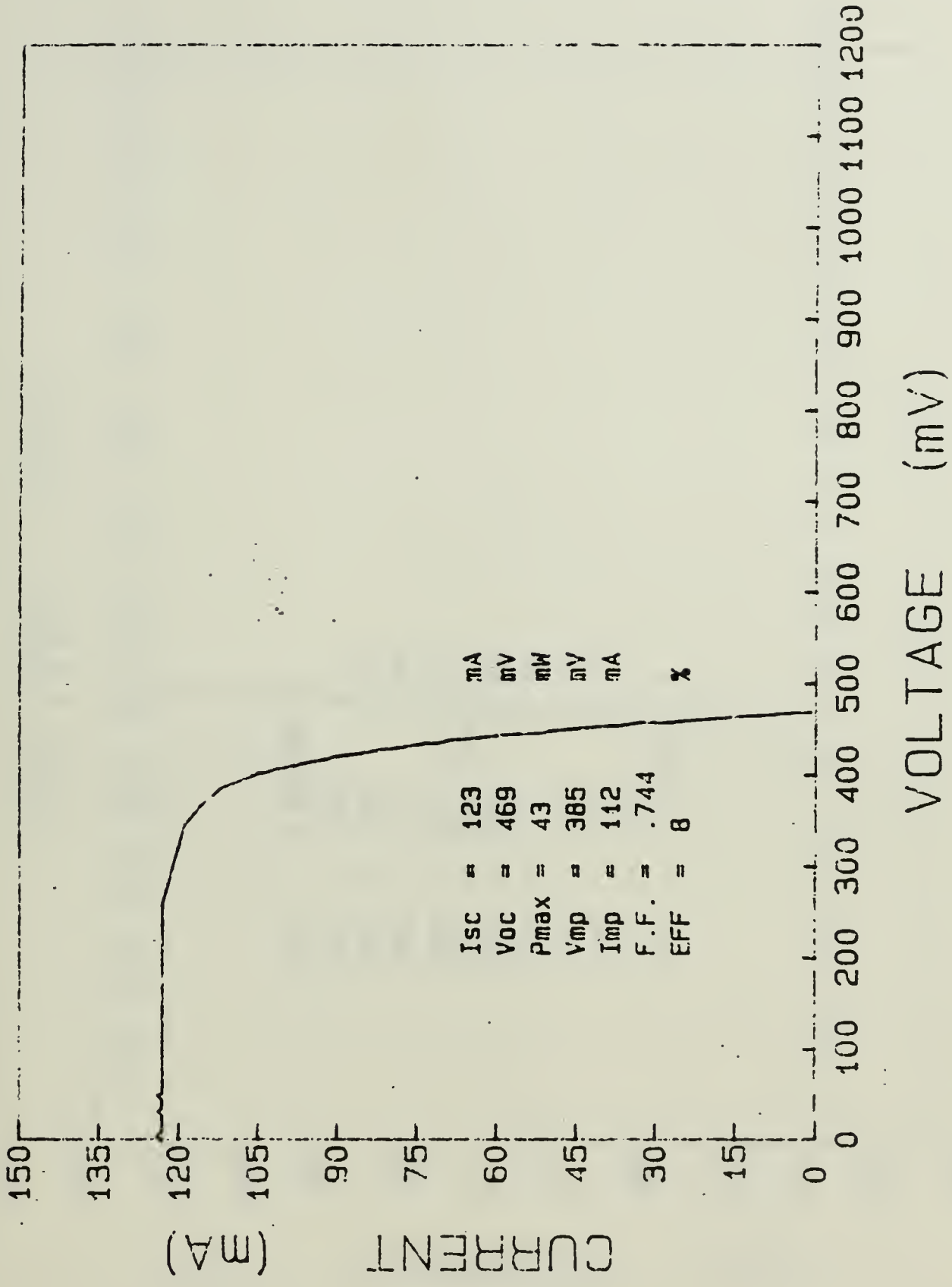

Figure 6.29 I-V Curve for Silicon Solar Cell Sil-89C, Annealed at 100°C Under a 1.250 A cm^2 Foward-bias Current for 24 Hours.

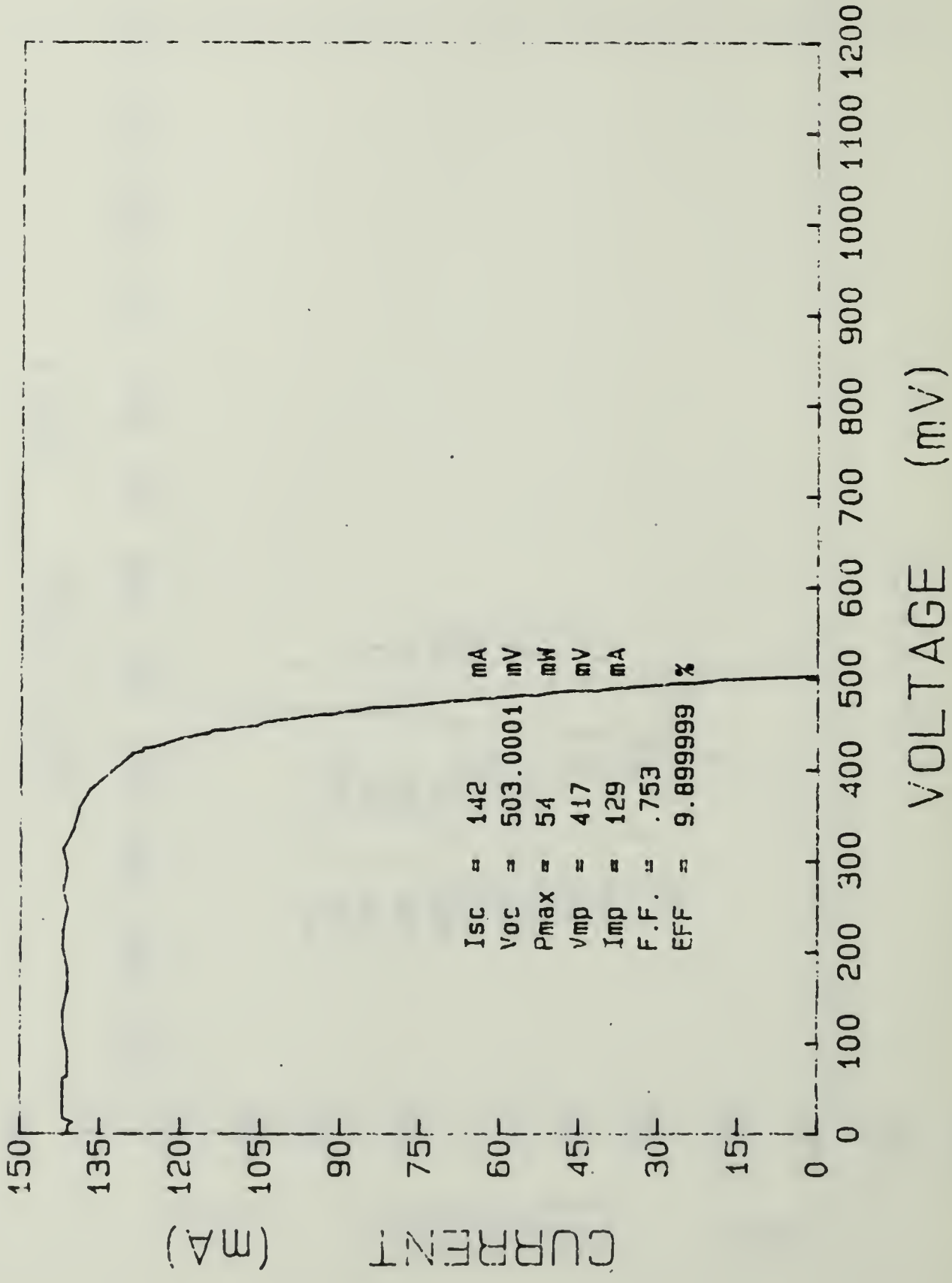

Figure 6.30 I-V Curve for Silicon Solar Cell Sil-90A, Irradiated to a Fluence of 3.7×10^{13} e cm^2 by 1-Mev Electrons.

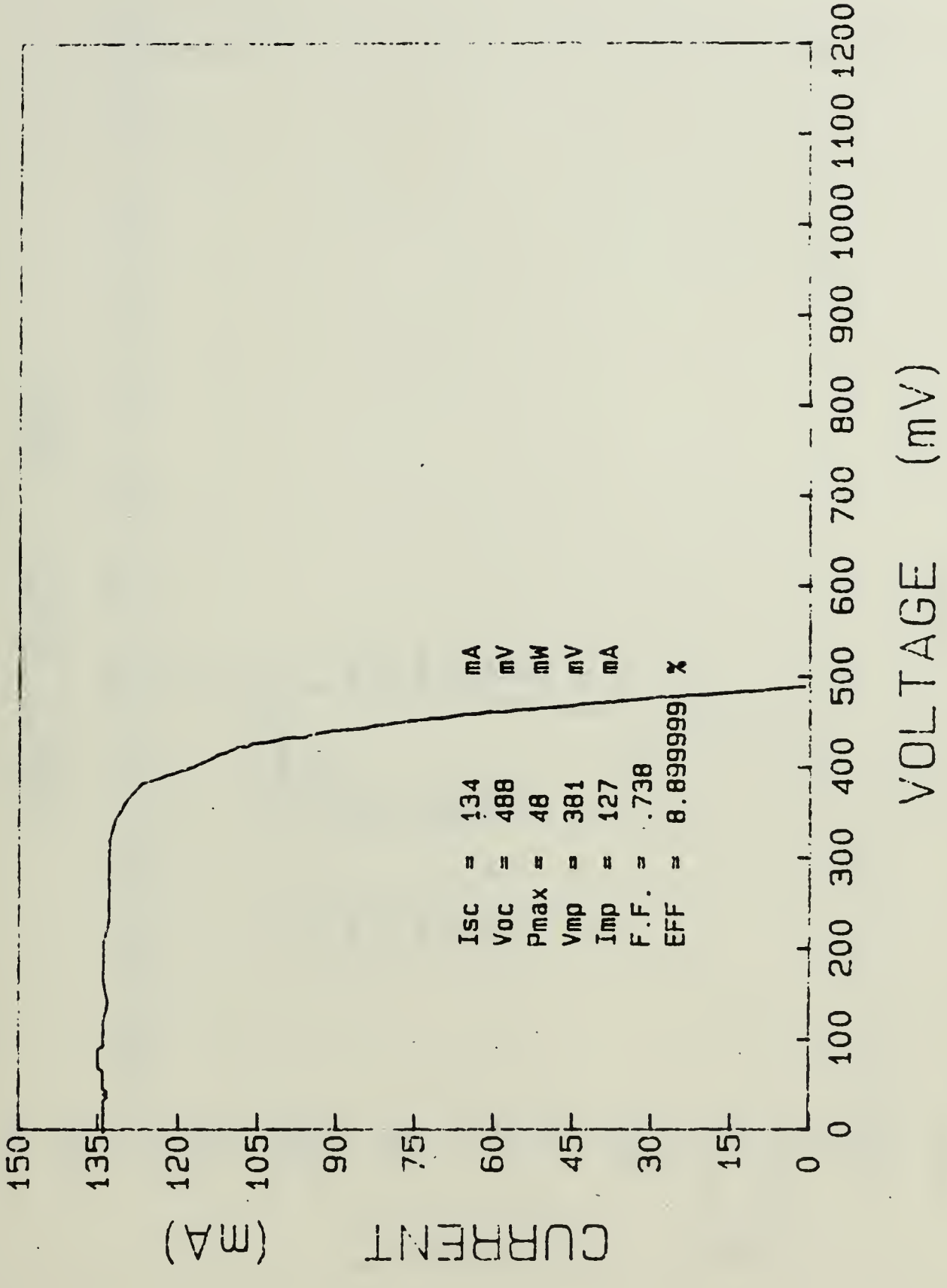

Figure 6.31 I-V Curve for Silicon Solar Cell Sil-90C, Annealed at 120°C Under a 0.250 A/cm^2 Foward-bias Current for 45 Hours.

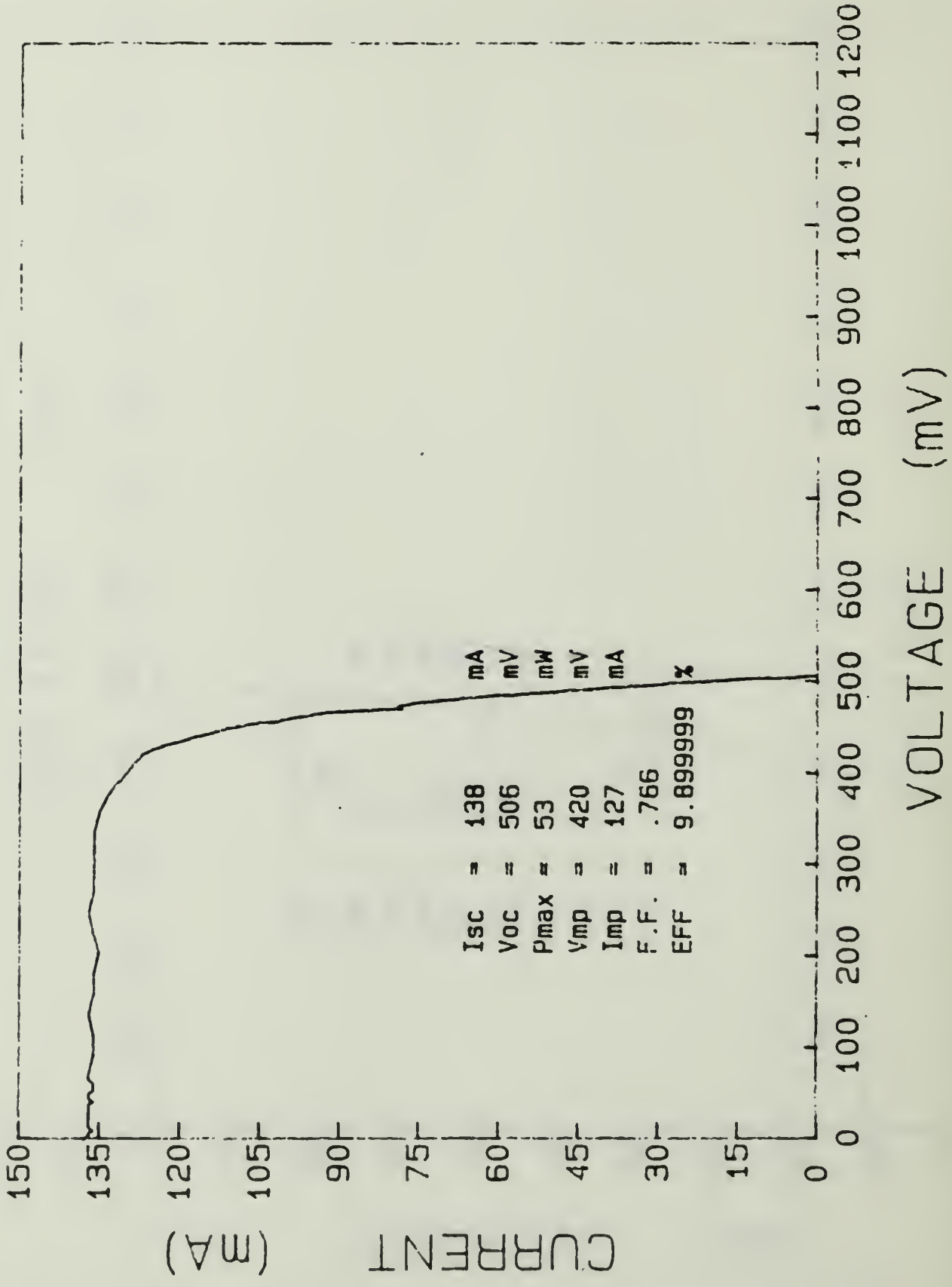

Figure 6.32 I-V Curve for Silicon Solar Cell Sil-91A, Irradiated to a Fluence of 3.7×10^{13} e/cm^2 by 1-Mev Electrons.

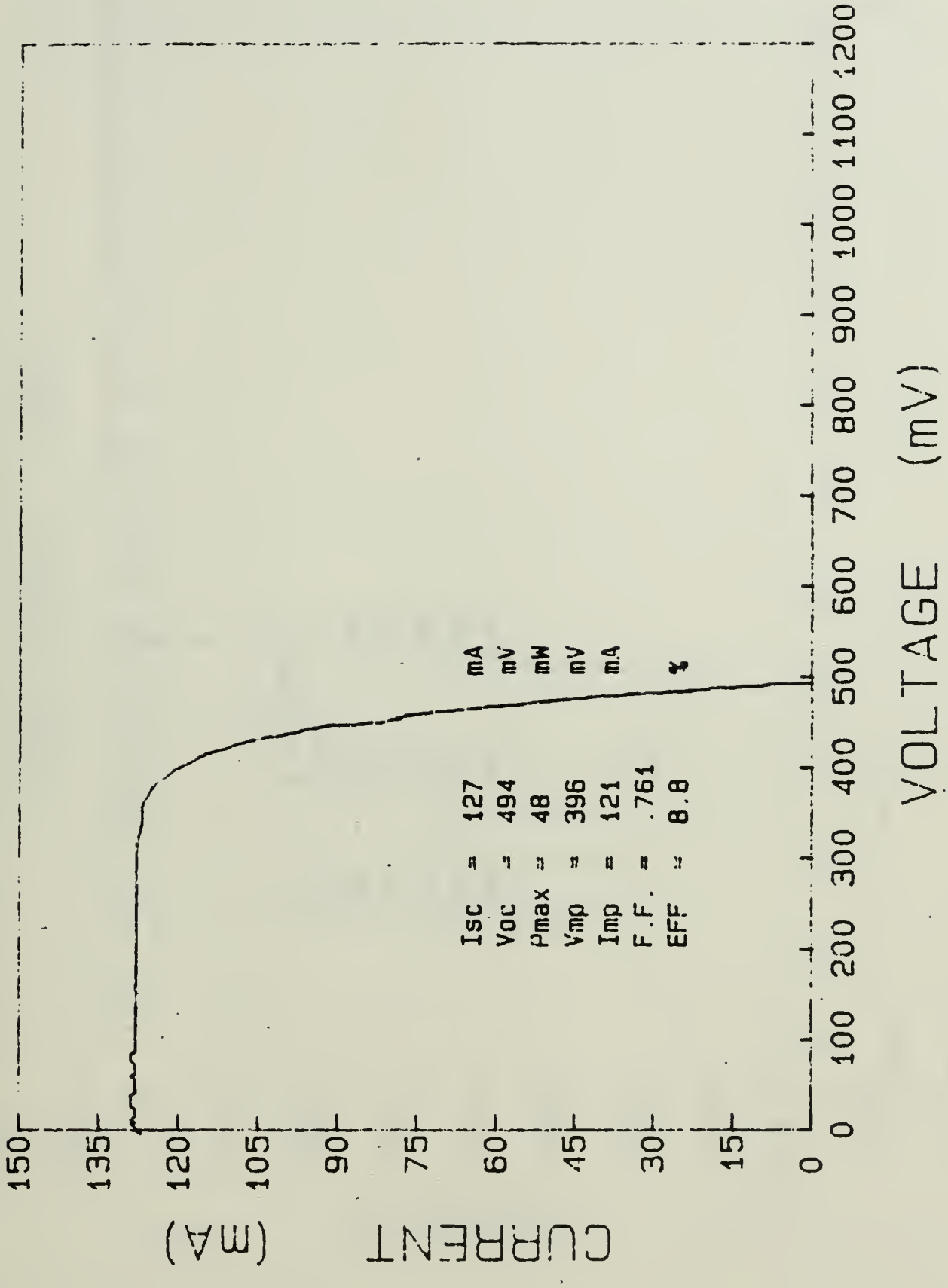

Figure 6.33 I-V Curve for Silicon Solar Cell Sil-91C, Annealed at 120°C Under a 0.500 A/cm^2 Foward-bias Current for 23 Hours.

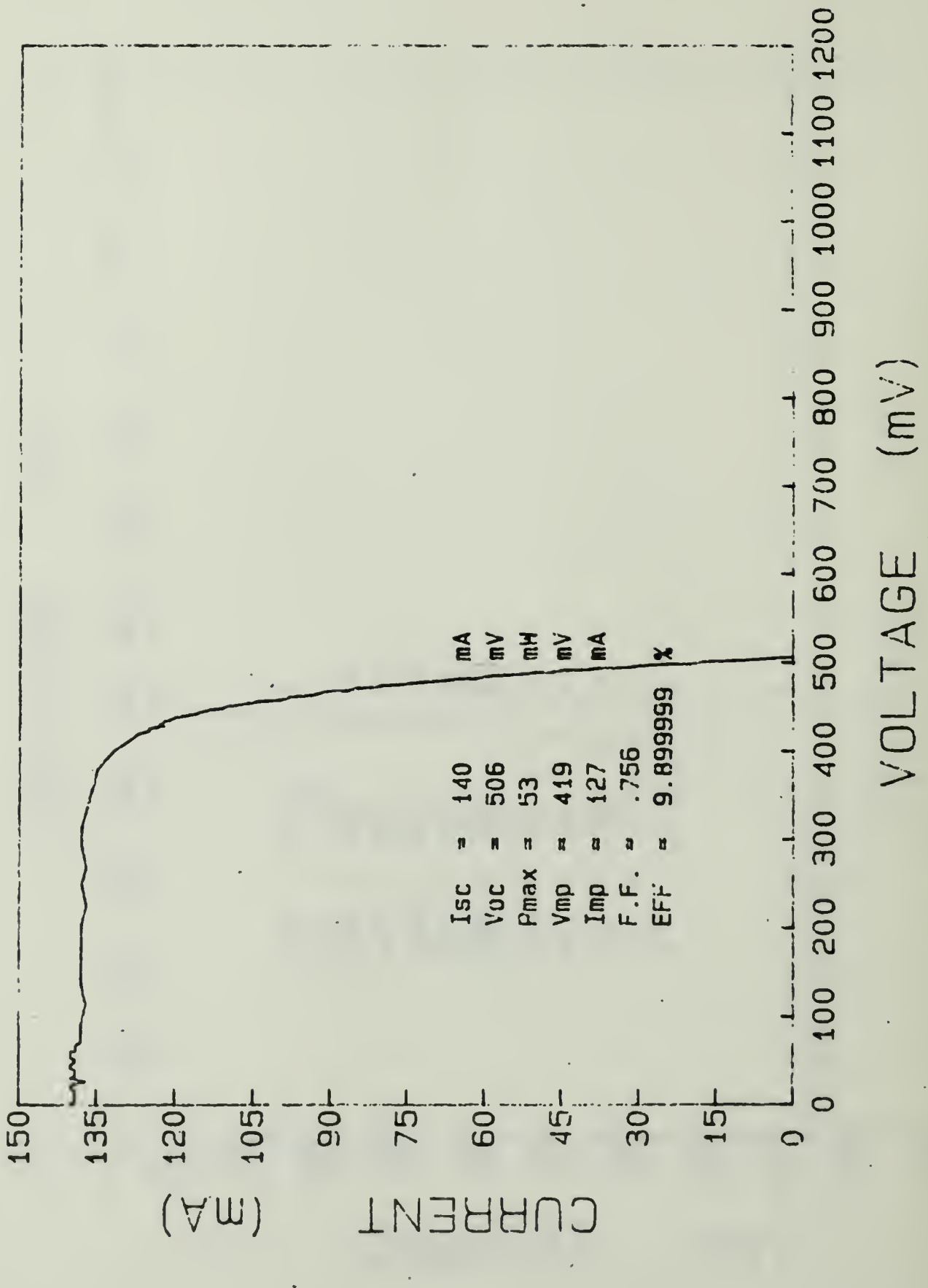

Figure 6.34 I-V Curve for Silicon Solar Cell Sil-92A, Irradiated to a Fluence of 3.7×10^{13} e cm^{-2} by 1-Mev Electrons.

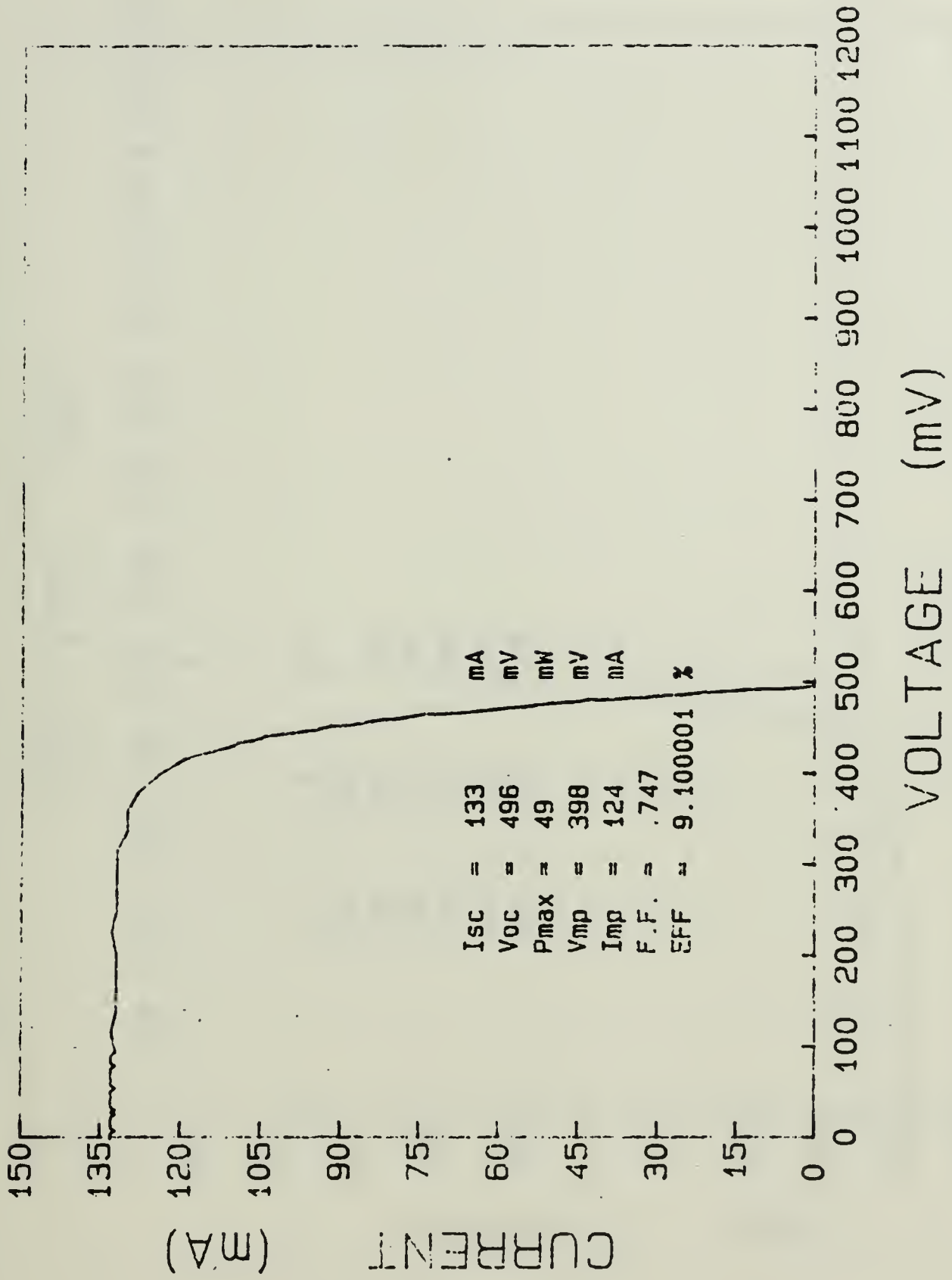

Figure 6.35 I-V Curve for Silicon Solar Cell Sil-92C, Annealed at 120°C Under a 1.000 A/cm^2 Foward-bias Current for 23 Hours.

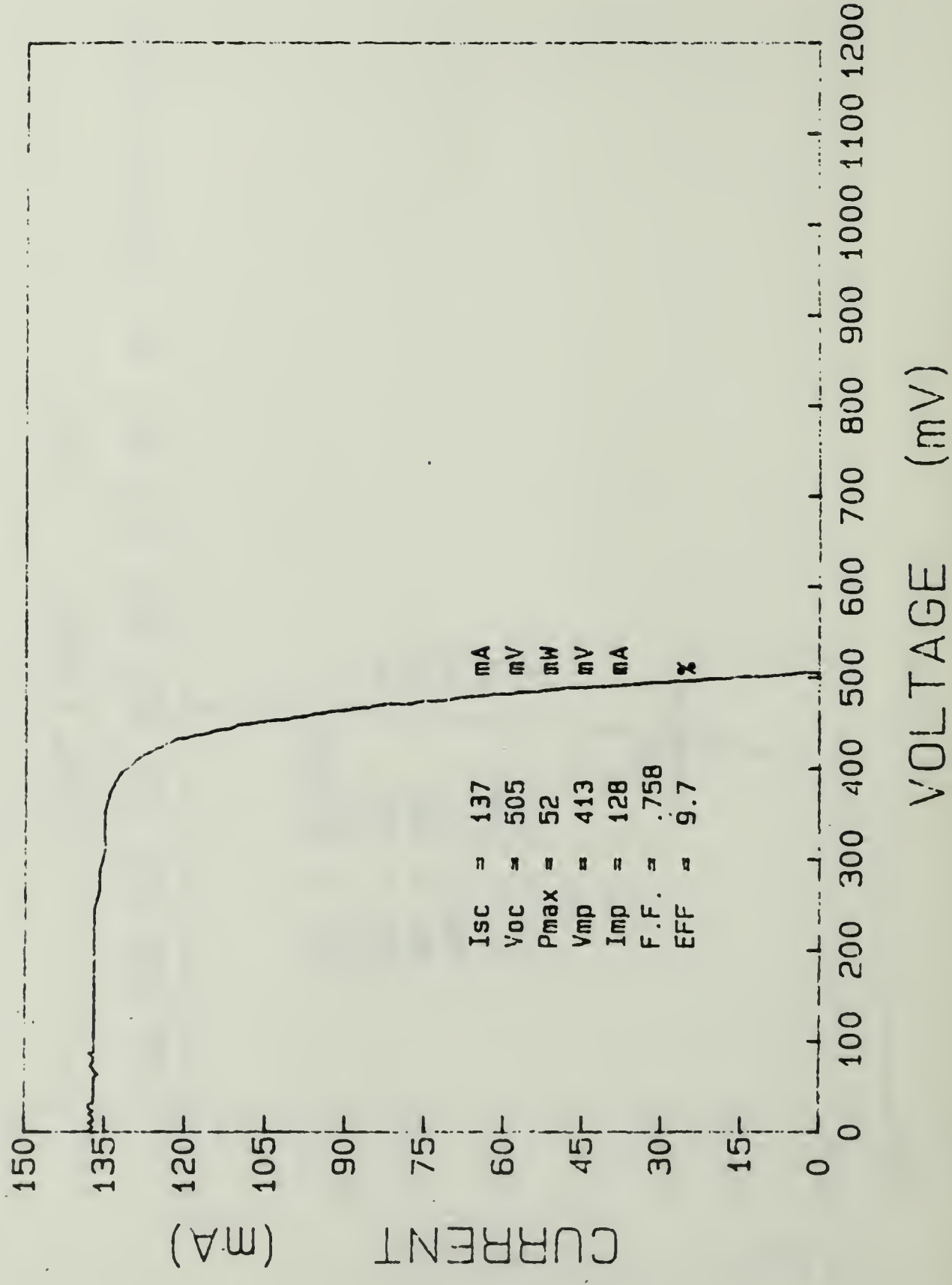

Figure 6.36 I-V Curve for Silicon Solar Cell Sil-93A, Irradiated to a Fluence of 3.7×10^{13} e, cm^2 by 1-Mev Electrons.

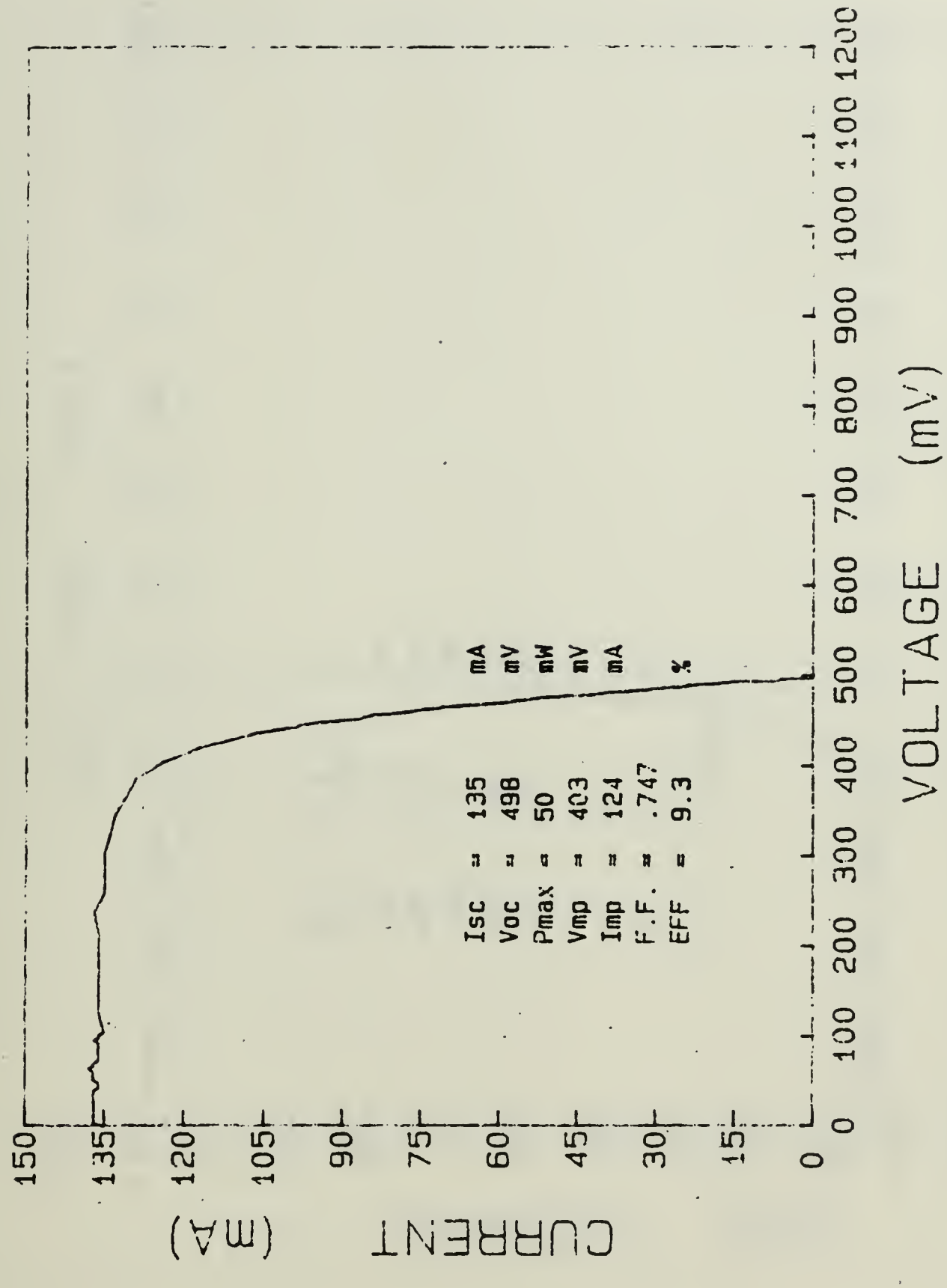

Figure 6.37 I-V Curve for Silicon Solar Cell Sil-93D, Annealed at 120°C Under a 1.250 A/cm^2 Foward-bias Current for 46 Hours.

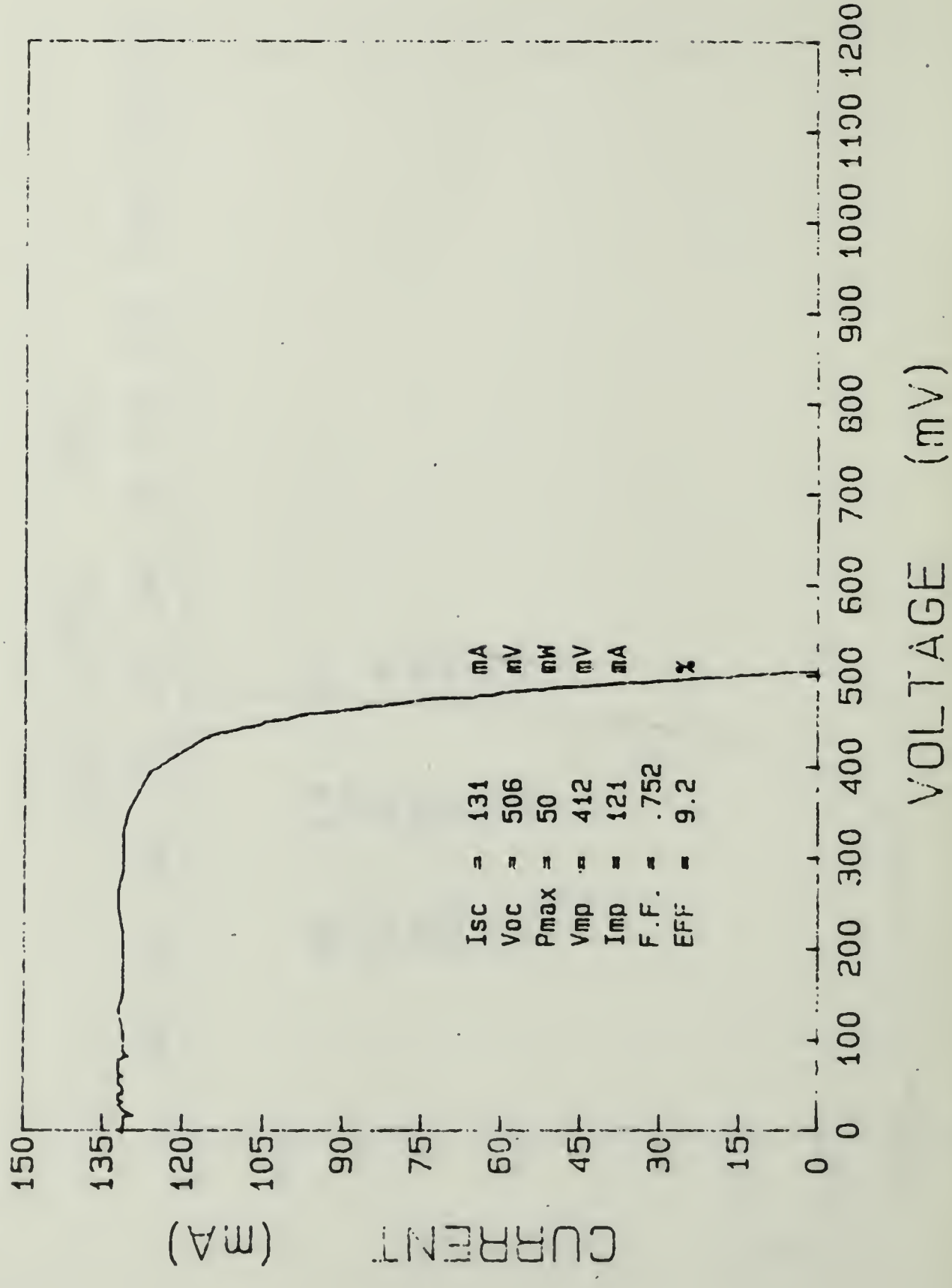

Figure 6.38 I-V Curve for Silicon Solar Cell Sil-94A, Irradiated to a Fluence of 3.7×10^{13} e/cm^2 by 1-Mev Electrons.

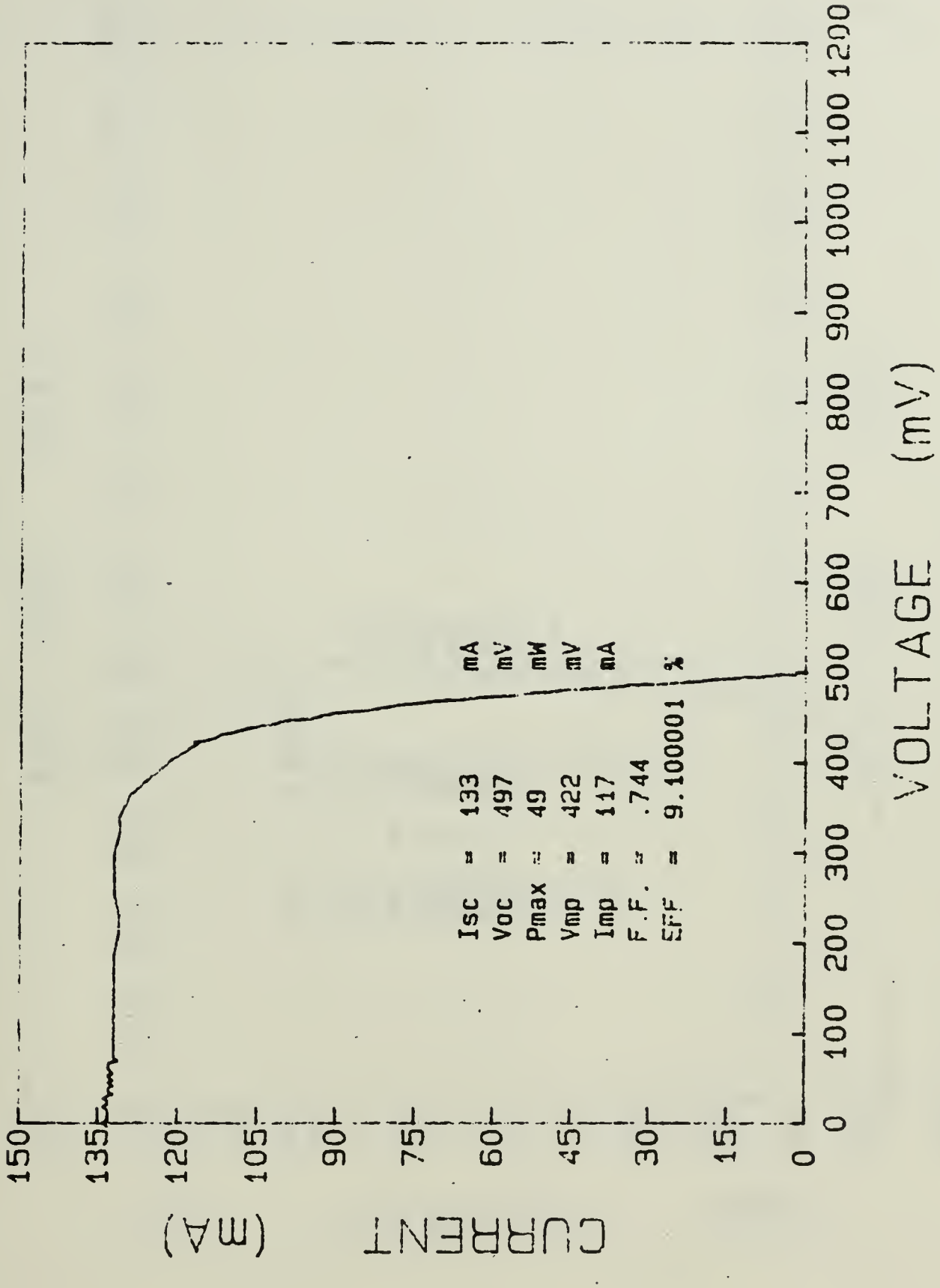

Figure 6.39 I-V Curve for Silicon Solar Cell Sil-94C, Annealed at 140°C Under a 0.250 A/cm^2 Foward-bias Current for 71 Hours.

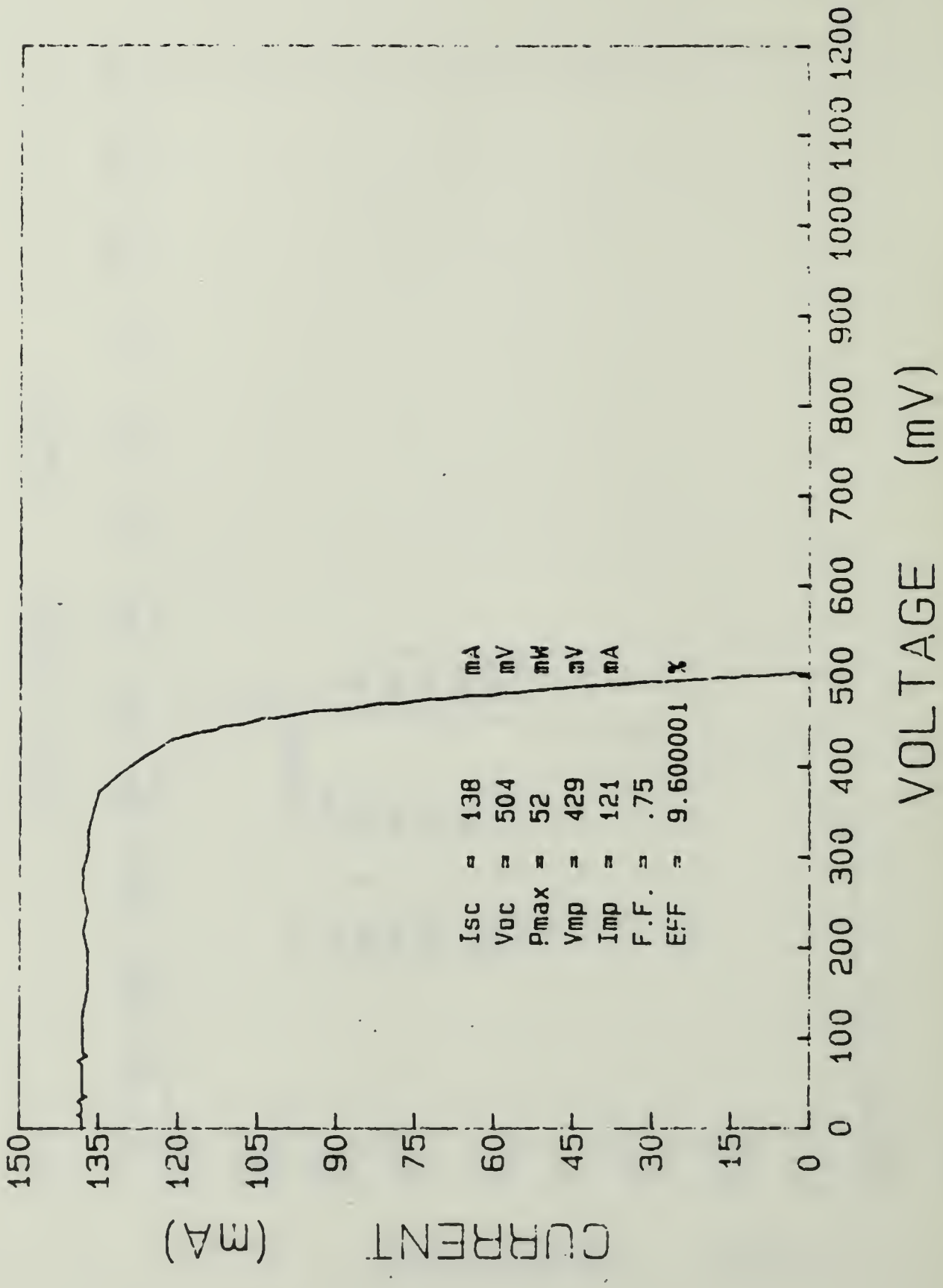

Figure 6.40 I-V Curve for Silicon Solar Cell Sil-95A, Irradiated to a Fluence of 3.7×10^{13} e cm^2 by 1-Mev Electrons.

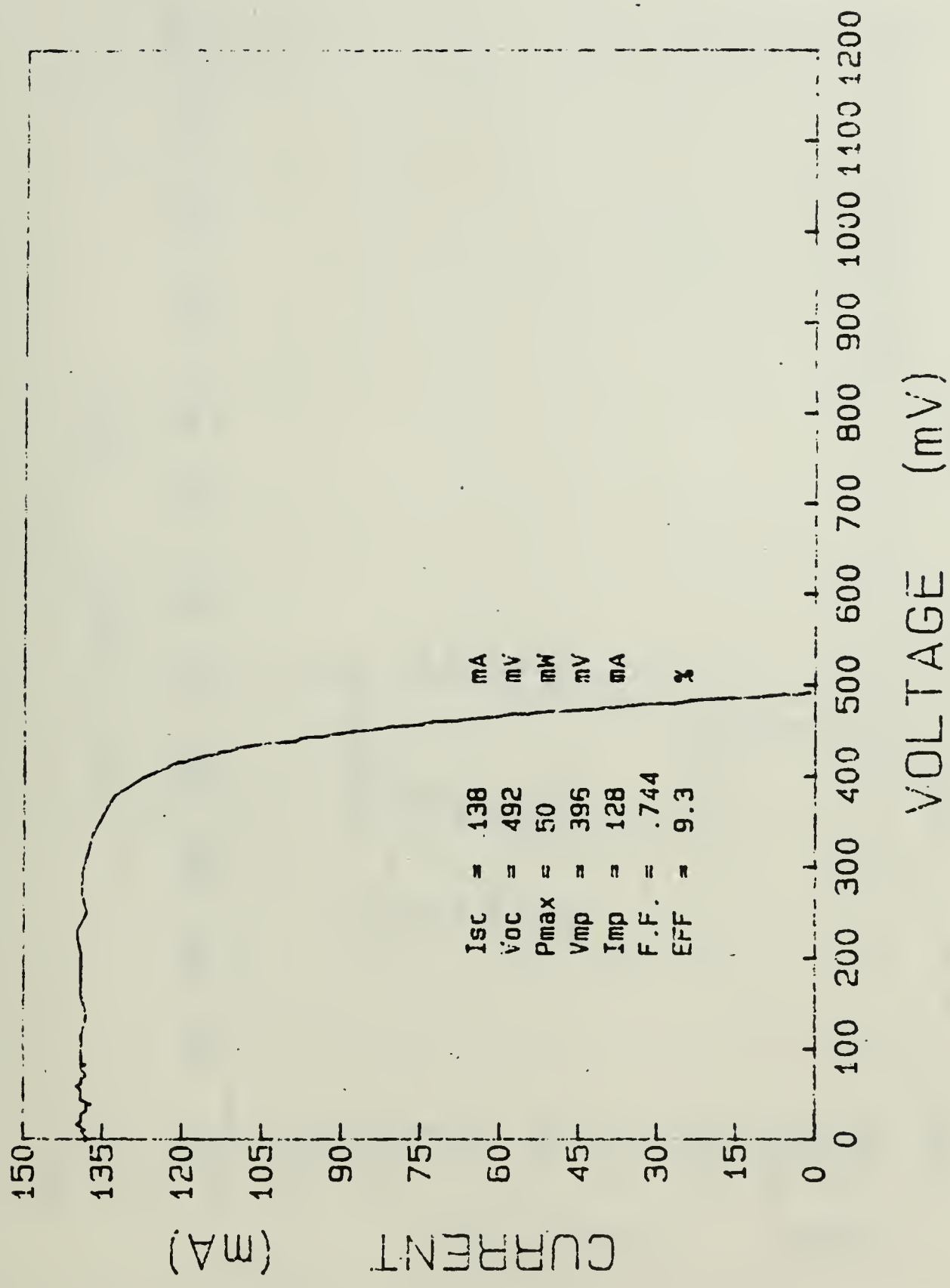

Figure 6.41 I-V Curve for Silicon Solar Cell Sil-95D, Annealed at 140°C Under a 0.750 A/cm^2 Foward-bias Current for 47 Hours.

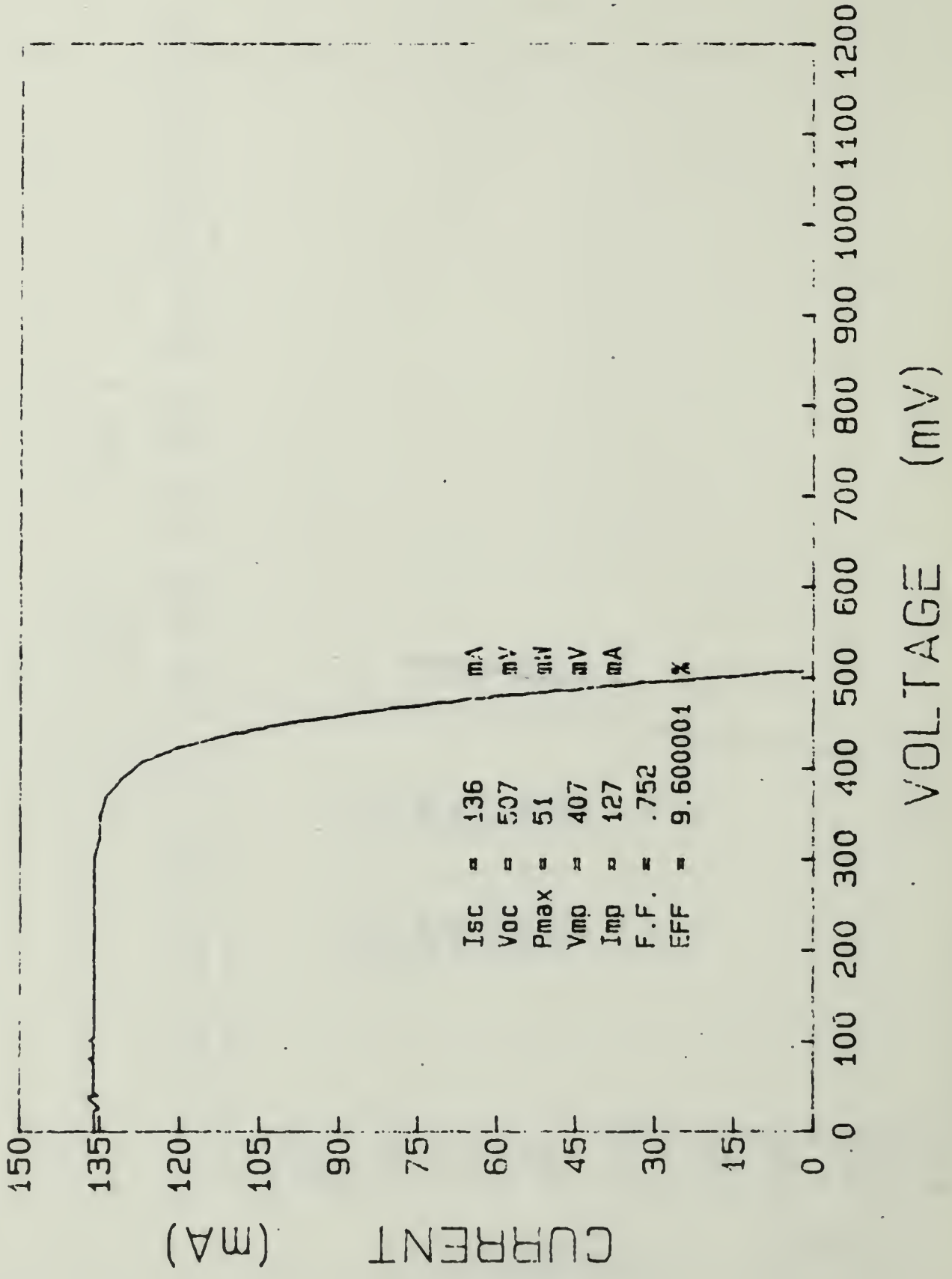

Figure 6.42 I-V Curve for Silicon Solar Cell Sil-96A. Irradiated to a Fluence of 3.7×10^{13} e/cm^2 by 1-Mev Electrons.

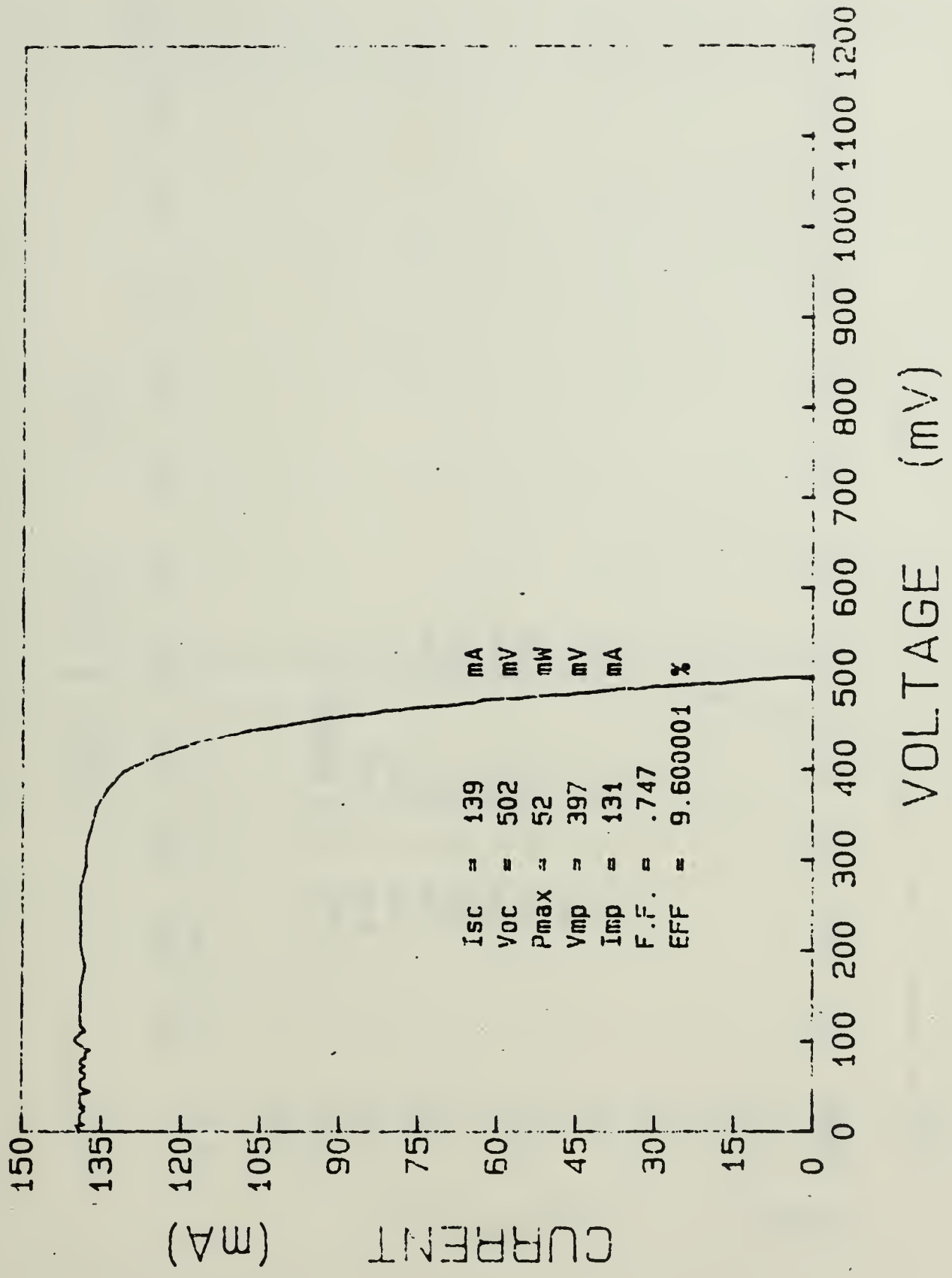

Figure 6.43 I-V Curve for Silicon Solar Cell Sil-96D, Annealed at 140°C Under a 1.250 A/cm^2 Foward-bias Current for 95 Hours.

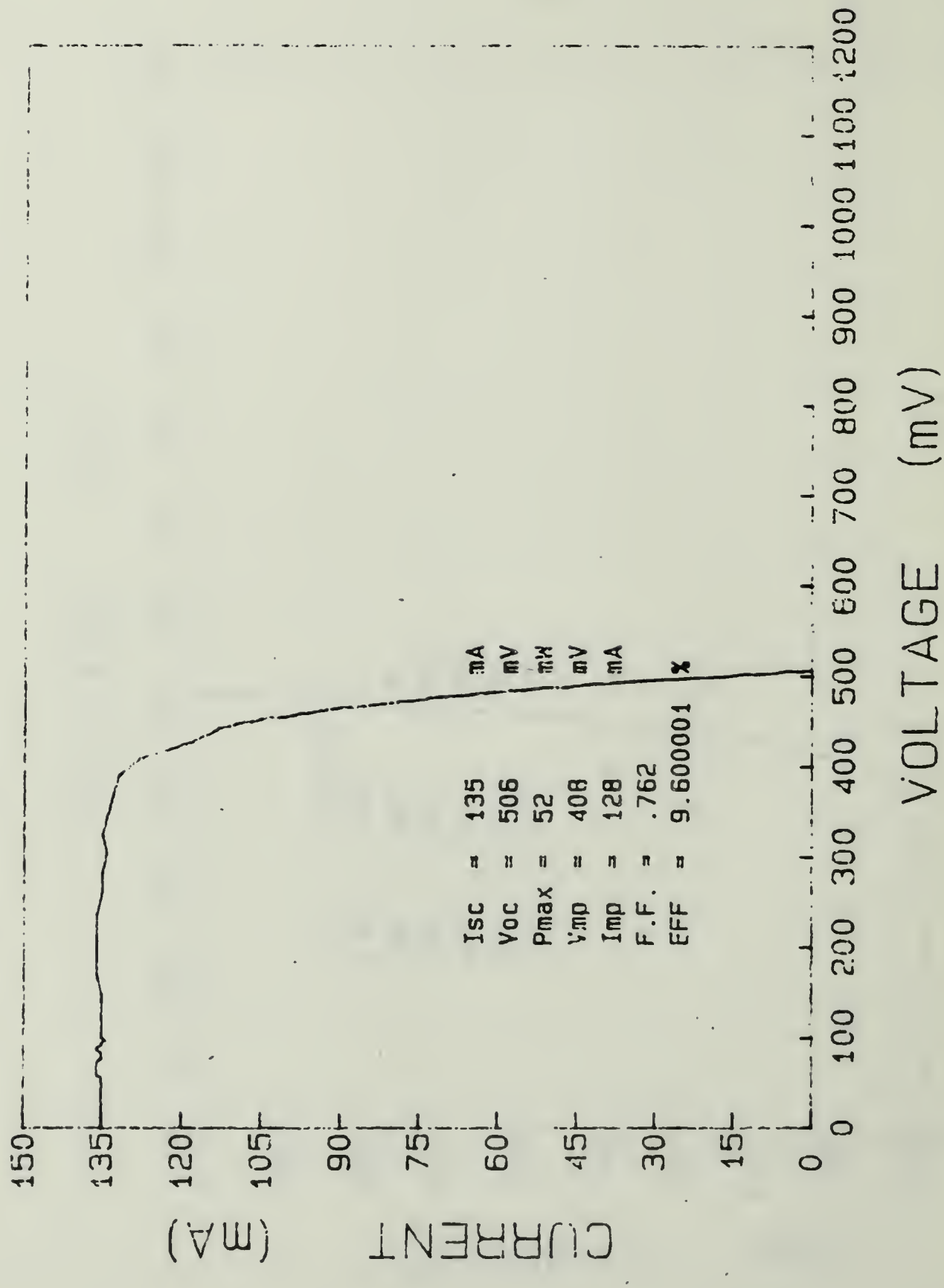

Figure 6.44 I-V Curve for Silicon Solar Cell Si-97A, Irradiated to a Fluence of 3.7×10^{13} e/cm^2 by 1-Mev Electrons.

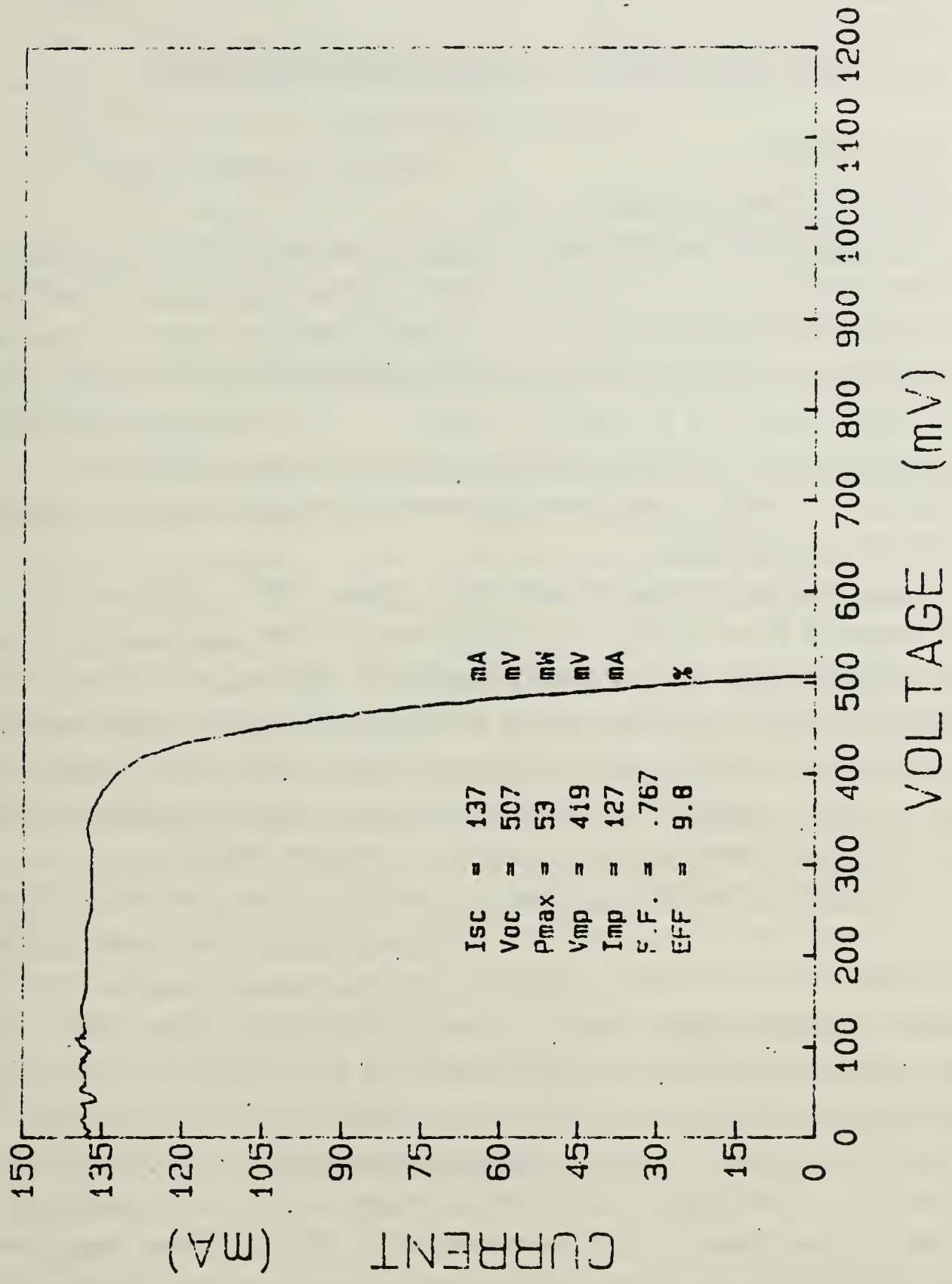

Figure 6.45 I-V Curve for Silicon Solar Cell Sil-97B, Annealed at 140°C Under a 1.250 A/cm^2 Foward-bias Current for 75 Hours.

VII. CONCLUSIONS AND RECOMMENDATIONS

A. CONCLUSIONS

1. GaAs Annealing Experiment

Examination of the experimental data from solar cells ASEC-4 and ASEC-5, which were annealed at 90°C and with varying current densities, proved difficult because of the randomness of the results. One exception was the apparant decrease in solar cell efficiency at a current density of 1.0 A/cm^2. Solar cells ASEC-7 and ASEC-8 showed similar decreases in all measured quantities when biased at 1.0 A/cm^2. A further attempt to anneal solar cell ASEC-9 at 1.250 A/cm^2 produced the same result. From this one can conclude that these cells cannot be annealed at current densities near or greater than 1.0 A/cm^2.

The annealing temperatures used were ambient, 100°C, 115°C and 130°C. Thermal annealing of cell ASEC-23 at 100°C shows that this mechanism does not contribute significantly to the overall annealing results. However, as described earlier in Chapter IV, the first thermal annealing recovery stage for GaAs cells begins at 150°C. This may account for the fact that no thermal effects were observed. No attempt was made to anneal at this higher temperature because the soldered metal contacts of the testing aparatus would not withstand the higher temperatures.

From Table 5, the efficiency of solar cell ASEC-10 was reduced from 16.5% to 16.0% after irradiation to a fluence of 1.0×10^{13} e/cm^2 by 20-Mev electrons. This damage reduced the cell efficiency to 96.97% of pre-irradiation levels. After Foward-bias Current Annealing at 100°C for 8 hours with a 0.750 A/cm^2 current density, cell efficiency increased to 98.79%. Similarly, from Table 7, the efficiency of solar cell ASEC-16 was reduced from 16.4% to 9.8% after irradiation to a fluence of 1.8×10^{14} e/cm^2 by 1-Mev electrons. This damage reduced the cell efficiency to 59.76% of pre-irradiation levels. After Foward-bias Current Annealing at 100°C for 50 hours with a 0.750 A/cm^2 current density, cell efficiency improved to 70.73%. Thus, Foward-bias Current Annealing does promote damage annealing in GaAs solar cells. The extent of recovery from this method depends on the magnitude of the fluence level. Since one cell was irradiated by 20-Mev electrons and the other by 1-Mev electrons, this may have had an additional effect on the annealing rate. Finally, the fact that solar cell

efficiency for cell ASEC-16 peaked at near 50 hours of annealing then decreased upon further annealing may indicate that there is a maximum annealing time limit. This could be due to diffusion of the dopant material away from the P/N junction which may ultimately reduce the potential barrier of the cell.

2. **Silicon Annealing Experiment**

Silicon solar cell Sil-99 was thermally annealed at 120°C for 46 hours, while solar cell Sil-100 was thermally annealed at 140°C for 119 hours. Neither of these cells showed a marked improvement in electrical parameters, as is expected, since silicon solar cells do not significantly anneal at temperatures below 200°C. Thus, the contribution of thermal annealing to the overall annealing rate on cells Sil-86 through Sil-97 is negligible.

Annealing temperatures used in this experiment were 100°C, 120°C and 140°C. Current densities ranged from 0.250 A/cm^2 to 1.250 A/cm^2, while annealing times varied from 22 hours to 95 hours. In all cases, the electrical characteristics of each cell decreased when the foward-biasing current was applied. These parameters continued to decline for cells Sil-86, Sil-87, Sil-88, Sil-90 and Sil-91 as the annealing time increased. Solar cells Sil-89 and Sil-92 stabilized after the initial decrease in electrical characteristics, while the efficiencies of cells Sil-93, Sil-94, Sil-95, Sil-96 and Sil-97 continued to improve with time. Examination of the data from Table 9 indicates that greater annealing temperatures, current densities and annealing times improves silicon solar cell annealing. However, none of the cells tested in this experiment annealed appreciably. Thus, Foward-bias Current Annealing under these conditions does not promote significant damage annealing.

3. **Gallium Arsenide Verses Silicon Annealing**

A comparison of both annealing experiments clearly demonstrates the superior ability of P/N junction GaAs solar cells to anneal over N/P junction silicon solar cells. Results from the silicon solar cell experiment would indicate that the damage annealing rate improves as the annealing temperature, annealing time and current density are increased. At levels greater than those used in this experiment, Foward-bias Current Annealing of silicon solar cells may even produce positive results. In the GaAs annealing experiment, there is a maximum current that will produce damage annealing. This current is less than 1.0 A/cm^2. Currents at or greater than 1.0 A/cm^2 cause significant degradation in all cell characteristics. Additionally, after 50 hours of annealing, the electrical characteristics of solar cell ASEC-16 began to degrade which may indicate a limit to the amount of time a GaAs solar cell may be annealed.

B. RECOMMENDATIONS

1. Gallium Arsenide Solar Cells

Several follow-on experiments are needed before Forward-bias Current Annealing of on-orbit solar arrays can be realized. These are:

a. Annealing a sufficient number of gallium arsenide solar cells irradiated to various fluence levels by 1-Mev electrons to provide statistical correlation between annealing rate and fluence levels.

b. Annealing 1-Mev irradiated GaAs solar cells to confirm/determine the maximum current density that can be used in Foward-bias Current Anealing.

c. Annealing 1-Mev irradiated GaAs solar cells to confirm/determine if there is a maximum annealing time after which solar cell efficiency decreases.

d. Annealing a sufficient number of irradiated GaAs solar cells to provide statistical correlation between annealing temperature, annealing time and current density.

e. Foward-bias Current Anneal a GaAs solar cell while the cell is exposed to radiation to more nearly approximate on-orbit annealing conditions.

2. Silicon Solar Cells

Experiments using greater annealing temperatures, annealing times and current densities may provide positive annealing rates. However, since a satellite's solar array temperature peaks at temperatures near 100°C, on-orbit annealing of silicon solar cells may be impractical because of higher annealing temperatures.

LIST OF REFERENCES

1. Agrawal, B. N., *Design of Geosynchronous Spacecraft*, Prentice-Hall, Inc., 1986.

2. Fuhs, A. E., *Launch Vehicles, Orbital Transfer Vehicles and Spacecraft Propulsion*, Naval Postgraduate School, 1984.

3. Solar Energy Research Institute, *Basic Photovoltaic Principles and Methods*, Van Nostrand Reinhold Co., 1984.

4. Jet Propulsion Laboratory Publication SP 43-38, *Solar Cell Array Design Handbook*, V.1, October 1976.

5. Jet Propulsion Laboratory Publication 82-69, *Solar Cell Radiation Handbook*, 3rd ed., by H. Y. Tada, J. R. Carter, Jr., B. E. Anspaugh and R. G. Downing, 1 November 1982.

6. John R. Barton, William G. Dunbar and Amy C. Reiss, *High Voltage Solar Array Plasma Protection Techniques*, in Eighteenth IEEE Photovoltaic Specialists Conference, pp. 411-417, 1985.

7. B. E. Anspaugh and R. G. Downing, *Radiation Effects in Silicon and Gallium Arsenide Solar Cells using Isotropic and Normally Incident Radiation*, in Seventeenth IEEE Photovoltaic Specialists Conference, pp. 23-30, 1984.

8. A. H. Kalma, R. A. Berger, C. J. Fischer and B. A. Green, *Energy and Temperature Dependence of Electron Irradiation*, IEEE Transactions of Nuclear Science, NS-22, p. 2277, 1975.

9. W. L. Wang and Sheng S. Li, *Studies of Deep-Level Defects and Recombination Parameters in 1-Mev Electron and Low Energy Proton Irradiated (AlGa)As-GaAs Solar Cells*, in Seventeenth IEEE Photovoltaic Specialists Conference, p. 161, 1984.

10. M. A. Green, A. W. Blakers, S. R. Wenham, S. Narayanan, M. R. Willison, M. Taouk and T. Szpitalak *Improvements in Silicon Solar Cell Efficiency* in Seventeenth IEEE Photovoltaic Specialists Conference, pp. 39-42, 1984.

11. A. C. Day, W. E. Horne, and I. Arimura, *Proton Damage Annealing for use in Extended Life Solar Arrays*, IEEE Transactions on Nuclear Science, Vol. NS-27, No. 6, pp. 1665-1669, December 1980.

12. Masufumi Yamaguchi and Chikara Amano, *^{60}Co γ-ray and Electron Irradiation Damage of GaAs Single Crystals and Solar Cells*, Journal of Applied Physics, Vol. 54, No. 9, pp. 5021-5029, September 1983.

13. R. Y. Loo, G. S. Kamath, and R. C. Knechtli, *Effect of Electron Flux on Radiation Damage in GaAs Solar Cells*, in Sixteenth IEEE Photovoltaic Specialists Conference, pp. 307-309, 1982.

14. Clark T. F., *An Experimental Test of Minority Carrier Annealing on Gallium Arsenide Solar Cells Using Foward-Biased Current*, Masters Thesis, Naval Postgraduate School, Monterey, California, September 1986.

15. Gold D. W., *High Energy Electron Radiation Degradation of Gallium Arsenide Solar Cells*, Masters Thesis, Naval Postgraduate School, Monterey, California, March 1986.

INITIAL DISTRIBUTION LIST

		No. Copies
1.	Defense Technical Information Center Cameron Station Alexandria, VA 22304-6145	2
2.	Library, Code 0142 Naval Postgraduate School Monterey, CA 93943-5002	2
3.	Professor S. Michael Code 62Mi Naval Postgraduate School Monterey, CA 93943	2
4.	Chairman, Code 62 Department of Electrical and Computer Engineering Naval Postgraduate School Monterey, CA 93943	2
5.	Professor R. Panholzer Code 62Pz Naval Postgraduate School Monterey, CA 93943	2
6.	Department of the Navy Commander Space and Naval Warfare Systems Command, PDW 106-483 Attn: Lcdr. R. Harding Washington, D.C. 20363-5100	2
7.	Naval Space Command Code N13 Dahlgren, VA 22448	2
8.	United States Space Command Attn: Technical Library Peterson AFB, CO 80914	2
9.	Naval Research Laboratory Code 6623 4555 Overlook Ave., SW Washington, D.C. 20375	2

10. LT Richard L. Staats 4
Defense Communications Engineering Center
Code R420
1860 Wiehle Avenue
Reston, VA 22090